Interference Mitigation in Wireless Communications

A Thesis
Presented to
The Academic Faculty

by

Kihong Kim

In Partial Fulfillment
of the Requirements for the Degree
Doctor of Philosophy

School of Electrical and Computer Engineering
Georgia Institute of Technology
December 2005

Interference Mitigation in Wireless Communications

Approved by:

Professor Gordon L. Stüber,
Advisor and Committee Chair
Electrical and Computer Engineering

Professor Ye (Geofferey) Li
Electrical and Computer Engineering

Professor Mary Ann Ingram,
Electrical and Computer Engineering

Professor Douglas B. Williams,
Electrical and Computer Engineering

Professor Alfred Andrew,
Mathematics

Date Approved: 23 August 2005

To,

My wife, Yeongseon, my daughter, Jeeyoon

and our parents

for their love for all these years.

ACKNOWLEDGEMENTS

This dissertation could not be completed without influences from several individuals, to whom I am grateful for their contributions, direct or indirect, to the completion of this research.

First and foremost, I would like to acknowledge a tremendous debt of gratitude towards my advisor, Prof. Gordon Stüber, whose patience, understanding, and guidance to me cannot be overstated. In addition to his academic supervision, I am also grateful for his financial support throughout my study. Most of all, I have learned a lot more than research work through his loyalty to integrity as an academic professional.

Next, I thank the reading committee members of my dissertation committee, Prof. Ye (Geofferey) Li and Prof. Mary Ann Ingram for their time, effort, and valuable suggestions necessary to complete this work. I also extend my thank to Prof. Douglas Williams and Prof. Alfred Andrew for having dedicated their valuable time to participate my dissertation committee, and having provided insightful comments and feedbacks for this research.

I thank all other members of Wireless Systems Laboratory (WSL), past and present, Dr. Jinsoup Joung, Dr. Hasung Kim, Heewon Kang, Joon Beom Kim, Chirag Patel, Alenka Zajic, and Qing Zhao, in no particular order, for all the time and discussions we shared during my stay at WSL. Especially, I give thanks to Dr. Apurva Mody. His optimism in academic and personal life has always made me focus on the light at the end of the tunnel. I also thank Dr. Tom Pratt and Galib Asadullah for their dedicated collaboration on the GSM project.

Lastly, I owe a debt of gratitude to my family for their love, support, and sacrifice along the path of my academic pursuits. For all this and much more, I dedicate this thesis to them.

Thank God for showing me the beginning and the end of a segment of the path of my life.

TABLE OF CONTENTS

LIST OF TABLES

LIST OF FIGURES

LIST OF ABBREVIATIONS

ACI	Adjacent-channel interference
ACL	Asynchronous Link
ARQ	Automatic repeat request
AWGN	Additive white Gaussian noise
BER	Bit error rate
BLAST	Bell-labs layered space-time algorithm
BPSK	Binary phase shift keying
CCI	Co-channel interference
CDF	Cumulative distribution functions
CDMA	Code-division multiple access
CIR	Carrier-to-interference ratio
CPM	Continuous phase modulation
CPPE	Conditional probability of packet error
CRC	Cyclic redundancy check
CSI	Channel state information
DDF	Dual-decision feedback
DFE	Decision-feedback estimation
DDFSE	Delayed decision-feedback sequence estimation
DSSS	Direct-sequence spread spectrum
ECC	Error correction codes
EDGE	Enhanced data rates for GSM evolution
EGC	Equal gain combining
FDMA	Frequency division multiple access
FCC	Federal communications commission
FEC	Forward error correction
FER	Frame error rate

FHSS	Frequency-hopping spread spectrum
GFSK	Gaussian-filtered frequency shift keying
GMSK	Gaussian-filtered minimum shift keying
GSM	Group special mobile
IRC	Interference rejection combining
ISI	Intersymbol interference
LGMSK	Linearized Gaussian-filtered minimum shift keying
LLR	Log-likelihood ratio
LMS	Least-mean squares
LOS	Line-of-sight
LS	Least squares
MAC	Medium access control
MAI	Multiple access interference
MAP	Maximum a posteriori
MIMO	Multiple-input multiple-output
MMSE	Minimum mean-square error
ML	Maximum likelihood
MLSE	Maximum likelihood sequence estimation
MRC	Maximal ratio combining
MUD	Multi-user detection
NBAA	Narrow beam adaptive antenna
NBI	Narrow-band interference
OBS	Obstructede channels
OC	Optimal combining
OP	Outage probability
OFDM	Orthogonal frequency division multiplexing
OSTBC	Orthogonal space-time block coding

PDF	Probability density function
PIC	Parallel interference cancellation
PN	Pseudo noise
PSK	Phase shift keying
QAM	Quadrature amplitude modulation
QoS	Quality of service
QPSK	Quadrature phase-shift keying
RLS	Recursive least squares
SCO	Synchronous Link
SDMA	Space division multiple access
SIC	Serial interference cancellation
SIMO	Single-input multiple-output
SISO	Soft-input soft-output
SINR	Signal-to-interference-plus-noise ratio
SNR	Signal-to-noise ratio
SOVA	Soft-output Viterbi algorithm
SVD	Singular value decomposition
STBC	Space-time block coding
STTC	Space-time trellis coding
TDL	Tapped delay line
TDMA	Time division multiple access
TSS	Training symbol sequence
UL	Unlicensed band
WBI	Wide-and interference
WLAN	Wireless local area network
WPAN	Wireless personal area network
ZF	Zero forcing

SUMMARY

Co-channel interference (CCI) is a major source of impairments in wireless communications. The primary objective of this thesis is to design advanced interference resilient schemes for asynchronous slow frequency hopping wireless personal area networks (FH-WPAN) and time division multiple access (TDMA) cellular systems in interference dominant environments. We also propose an interference-resilient power allocation method for multiple-input-multiple-output (MIMO) systems.

For asynchronous FH-WPANs in the presence of frequent packet collisions, we propose a single antenna interference cancelling dual decision feedback (IC-DDF) receiver based on joint maximum likelihood (ML) detection and recursive least squares (RLS) channel estimation. The single antenna IC-DDF receiver suppresses the CCI from packet collisions and the ISI from modulation waveform by jointly detecting two co-channel signals in low-Doppler frequency-nonselective fading channels at reduced complexity. For the system level performance evaluation, we propose a novel geometric method that combines bit error rate (BER) and the spatial distribution of the traffic load of CCI for the computation of packet error rate (PER). We also derived the probabilities of packet collision in multiple asynchronous FH-WPANs with uniform and nonuniform traffic patterns. Combined with the forward error correction (FEC) schemes of the packets, the proposed method can effectively evaluate the performance of interference cancelling receivers in heavy traffic load conditions resulting from multiple asynchronous FH-WPANs in close proximity.

For the design of TDMA receivers resilient to CCI in frequency selective channels, we propose a soft output joint detection interference rejection combining delayed decision feedback sequence estimation (JD IRC-DDFSE) scheme. In the proposed scheme, IRC suppresses the CCI, while DDFSE equalizes ISI with reduced complexity. Our preliminary results show that the joint detection method, associated with a joint least squares (LS) channel estimation algorithm, is highly efficient in suppressing high power CCI in various

channel models. Also, the soft outputs are generated from IRC-DDFSE decision metric to improve the performance of iterative or non-iterative type soft-input outer code decoders.

For the design of interference resilient power allocation scheme in MIMO systems, we investigate an adaptive power allocation method using subset antenna transmission (SAT) techniques. Motivated by the observation of capacity imbalance among the multiple parallel sub-channels, the SAT method achieves high spectral efficiency by allocating power on a selected transmit antenna subset. Increased transmit power per transmit antenna with SAT scheme achieves larger spectral efficiency than all-antenna transmission method in the presence of high power CCI. For 4×4 V-BLAST MIMO systems, the proposed scheme with SAT showed analogous results. Adaptive modulation schemes combined with the proposed method increase the capacity gains. From a feasibility viewpoint, the proposed method is a practical solution to CCI-limited MIMO systems since it does not require the channel state information (CSI) of CCI.

CHAPTER I

INTRODUCTION

During the last two decades, wireless communication has evolved from an optional convenience to an indispensable necessity in daily life. Advances in digital signal processing, digital computing, and radio transmission technologies have facilitated the introduction of a wide range of wireless communication services. Second generation wireless mobile communication systems such as GSM, IS-95, IS-136 and PDC provide people reliable narrowband communication links mostly for voice and text traffics with high mobility, and high-speed private- and public-access wireless local/personal area networks (WLAN/WPAN) such as Wi-Fi and Bluetooth deliver broadband multimedia traffic with limited mobility. However, increasing demands on high-capacity wireless multimedia services with sufficient mobility have created challenging tasks to the designers of next generation wireless mobile communication systems.

Because of the randomness of the mobile propagation channels and limited radio spectrum, co-channel interference (CCI), fading and intersymbol interference (ISI) are major impediments to high-capacity transmission in power- and bandwidth-limited wireless communication systems. Fading is traditionally countermeasured by channel coding and interleaving techniques as well as transmit/receive antenna diversity schemes. ISI from multipath reception can be combated by various linear/nonlinear type equalization techniques employing symbol-by-symbol detection methods such as decision feedback equalizer (DFE) or sequence-estimation methods such as maximum likelihood sequence estimation (MLSE).

In cellular networks, CCI is the interference from neighboring cells using the same radio channels. As the frequency reuse factor decreases from seven to three, then to one, CCI is unavoidable due to the channel reuse in adjacent cells. On the other hand, in ad-hoc type wireless networks such as WLAN and WPAN, the signals transmitted from multiple networks operating in close proximity behave as CCI to each other. Given perfect knowledge

of the channel coefficients of all co-channel signals, CCI is best handled by the joint MLSE (J-MLSE) receiver, but J-MLSE is generally too complex. Less complex linear filter type receivers suppress CCI by controlling the filter coefficients in the sense of maximizing the signal-to-interference-plus-noise ratio (SINR).

In typical wireless mobile communication systems, CCI, ISI and fading often arise together. Hence, the receiver designs for mitigating these impairments in joint fashions are quite common. In filter-based approaches, CCI is suppressed by a feedforward linear filter while ISI is mitigated by a concatenated decision feedback filter [97]. For the receivers with multiple antennas, diversity combining techniques broaden the freedom in interference mitigation receiver designs. Combined with MLSE or DFE type receivers, diversity combining combat ISI and fading jointly. For the suppression of CCI in flat fading channels, an optimum linear minimum mean square error (MMSE) combining technique was suggested by Winters [146]. Also, joint mitigation of CCI and ISI employing sequence estimation techniques can be found in many references. Concatenation of MMSE filtering and MLSE has been proposed by Bottomley *et al.* [27], and extended to an interference rejection combining MLSE (IRC-MLSE) receiver [28]. The complexity issue of MLSE structure in channels with long channel impulse responses has been handled by employing less complex delayed decision feedback sequence estimation (DDFSE) [84].

Multiuser detection (MUD) algorithms detect all co-channel signals unlike the filter-based methods treating all co-channel signals, except the desired one, as interference. After Van Etten [46] suggested a joint detection of co-channel signals by extending Forney's maximum-likelihood receiver [50], diverse MUD algorithms based on linear/nonlinear techniques such as joint MLSE, decorrelator, linear MMSE, and parallel/successive interference cancellation (PIC/SIC) have been proposed for practical code/time division multiple access (CDMA/TDMA) receiver designs [29, 39, 40, 118, 140, 143, 148].

In multiple-input multiple-output (MIMO) systems, large spectral efficiency can be achieved if the spatially multiplexed data streams, which manifest themselves as CCI to each other, are properly separated [51]. Accordingly, CCI mitigation techniques developed for single antenna systems have been applied in decoding of multi-channel data streams

in MIMO systems. In the Bell Labs layered space-time (BLAST) architectures, successive decoding of spatially multiplexed data streams have been suggested by using zero-forcing (ZF) or MMSE type linear receivers [52,147]. On the other hand, the spectral efficiency of a MIMO system, which heavily depends on the optimality of the power allocation algorithm, reduces in the presence of CCI [26]. For additive white Gaussian noise (AWGN) channels, the power allocation based on a water-filling and equal-distribution algorithms are known optimum to attain channel capacity when transmitters have channel state information (CSI) or not, respectively [34, 51]. However, in the presence of unknown high power CCI or noise, eigenmode imbalance in channel matrices wastes the power allocated to the eigenmodes with small eigenvalues when the CSI of CCI is not available [74]. Accordingly, antenna subset selection techniques have attracted significant attention because of the benefit of reduced cost in hardware implementation while improving error performance of linear/nonlinear receivers and transmitters [57, 69, 120].

1.1 Problem and Solution

The impairments from CCI and ISI have been major obstacles to reliable communication in *long-range* cellular networks and in *short-range* wireless local- and personal-area networks. Linear filtering, equalization, and diversity combining techniques have been traditional means to combat the impairments in separate or joint fashions. Also, the interference-cancelling techniques designed for decoding of multiple single-user signals have been applied in decoding of spatially multiplexed data streams in MIMO systems [52]. However, the impairments from high-power CCI and ISI in time-varying channels still impose severe constraints in the design of practical interference resilient receivers [26, 28, 156]. In the following, some of problems encountered in the design of interference mitigation receivers in the area of asynchronous FH-WPANs, TDMA cellular systems, and MIMO systems are presented along with the proposed solutions.

1.1.1 Interference Cancellation in Asynchronous Slow FH Networks

1.1.1.1 Dual Decision-Feedback Interference Cancellation

The packets transmitted from multiple ad-hoc Bluetooth piconets operating in the industrial, scientific and medical (ISM) bands manifest themselves as CCI to each other. By regulation of the FCC, the Bluetooth receivers are designed to combat the CCI by using a frequency hopping spread spectrum (FHSS) technique [1, 6]. However, for asynchronous slow FH Bluetooth piconets, packet collisions are unavoidable as the number of actively transmitting Bluetooth piconets increases [43, 127, 155]. Also, Bluetooth receivers face ISI introduced by the non-Nyquist Gaussian transmit filter. Though the joint MLSE (J-MLSE) using a Viterbi algorithm is known optimum for the detection of multiple co-channel signals with ISI [46], interference cancelling techniques based on symbol-by-symbol detection can be alternative solutions for simple-and-economic Bluetooth receivers. To compute the decision metrics for joint detection receivers, the channel impulse responses of all co-channel signals are required, so that adaptive channel estimation is needed for time-varying channels. The tracking properties of the least mean squares (LMS) algorithm is quite similar to that of the recursive least squares (RLS) algorithm [44, 98]. The LMS algorithm converges slowly in training mode, and the accuracy in data mode is sensitive to the initial channel estimate obtained in the training mode. The fast converging RLS algorithm requires complex computation.

In this study, we propose a single antenna interference cancelling dual decision-feedback (IC-DDF) maximum likelihood (ML) receiver that jointly detects two co-channel signals. The DDF function diminishes the impairments from ISI and CCI by subtracting the postcursor parts of the all estimated co-channel signals simultaneously. Also, an adaptive channel estimation with a simplified recursive least squares (RLS) algorithm was developed for the joint channel estimation and tracking in slow flat fading channels. The new algorithm reduced the complexity of the covariance matrix update function by using a constant covariance matrix.

1.1.1.2 Link-Level Performance Evaluation for Multiple Bluetooth Piconets

For multiple Bluetooth piconets operating in proximity, transmission of packets is impaired by the collisions between the packets from different piconets rather than by the randomness of propagation channels. Packet error rate (PER) has been widely used as a link-level performance measure of communication links and is one of the key parameters defining the quality of service (QoS) of a traffic link. Traditionally, PER has been computed either by using channel models [125, 127, 154] or by using packet collision probabilities [43, 80] in separate fashions. However, each separate approach does not provide comprehensive understanding of the link-level performance of multiple packet networks experiencing frequent packet collisions in time-varying channel conditions.

In this study, we propose a novel method that effectively combines the influence from faded channels and the packet collision statistics for the link-level performance evaluation of interference cancelling Bluetooth receivers. In the proposed method, the PER is computed by using the probability density function (pdf) of received carrier-to-interference ratio (CIR), raw BER of the receiver, and packet collision statistics of multiple piconets. The pdf of CIR is derived from the spatial distribution of co-channel interference, rather than from the fading statistics, by using a geometric method. In addition, the probabilities of packet collisions in multiple slow FH Bluetooth piconets with various traffic patterns have been derived and used in overall link throughput computation.

1.1.2 Joint Detection Interference Rejection Combining TDMA Receiver

In TDMA cellular systems, CCI from neighboring co-channel cells degrades the receiver performance due to multipath fading, non-ideal terrain structures, and dense frequency reuse schemes [128]. Many linear/nonlinear type interference cancelling receivers based on single-user detection (SUD) techniques have been documented in literature. However, the performance of SUD-based receivers is marginal in the presence of high-power CCI. In this condition, the joint detection of co-channel signals is a feasible solution to the high-power CCI mitigation problem at the cost of increased complexity [46, 118, 135]. On the other hand, diversity combining techniques are known effective in CCI suppression for the systems

with multiple receive antennas. Winters [146] has proposed a optimum linear diversity combining scheme for CCI suppression in flat fading channels by using channel coefficients of all co-channel signals, but achieving the channel coefficients of all co-channel signals is a challenging task in practical systems. To mitigate CCI and ISI jointly, Bottomley [27] has proposed an IRC-MLSE receiver, and Joung *et al.* [84] have proposed a reduced complexity scheme by employing a DDFSE technique. The IRC-MLSE scheme requires only desired signal's channel information and successfully suppresses the interference from one co-channel user. However, the performance of IRC-MLSE drops sharply as the number of CCI increases.

The objective of this study is to design a practical CCI resilient receiver for synchronous GSM cellular networks that provides reliable communication links to remote BSs against the strong co-channel signals from the nearby BSs for intelligence or emergency operations. The receiver should be operable at CIR levels that are far below the range that conventional receivers are usually designed to operate in. We propose a soft output fractionally spaced joint detection IRC-DDFSE (JD IRC-DDFSE) scheme with joint least squares (LS) channel estimation. The joint detection of the desired and the strongest co-channel signals significantly reduces the impairments from the strong CCI. The complexity increase from joint detection is compensated by using reduced state DDFSE. The effect of the number of received CCI is assessed by a heuristic method based on measurement data of narrow beam adaptive antenna (NBAA) and sector antenna schemes [15]. The soft outputs generated from a Log-MAP algorithm improve the performance of a Viterbi type outer code decoder in binary and non-binary signaling systems. Joint LS channel estimation reduces the estimation error from the cross-correlation between two training symbol sequences (TSS) by using the tools of linear algebra [118]. In addition, we investigate the effect of unequal CCI power distribution over antenna branches by computer simulations.

1.1.3 CCI Mitigation in Space-Time MIMO Communication Systems

Recent research in information theory showed that a large channel capacity exists for wireless systems with multiple transmit and receive antennas if the richness in multipath is

properly exploited [51]. The capacity of a MIMO system depends on the number of transmit/receive antennas, the correlation between the channel coefficients of individual paths, and the power allocation scheme over the transmit antennas [126,147]. For AWGN channels, the power allocation based on a water-filling algorithm is known to attain capacity when the transmitters have CSI [34]. Likewise, the equal power distribution is an alternative solution if CSI is not available at the transmitter [51]. Unlike the Gaussian noise, however, CCI is generally treated as colored noise having non-zero off-diagonal terms in its covariance matrix. Hence, the power allocation must be optimized with an equivalent channel matrix derived from the CSI of desired and interfering signals [48]. However, the estimation of the CSI of interfering signals, which is an essential part of the equivalent channel matrix, is a challenging task in many practical systems. Also, the equal power distribution is not promising in the presence of high-power interference-plus-noise because of the elimination of all but a few largest eigenvalues in such conditions [22,111]. To mitigate the capacity loss from CCI, MIMO multiuser detection and adaptive power allocation by subspace tracking were proposed [26, 64, 153]. But, they are impractical when the transmitter either has a large number of antennas or does not have the CSI for all co-channel signals.

In this study, we investigate the effect of adaptive power allocation by using subset antenna transmission (SAT) on the capacity of MIMO systems in the presence of co-channel interference (CCI). In the SAT scheme, the transmit power is redistributed equally across a selected subset of the transmit antennas. The subset is determined from a criteria obtained from the CSI of the desired signal, while CSI of the CCI is not needed. The capacity gain from the proposed method is evaluated by numerical methods. For comparison, the performance of a space-time diversity coding (STDC) scheme in terms of interference mitigation is also provided.

1.2 Thesis Outline

This thesis is organized as follows. Chapter 2 reviews a brief background information on interference sources in wireless communications and interference mitigation techniques for various system models. Chapter 3 presents interference cancellation in Bluetooth networks,

where a cost-effective single antenna joint detection interference cancelling receiver and an associated system level performance evaluation scheme are proposed. Chapter 4 considers a practical soft output joint detection IRC-DDFSE TDMA receiver that mitigates the effect of a strong CCI signal. Computer simulations were carried out to evaluate the performance of the proposed receiver design for various GSM channel models. Chapter 5 analyzes the performance of the proposed subset antenna transmission method for MIMO systems in the presence of high-power interference and noise. Comparisons are made between the SAT scheme and the conventional all-antenna transmission scheme in information theoretic capacity and realistic capacity of vertical-BLAST (V-BLAST) systems. Chapter 6 summarizes the results obtained in this thesis, and proposes some topics for further study.

CHAPTER II

BACKGROUND

2.1 Interference in Wireless Communications

2.1.1 Propagation Channels

In wireless mobile communications, the transmitted signal is subject to various impairments caused by the transmission medium combined with the mobility of transmitters and/or receivers. Path-loss is an attenuation of the signal strength with the distance between the transmitter and the receiver antenna, and the frequency reuse technique in cellular systems is based on the physical phenomena of path-loss. Unlike the transmission in free space, transmission in practical channels, where propagation takes place in atmosphere and near the ground, is affected by terrain contours. As the mobile moves, the slow variation in mean envelope over a small region, *shadowing*, appears due to the variations in large-scale terrain characteristics, such as hills, forests, and clumps of buildings. The variations resulting from shadowing, are often described by a log-normal distribution with standard deviation ranging from 4 to 13 dB [62, 128]. Power control techniques are often used to combat the slow variation in mean received envelope due to the path-loss and shadowing.

Compared to the large-scale fading due to the shadowing, multipath fading, often called fast fading, refers to the *small-scale* fast fluctuation of the received signal envelope resulting from multipath reception and transmitter and/or receiver movement. Multipath fading results in the constructive or destructive addition of arriving plane wave components, and manifests itself as large variations in amplitude and phase of the composite received signal in time [82]. When the channel exhibits a deep fade, fading causes a very low instantaneous signal-to-noise ratio (SNR) or carrier-to-noise ratio (CNR). Diversity and coding techniques are well known methods for combating multipath fading by reducing the probability that the received signal is weak.

2.1.2 Intersymbol Interference (ISI)

In radio channels for digital communication, ISI is due to multipath propagation when the delay spread of the channel is large compared to the duration of modulated symbol [108]. Also, ISI can be introduced by an over transmit and receive filter response that is not a Nyquist pulse. The ISI results in non-flat transfer function in frequency domain such that the all frequency components in the transmitted signal may not experience similar amplitude and phase variations [108]. An equalizer is a digital filter used in digital communications to correct or *equalize* ISI. Two types of equalizers are used to mitigate ISI by using linear or nonlinear techniques: symbol-by-symbol equalization such as DFE and sequence estimation such as MLSE [116].

2.1.3 Co-Channel and Adjacent-Channel Interference (CCI and ACI)

CCI is introduced when a frequency band is shared by multiple users at the same time. In cellular systems, CCI arises by the frequency reuse in neighboring cells. As frequency reuse factor decreases to increase the system capacity, CCI increases as the distance between the co-channel cells decreases. Therefore, the performance of a frequency reuse system is limited by CCI rather than by additive noise. For wireless communication systems such as EDGE [11], which uses smaller cell size and an aggressive frequency reuse strategy, CCI mitigation is an important issue for spectral efficiency increase [31]. Diversity combining and multiuser detection (MUD) approaches have been known effective for mitigating CCI [118, 146]. Similarly, the ACI, signals received from one channel but smeared into adjacent channels due to imperfect receive filtering or imperfect frequency offset estimation, degrades the receiver performance. In frequency reuse cellular systems, ACI can be minimized by avoiding the use of adjacent channels within a cell [94]. However, as the frequency reuse factor approaches one, the distortions from ACI cannot be neglected in the receiver design.

Table 1: Summary of interferences in 2.4 GHz ISM band

Characteristics	Interference Sources			
	WPAN (Bluetooth)	WLAN	MW Oven	Cordless Phone
BW (MHz)	1	22	$2 \sim 60$	0.180
Power (mW)	$1 \sim 100$	$10 \sim 1000$	(leakage)	$10 \sim 100$
Popularity	medium	medium	small($\sim$1)	small($\leq$3)
Multiple Access	FHSS/TDD	DSSS/FDD	N/A	Proprietary
Modulation	GFSK	BPSK	CW	Proprietary
Range (m)	$\leq$10	$10 \sim 100$	$\leq$10	$10 \sim 100$
Specification	Yes	Yes	safety only	proprietary

2.1.4 Interference in ISM Bands

Since the Federal Communications Commission (FCC) opened a broad radio spectrum in 2.4 GHz band for industrial, scientific, and medical (ISM) uses, various applications have been benefited from the wide band of license-free radio spectrum [1, 6, 136]. In the ISM band, wireless networks operate without coordinated or centralized control for avoiding mutual interference. Instead, the CCI in ISM bands is governed by using spread spectrum techniques and strict transmit power level control [1,6]. As a result, a communication device operating in the ISM band may encounter interference from many sources, for example, Bluetooth WPAN devices, IEEE 802.11 WLAN devices, cordless phones, remote sensing devices, and even microwave ovens as listed in Table 1 [56, 136]. As a wave of commercial products were arriving for use in ISM bands, the coexistence of multiple collocated systems with different radio interfaces has been a technically challenging issue both for medium access control (MAC) and physical (PHY) layer designs [45, 65, 66, 79, 124, 156]. Also, the CCI between multiple Bluetooth piconets operating in close proximity in places such as shopping malls and airport lounges has been receiving a technical concern as the number of deployed Bluetooth applications grows rapidly [6, 127].

2.2 Interference Mitigation Techniques

The characteristics of CCI and ISI of a wireless communication system is determined by the radio interface and the network topology of the system. Accordingly, a broad range

of interference mitigation techniques have been employed at transmitter and/or receiver as illustrated in Figure 1 [93].

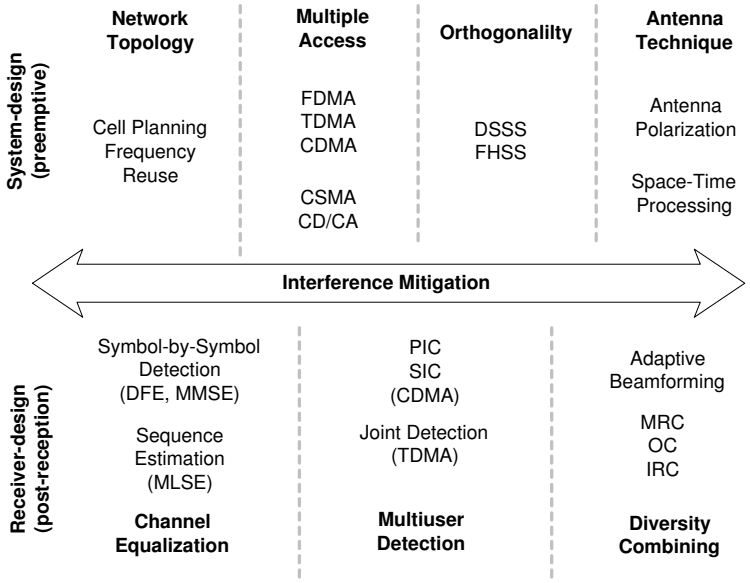

Figure 1: Interference mitigation techniques.

In system-design approaches, transmission of co-channel signals is properly managed so that the power of received CCI is maintained below an acceptable level [55, 62, 128]. In contrast, receiver-design approaches actively mitigate the CCI/ISI which cannot be separated by the preemptive system-design approaches. In practical systems, both approaches are employed in joint fashions to reduce the interference.

2.2.1 Frequency Reuse and Multiple Access

Information streams from multiple users can be transmitted in parallel through a shared radio spectrum by isolating signals from different users from each other in multiple domains [62]. In time, frequency, and code division multiple access (TD/FDMA) techniques, signals from multiple users are transmitted by using nonoverlapping time slots, nonoverlapping frequency bands, and codes having very small crosscorrelations, respectively, so that signals from different users are easily separated. Two forms of CDMA, frequency hopping (FH) and direct sequence (DS), are widely used in military and commercial applications [114]. The second generation digital cellular systems based on IS-95, IS-136, GSM

and PDC standards are designed using a combination of the three multiple access techniques to accommodate more channels [55].

Frequency reuse is an example of space division multiple access (SDMA) techniques that separates CCI in cellular systems by utilizing path loss phenomena and radio spectrum partitioning [55,94]. In a frequency reuse scheme, clustered radio channels are reused in distant co-channel cells in repeating patterns. The transmit power is properly controlled to keep the amount of CCI at a tolerable level. However, the received CIR at a receiver is not guaranteed statistically because of the dynamic nature of the fading channels especially in high capacity wireless systems where more aggressive frequency reuse schemes are employed [11].

Wireless packet networks (WLAN and WPAN) based on IEEE802.11 and Bluetooth standards provide complementary wireless solutions for low-mobility broadband multimedia traffic in the unlicensed ISM band [1, 6, 10]. The WLANs and WPANs operate in two different network topologies: access-point and ad-hoc network. Without any centralized multiple access control among collocated networks, independent multiple access control (MAC) in each network such as carrier sensing multiple access with collision avoidance (CSMA/CA) cannot avoid the collision between packets from different networks. Therefore, CCI from packet collisions can only be mitigated by using direct sequence or frequency hopping spread spectrum techniques at physical (PHY) layer signal processing.

2.2.2 Adaptive Filtering

Interference cancelling receiver design is often viewed as an adaptive filtering with feedforward and feedback filters as illustrated in Figure 2 [93]. This technique finds its root in adaptive equalization research, which primarily focuses on mitigating ISI with single antenna by using linear and nonlinear techniques. However, previous works of Lo *et al.* [100], Petersen *et al.* [112], and Yoshino *et al.* [151] showed that equalization techniques effectively mitigate CCI as well ISI. Two types of equalizers using linear or nonlinear techniques can be found in many references: symbol-by-symbol equalizers and sequence estimators.

The most common structure for the linear equalizer is the transversal filter in which the current and past values of the received signal are weighted by equalizer coefficients

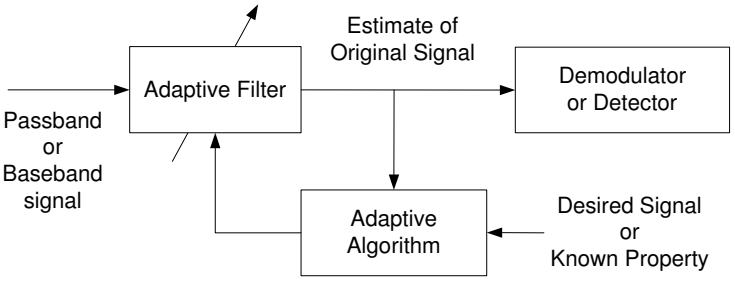

Figure 2: An adaptive filter model for interference mitigation.

and summed to produce the output for symbol-by-symbol decisions on the received symbol sequence. The equalizer coefficients are adjusted to minimize some error criterion. The equalizer that forces ISI to zero is called zero-forcing (ZF) equalizer. The MMSE equalizer outperforms the ZF equalizer in performance and convergence properties by mitigating the noise enhancement [115, 116]. Nonlinear decision feedback equalizer (DFE) combined with a linear feedforward filter has been proposed to reduce the effect of noise enhancement from precursor and postcursor ISI. Lo *et al.* [100] showed that a directly adapted RLS DFE equalizer outperforms an MMSE equalizer, which employs estimates of channel impulse response and the autocorrelation of interference-plus-noise in frequency selective channels in the presence of CCI [100]. One drawback of the DFE type receivers is error propagation when the desired signal is in a deep fade, or when the received CIR is low. Uesugi *et al.* [135] also proposed a DFE type single/double feedback interference cancelling (SF/DF-IC) receiver to mitigate CCI by subtracting the ISI components of the estimated co-channel signals.

The optimum maximum-likelihood sequence estimation (MLSE) receiver for signals corrupted with ISI and AWGN was proposed by Forney [50]. MLSE uses a whitened-matched filter (WMF) followed by a Virerbi decoder to combine equalization and decoding. An MLSE type receiver requires the channel information for sequence estimation, and its complexity increases exponentially with the length of the channel and the size of the signal constellation. For tracking rapidly time-varying channels, adaptive algorithms such as the LMS and the RLS algorithms are usually employed [135,151]. The suboptimum sequence estimation techniques were investigated for solutions with reduced complexities. Duel-Hallen

Table 2: Weight functions of diversity combining techniques with CCI

	Weight	Notes
EGC	$\mathbf{W} = [1, \ldots, 1]$	Co-phased and equally weighted
MRC	$\mathbf{W} = [g_{1d}^*, \ldots, g_{Nd}^*] = \mathbf{g}_d^*$	ML with CSI
OC	$\mathbf{W} = \alpha \mathbf{R}^{-1} \mathbf{g}_d^*$ where $\mathbf{R}^{-1} = \sigma^2 \mathbf{I} + E[\mathbf{g}_i^* \mathbf{g}_i^T]$	Optimal in sense of Max. SINR
IRC	metric $= \arg\min\{\exp(-\mathbf{g}_i^* \mathbf{R}^{-1} \mathbf{g}_i^T)\}$	MLSE from impairment vector

and Heegard proposed a delayed decision-feedback sequence estimator (DDFSE) [41]. This algorithm provides tradeoffs between complexity and performance by using a truncated state trellis and decision-feedback to compute branch metric. A reduced-state sequence estimation (RSSE) was proposed by Eyuboglu *et al.* [47] by using the idea of set-partitioning algorithm initially proposed by Ungerboeck [137].

2.2.3 Spatio-Temporal Interference Mitigation

Faded signal reception results in a large penalty in SNR when the receiver has only one set of received signals from a single antenna. For example, a DFE type receiver with a single antenna experiences error propagation during the signal reception in a deep fade. The use of multiple antennas at receiver creates multiple-input multiple-output (MIMO) channels in CCI mitigation [128], and the existing CCI mitigation techniques for multiple-input single-output (MISO) channels can be extended to spatio-temporal interference mitigation techniques by using diversity combing techniques. One advantage of the spatio-temporal approach is a joint suppression-and-equalization of CCI and ISI [27, 84, 97].

2.2.3.1 Diversity Combining for CCI Suppression

Figure 3 illustrates an architecture of the $1 \times N$ diversity combining receiver with channel vectors $\mathbf{g}_d = [g_{1d}, \ldots, g_{Nd}]$ and $\mathbf{g}_i = [g_{1i}, \ldots, g_{Ni}]$ of the desired and interfering signals, respectively. Weight functions of four different diversity combining techniques are summarized in Table 2. Aalo *et al.* [12], Hafeez *et al.* [72], Shah *et al.* [122], and Rao *et al.* [119]have analyzed the performance of optimum combining (OC) and MRC techniques with non-Gaussian CCI in flat fading channels in terms of outage probability. Suzuki [130]

and Yoshino*et al.* [151] showed that the MRC has an interference cancelling effect in CCI environments. The optimum linear minimum mean square error combining technique for flat fading channels was proposed by Winters [146] by using the channel information of all co-channel signals in updating the antenna weight coefficients. Unlike MRC which mitigates CCI by enhancing the received SINR at the antenna outputs, OC jointly combats the effects of fading and CCI through digital beamforming with a multiple-element spatial diversity combiner [128]. Though OC is not effective in ISI equalization, this drawback can be compensated for by using a concatenated symbol-by-symbol equalizer or sequence estimator.

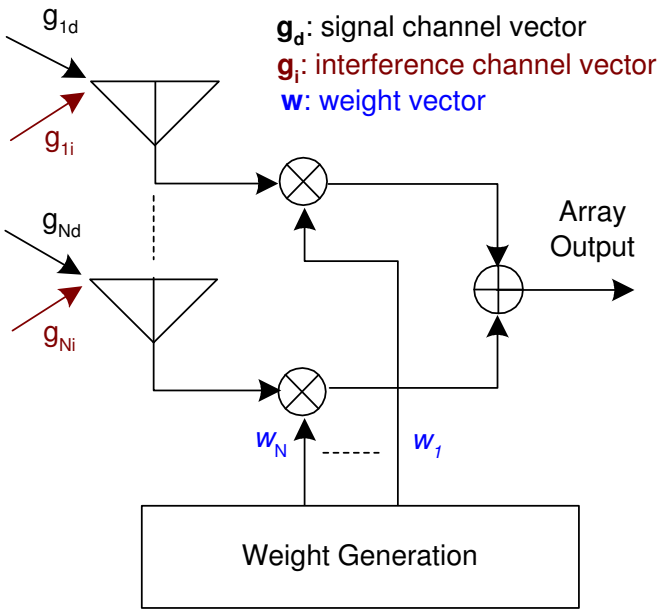

Figure 3: A schematic of diversity combining.

2.2.3.2 Two-Stage Interference Cancellation

In frequency selective fading channels, all co-channel signals experience ISI. Liang *et al.*'s work [97] on two-stage CCI/ISI reduction method was motivated by this observation. In the two-stage interference mitigation, the CCI is suppressed by a space-time filter in the first stage and the ISI is cancelled by a Viterbi type equalizer in the second stage [99]. Duel-Hallen [38] and Uesugi *et al.* [135] have suggested DFE-based approaches for joint

suppression-and-equalization in MIMO channels. Li *et al.* [96] also proposed CCI/ISI mitigation for IS-136 TDMA systems by using MMSE spatial-temporal DFE and linear equalizer (LE).

With sequence estimation equalizers, joint MLSE (J-MLSE) is the maximum-likelihood solution to the signal detection in the ISI channels with CCI [46]. Besides its computational complexity, J-MLSE requires channel coefficients of all co-channel signals, which is mostly infeasible in practical systems. As an alternative solution to J-MLSE, an interference rejection combining MLSE (IRC-MLSE) receiver, which only requires channel information of the desired user, was proposed by Bottomley *et al.* [27]. The IRC-MLSE receiver structure exploits the cross-correlation of the signal impairments of interference-plus-noise across the antenna arrays and combines diversity branches in the metric of the MLSE receiver. The IRC-MLSE technique has been considered a practical solution in many interference-resilient TDMA receiver designs [59, 86, 117].

Joung *et al.* [84] suggested a fractionally-spaced reduced complexity IRC-DDFSE receiver by employing the DDFSE technique initially proposed by Duel-Hallen [41]. The IRC-DDFSE receiver uses a $T/2$-spaced noise whitening filter depending only on the transmit pulse as suggested by Hamied and Stüber [73]. This receiver structure not only gives an advantage of immunity to symbol timing errors but also requires no ideal bandpass filter. In addition, generation of soft outputs from diversity combining metrics and their use in joint detection and channel estimation have been suggested [18, 152]. An iterative soft output decoding technique was also proposed for multiuser detection in TDMA systems [138].

For diversity combining receivers, the received CIRs at antenna branches are generally assumed equal. However, this assumption is not always applicable, especially in diversity combining with directional antennas. Mallik *et al.* [103] showed that the imbalance of Gaussian noise across antenna branches degrades the performance of equal gain combining (EGC) in correlated Rayleigh faded channels, and Lin [99] showed that optimal and selective combining receivers with linear/nonlinear equalizers achieve minimum BER when all antenna branches have equal received SNRs.

2.2.3.3 Beamforming and Transmit Diversity

Beamforming and transmit diversity are two complementary techniques for using multiple antennas in wireless communication systems. Beamforming achieves an array gain by linearly combining tap gains of an antenna array in highly correlated channels while transmit diversity obtains a diversity gain by exploiting the independence among channels [53]. In highly correlated line-of-sight (LOS) indoor channels, beamforming techniques provide CCI-mitigation through spatial filtering [125]. The spatial filtering of CCI is achieved either by shaping beams to have nulls in the directions of co-channel signals or by forming beams to have a large gain in the direction of the desired signal [142]. For this reason, beamforming requires estimation of the direction of arrival (DoA) of the desired or interfering signals.

Several variations of beamforming have been proposed: fixed, switched, and adaptive beamforming. In fixed beamforming (FB) networks, an antenna array forms narrow multiple beams in pre-selected directions for low-mobility users and suppresses the interference from outside of the beamwidth. The multichannel multipoint distribution service (MMDS) for broadband wireless access (BWA) is one example of FB networks [9, 123]. The switched beamforming (SB) technique uses a switch to select the best beam to receive a particular signal in FB networks. As the realizations of the space division multiple access (SDMA) technique, the fixed and switched beamforming have been applied to existing TDMA cellular networks [72, 81, 104]. In cellular systems, adaptive control of antenna array is required to track the time-varying distribution of mobile users. Anderson *et al.* [15] has suggested an adaptive antenna system for GSM and TDMA systems by using an adaptive beamforming (AB) technique in downlink and an interference rejection combining technique in uplink. The LMS or RLS algorithms are used in updating of the spatial characteristics of the AB array.

Unlike the beamforming technique which changes the radiation pattern of an antenna array to achieve array gains and CCI-mitigation by controlling the weights of array elements in radio frequency (RF) level, the diversity gain of the transmit diversity (TD) is achieved by combining the signals in baseband or intermediate frequency (IF) level [63]. As a result, TD allows a lot of freedom in transmitter/receiver designs by combining coding and space-time

diversity techniques [37]. Space-time encoding techniques employed in transmitter helps the separation of transmitted signals at the receiver by using the orthogonality between space-time code matrices. In other words, CCI mitigation in transmit diversity is achieved by using the space-time coding as well as the antenna diversity. Another advantage of the transmit diversity scheme is the simplified receiver structure without loosing diversity gains. Li *et al.* [95] suggested a simplified CCI/ISI mitigation receiver design based on a transmit diversity scheme, and Tarokh and Jafarkhani [131] proposed a simplified differential detection scheme which requires no channel information at transmitter and receiver by using a differential coding across transmit antennas.

The third generation (3G) wireless communication systems W-CDMA [8] and cdma2000 [7] have considered time diversity techniques as their key contributing technologies. Orthogonal TD (OTD) [7] is an open loop method in which coded interleaved symbols are split into even and odd symbol streams and transmitted using two different Walsh codes. Space-time transmit diversity (STTD) [8] and space-time spreading (STS) [7] techniques use Wlash codes and transmit diversity techniques which are very similar to the one proposed by Alamouti [14]. Closed loop techniques are adaptive in nature. Switched TD (STD) was adopted by cdma2000 as an extension of the open loop technique, time-switched time diversity (TSTD). The mobile station (MS) uses the average received power from the common pilots from each antenna, and makes a decision from which antenna it would like the BS to transmit. W-CDMA adopted a more aggressive transmit adaptive array (TXAA) method which optimizes the transmitter weight to deliver maximum power to the MS. The MS computes the weights and transmits to the BS. The precision, feedback error and feedback delay are the technical issues requiring further research.

2.2.4 Multiuser Detection

Distinguished from single-user detection techniques, which treats signals from co-channel users as interference, multi-user detection (MUD) detects all co-channel signals simultaneously. Since MUD techniques not only increase the system capacity but also improve the quality of an individual communication link by eliminating CCI from multi-users [16], MUD

has been an important technology in interference-limited communication systems such as GSM, IS-54/IS-136, and IS-95 regardless of the multiple access schemes [77].

After the concept of MUD based on the J-MLSE technique was introduced by Van Etten [46] in 1976, a number of optimum and suboptimum MUD receiver designs have been suggested mostly for CDMA cellular systems. In CDMA cellular systems based on DSSS techniques, all co-channel users behave as wideband interference (WBI) to each other because of the low cross-correlation spreading codes [5, 91]. However, the near-far problem and imperfect power-control limit the system capacity of the existing single-user detection systems. The optimum multiuser detector for asynchronous CDMA systems was proposed by Verdú [143]. However, the complexity of the optimum detector, which increases proportional to $\mathcal{O}(M^k)$ where M is the alphabet size and k is the number of users, has prompted the research on reduced-complexity suboptimum receivers. These suboptimum receiver designs include the decorrelator detectors [101, 102], linear MMSE detectors [148], nonlinear decision feedback detectors [39, 40], and multi-stage detectors with successive and parallel interference cancellations (SIC/PIC) [29,140,141]. SIC is known to outperform PIC in realistic conditions where the users have unequal received power levels [109]. Imperfect channel estimation and power control are the major sources of performance loss in SIC. An unequal weighting technique and a binary iterative feedback algorithm have been suggested by Andrew *et al.* [17] and Agrawal *et al.* [13] , respectively, to improve the channel estimation and power control efficiency in SIC.

Similarly, a joint interference cancelling receiver based on DFE technique was suggested by Uesugi *et al.* [135] for the Japanese TDMA celluar system, and Hafeez *et al.* [71], Hoeher *et al.* [76], and Ranta *et al.* [118] proposed practical MUD receives for TDMA-based GSM, EDGE, and IS-54/IS-136 systems, respectively, by using joint sequence estimation techniques based on J-MLSE. To reduce the state of the J-MLSE method, reduced-state joint detection algorithms based on the DDFSE technique have been suggested [76, 88]. Also, the single-antenna interference cancellation (SAIC) techniques for TDMA cellular systems have been considered as practical solutions for capacity increase without modifying existing infrastructures [20]. The results from computer simulations and field trials witnessed

the feasibility of the SAIC techniques based on joint-demodulation and blind interference cancellation techniques in existing TDMA networks [32, 113].

2.3 Packet-Level Performance in Wireless Communication

In present and future wireless digital communication systems such as GSM/EDGE, 3G cellular systems, Wi-Fi, and Bluetooth, the transmission of multimedia traffic is organized and transmitted in packets [1, 4, 6, 11]. The transmission of a packet is often protected by a forward error correction (FEC) scheme. When a packet arrives with more bit errors than the FEC scheme can restore, a packet error occurs and the erroneous packet generally needs to be retransmitted. Also, FER is one of the key parameters defining the quality-of-service (QoS) of a communication network [49]. As a result, PER is widely accepted as a performance measure of wired and wireless communication networks regardless of the nature of the propagation channels.

2.3.1 AWGN Channels

In AWGN channels, the transmission of each uncoded bit can be considered an independent and identically distributed (i.i.d) process. With this assumption, the probability of packet error $P_{pkt}(e)$ can be represented in a binomial distribution with the probability of bit error $P_{bit}(e)$ as

$$P_{pkt}(e) = 1 - \sum_{i=0}^{N_{max}} \binom{L}{i} (P_{bit}(e))^i (1 - P_{bit}(e))^{L-i} \tag{1}$$

where L, N_e, and N_{max} represent the packet length, the number of bit errors during packet transmission, and the number of maximum bit errors which can be corrected with a given FEC scheme, respectively.

2.3.2 Time-Varying Fading Channels

In mobile communications, transmitted signals experience time-varying fading channels due to the multipath reception and mobility of receivers and/or transmitters. For fast fading channels where the received signal power changes rapidly bit-by-bit, transmission of each bit and corresponding bit error probability can be considered an i.i.d process [154]. The systems employing ideal interleavers employ the same model even in slow fading channels [25].

For slow fading channels where fades maintain for more than a one-bit baud interval but change during the block transmission, the signal transmission at every baud interval cannot be considered as an i.i.d process unless the transmitted bits are ideally interleaved. In these channel conditions, a packet error is determined by the fade duration and the FEC function of the packet [25,92]. In a packet error model proposed by Lai and Mandayam [92], a packet is considered lost if the sum of the fade durations $\tau_f = \sum_i \tau_{bi}$ is greater than a given threshold τ_{th}, where $\tau_{th} = T_b \times N_{max}$ is the baud duration multiplied by the maximum number of bit errors allowed with a given FEC scheme. In Rayleigh faded channels, the probability of packet error is given as [92]

$$P_{\tau_f}(\tau_f > \tau_{th}) = \frac{2}{u} I_1(\frac{2}{\pi u^2}) \exp(-\frac{2}{\pi u^2}) \tag{2}$$

where $I_1(z)$ is a Bessel function of imaginary argument and u is the normalized fade duration $u = \tau_{th}/\bar{\tau}_{th}$ with the mean duration of $\bar{\tau}_{th}$. Figure 4 illustrates the effect of the fade duration during a packet reception.

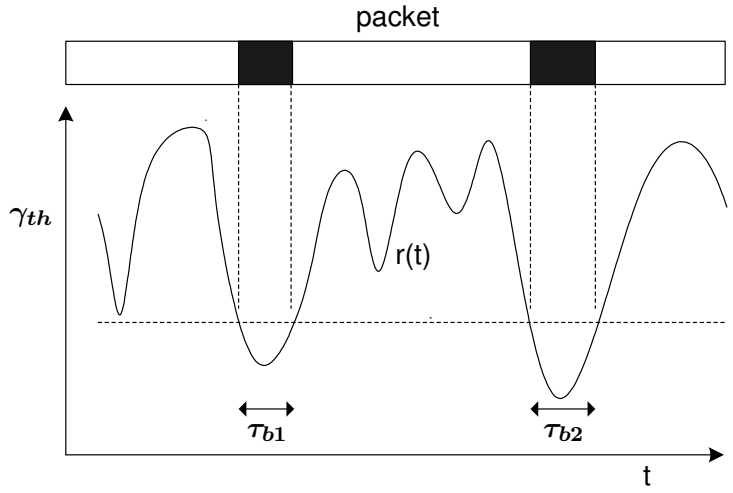

Figure 4: Packet reception in slow faded channels.

The block fading channel model, in which the channel state is assumed to change at every block interval and to remain unchanged during the block transmission, is widely accepted for packet error modelling in quasi-static channels [125]. Zorzi *et al.* [154] has suggested a packet success/failure model for noninterleaved packets in block fading channels by using a

first-order Markov process. In fast fading channels, the Markov process degenerates into an i.i.d process. In a simplified threshold-type PER computation model suggested by Souissi and Meihofer [127], a packet is considered erroneous if its received SINR γ_{rx} is smaller than a given threshold γ_{th} as

$$P_{pkt}(e) = P(\gamma_{rx} < \gamma_{th}). \tag{3}$$

2.3.3 Uncoordinated Wireless Packet Networks

For multiple asynchronous wireless packet networks operating in close proximity, the probability of packet error can be defined as

$$P_{pkt}(e) = P_{pkt}(e|c)P(c) + P_{pkt}(e|nc)(1 - P(c)) \tag{4}$$

where $P_{pkt}(e|c)$ and $P_{pkt}(e|nc)$ are the conditional probabilities of packet error with and without collision, respectively, with a given probability of collision $P(c)$. In short-range low-mobility wireless communication systems such as WLAN and Bluetooth WPAN, transmitted packets face negligible distortion from low-Doppler high-visibility propagation channels, and the probability of packet error defined in (4) is dominated by the first term of the right side of the equation [156].

In a simple packet collision model used by Howitt [80] for a Bluetooth interference modelling, a packet collision takes place if more than two packets share a radio channel simultaneously regardless of their received power levels. More complicated models proposed by Golmie *et al.* [66], Kamerman [85], and Van Dyck [139] have considered the capture effect, path loss, and the network topologies in combined ways in the decision of a packet collision. To compute the $P_{pkt}(e|c)$ in asynchronous packet collisions, Shellhammern [124] suggested the use of the number of the bits involved in the collision and the FEC scheme of the packet.

Previous studies on coexistence of WLAN and Bluetooth piconets in the ISM band have focused on the packet collision and associated link throughput in ad-hoc and access-point network topology models [66, 85, 124, 139, 156]. El-Hoiydi [43] simplified the computation of the probability of packet collisions between synchronous (SCO) and asynchronous (ACL) Bluetooth piconets by introducing the duty factors of the traffic links. Many analytical

models on the mutual interference among multiple collocated piconets carrying SCO/ACL traffic have been documented in literature [33, 80, 127, 155].

2.4 CCI and Channel Capacity in MIMO Systems

2.4.1 Channel State Information (CSI) and Power Allocation

In wireless communications, achieving a higher data rate is a challenging task for power and bandwidth limited systems. Recent researches in information theory showed that the capacity of a MIMO system depends on the number of transmit/receive antennas and the correlation between the channel coefficients of individual paths, and the capacity can be achieved by using a proper power allocation scheme over the transmit antennas [51,147]. The power allocation by a water-filling algorithm is known capacity-optimum when transmitters know CSI, while the equal power distribution is an alternative solution if CSI is not available at the transmitters [52, 106]. In a system having a single-user link on M transmit and N receive antennas ($M \leq N$), the mutual information of the MIMO channels is [34, 134]

$$\mathcal{I} = \log_2 \det(\mathbf{H}^H \mathbf{H} \mathbf{\Phi} + \mathbf{I}_M) \tag{5}$$

where $\mathbf{H}$, $\mathbf{\Phi} = E\{\mathbf{s}\mathbf{s}^H\}$, and $\mathbf{I}$ are the channel matrix, the covariance matrix of the transmitted signals $\mathbf{s}$, and an identity matrix, respectively. The random matrix $\mathbf{W} = \mathbf{H}^H \mathbf{H}$ has a $Wishart$ distribution, and the distribution of the eigenvalues and condition numbers of $\mathbf{W}$ is well explained in [42]. The parallel eigenmodes, which are represented with eigenvalues and corresponding allocated powers, can be modelled as multiple pipes with different diameters and corresponding amount of liquids running through them. When the CSI is available at transmitters, the channel capacity is achieved with water-filling method by choosing $\mathbf{\Phi}$ to maximize the mutual information with the power constraints $\mathrm{tr}(\mathbf{\Phi}) \leq P_T$ [34].

In contrast, if no CSI is available at transmitters, Foschini [52] showed that the equal power allocation scheme achieves the capacity. Considering the capacity achieved by water-filling method, the equal-power allocation method is suboptimum, but this is the only practical solution available if no CSI is available at the transmitters.

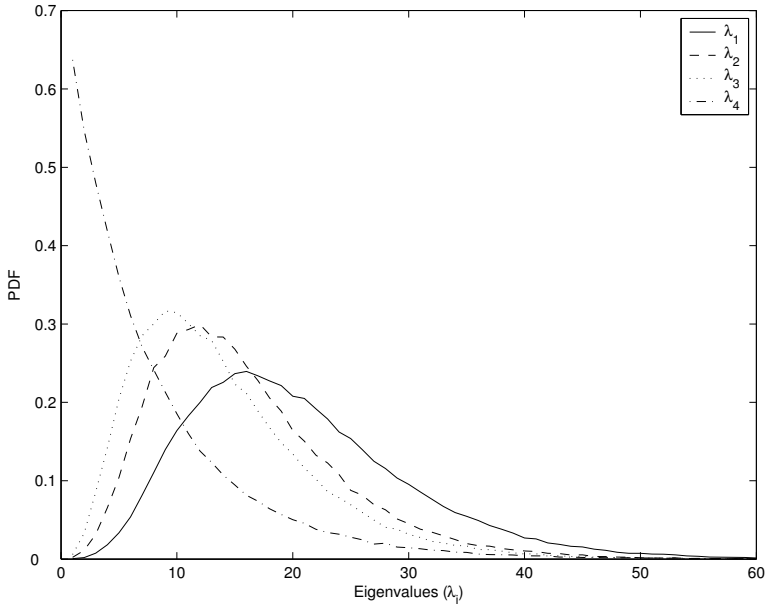

Figure 5: PDF of eigenvalues in MIMO systems: SNR = 30 dB, SIR = 10 dB, and $M = N = 4$.

2.4.2 Antenna Subset Selection in MIMO Systems

From the previous studies, rank deficiency or eigenmode imbalance in channel matrix has been observed as illustrated in Figure 5. These phenomena waste the power allocated to the eigenmodes with small eigenvalues of $\lambda_2, \ldots, \lambda_M$ when $\lambda_1 \gg \lambda_2, \ldots, \lambda_M$ in equal-power allocation scheme [74, 120]. To reduce the waste, transmission of signals through a selected antenna subset has been investigated [22,24,57,69,70]. Another advantage of subset antenna transmission/reception is the reduction of cost and complexity in transmter/receiver designs by employing a small number of expensive RF chains while utilizing a large number of less expensive antenna elements for increased diversity. For systems having more antennas at the transmitters than at the receivers ($M \geq N$), Banister and Zeidler [22] proposed a subspace tracking technique by shrinking the rank of the channel matrix over which power is equally allocated. However, this approach requires a complex subspace tracking algorithm, and the gain is negligible if $M \leq N$. Gore *et al.* [69] proposed norm based selection and incremental subset selection techniques for MMSE receivers. The authors also suggested a use of inverted transmit correlation matrix in transmit antenna selection for ZF receivers [68]. Gorokhov *et al.* [70] showed that decoupled selection of transmit and receive antenna subset achieves the

advantage of full diversity with reduced complexity. Gaur *et al.* [57] proposed a unified framework on antenna subset selection at transmitter/receiver for ZF and MMSE receivers which can be applicable to multiuser detection in the presence of co-channel interference. For 2×2 MIMO systems, Payaro *et al.* [111] proposed a switching-mode power allocation method. The switching between the modes of equal-power-allocation and all-power-over-one-antenna is controlled by the decision metric computed from the modulus of the complex channel coefficients and the trace of the covariance matrix of the signal vector.

For ad-hoc MIMO links, interference from adjacent MIMO links has been an obstacle to throughput enhancement. Park *et al.* [107] proposed a MAC protocol for throughput improvements by using antenna selection and space-time coding at transmitters. Demirkol and Ingram [36] proposed an algorithm controlling the number of transmit antennas in each transmitter to maximize the throughput of ad-hoc networks. Gaur *et al.*'s work [58] showed a middle-path approach providing a trade-off between the feedback signaling load and the network throughput performance. Also, adaptive modulation and bit loading techniques combined with non-equal power distribution methods have been investigated in contexts of link capacity [61, 74].

2.4.3 Space-Time MIMO Signalling

To realize the potential capacity of MIMO systems, several space-time MIMO signalling techniques and associated receiver designs have been proposed [14,60,110,129,133]. Figure 6 shows a schematic of a space-time MIMO system. Space-time MIMO signalling techniques can be categorized into two groups: space-time diversity coding (STDC) and spatial multiplexing (SM). The two types of space-time MIMO signallings are distinguished by the spatial code rate $r_s = K/T$, where K is the number of data symbols transmitted during T symbol periods: $r_s < 1$ (STDC) and $r_s = M$ (SM).

The STDC techniques extract the maximum available spatial diversity in the MIMO channels through appropriate construction of the transmitted space-time codewords: *precoding*. One example of space-time diversity coding is Alamouti scheme applied to two transmit antennas and any number of receiver antennas [14]. Alamouti scheme extracts

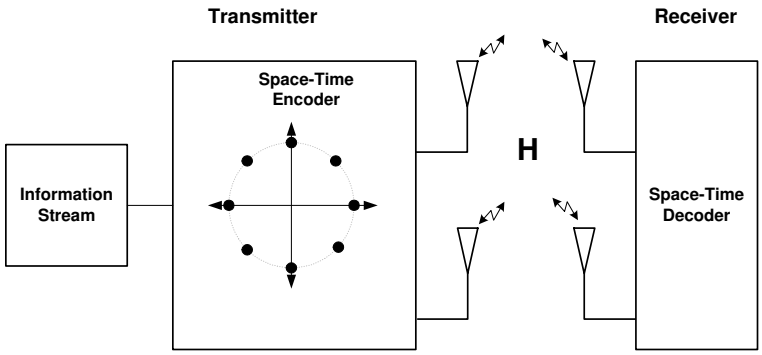

Figure 6: A schematic of a space-time MIMO system model.

$2N$th-order diversity gain with N receive antennas and can be extended to channels with more than two transmit antennas through the orthogonal space-time block coding (OSTBC) with low decoding complexity [132]. However, STDC signalling suffers capacity losses because of the small spatial code rate ($r_s < 1$). Another example of space-time diversity coding is the delay diversity which converts spatial diversity into frequency diversity by transmitting the data symbols from the first antenna and a delayed replica of that from the the second antenna [121]. The effective channel impulse response seen by the data symbols is a symbol spaced two-path SISO channel with independent fading paths and equal average path energy.

In spatial multiplexing, instead of maximizing the spatial diversity, the transmission rate is maximized by sending M independent data symbols per symbol period from M transmit antennas. By doing so, spatial multiplexing achieves a large spatial code rate $r_s = M$. For the transmission of M-symbol information streams, *horizontal*, *vertical* and *diagonal encoding* (HE, VE, and DE) schemes are employed by using different spatial multiplexing schemes [110].

2.4.4 Receiver Structures for Space-Time MIMO Systems

In space-time diversity coded systems, the orthogonality between the codes decouples the vector detection problem into scalar detections [132]. Hence, zero-forcing (ZF), minimum-mean square error estimation (MMSE), and ML sequence estimation (MLSE) type receivers

can be directly applied [110]. For the space-time trellis coded (STTC) systems, a Viterbi-type sequence estimator should be used [133].

In spatially multiplexed systems, the receiver design faces the problem of mutual interference between spatially multiplex information streams. Accordingly, there exists an analogy between multiuser detection (MUD) and the decoding of spatially multiplexed systems in terms of the complexity-performance tradeoff. The ML receiver performs vector decoding and is optimal in the sense of the error probability. A drawback of the ML type receiver design is the decoding complexity, which grows exponentially with the alphabet size and number of transmit antennas [144]. The complexity of ML decoding can be reduced by employing linear receiver front-ends [23]. One simple realization of the linear receivers is the ZF receiver which converts the joint decoding problem into M single stream decoding problems. The noise enhancement in ZF receivers can be reduced in MMSE type receivers by including the noise term in the front-end weight function. The MMSE receiver approaches the matched-filter receiver and the ZF receiver at low-SNR and high-SNR regions, respectively [110].

The nonlinear BLAST type MIMO systems are based on the idea of successive cancellation in MIMO system where each individual data stream is successively decoded and stripped away from the received data set for the reduced-interference decoding of the remaining data streams [51, 147]. For diagonally encoded systems (D-BLAST), the order of successive decoding is determined by the transmission structure while the received SINR determines the decoding order in vertically encoded systems (V-BLAST). MMSE and ZF type decoders can be used for the detection of chosen data symbols. The weight matrix for the decoding of i-th stage data streams is computed from the modified channel matrix with zeros in $1, \ldots, i-1$ of the columns [147].

CHAPTER III

INTERFERENCE MITIGATION IN ASYNCHRONOUS SLOW FREQUENCY HOPPING BLUETOOTH NETWORKS

3.1 Introduction

The Bluetooth system was developed for operation in the 2.4 GHz unlicensed ISM band. The slow frequency hopping (SFH) spread spectrum technique used in the Bluetooth system mitigates interference from other Bluetooth networks and other sources of interference by randomly hopping over a 79 MHz band with subcarriers spaced 1 MHz apart. However, as the number of Bluetooth piconets in the same location increases, the probability of packet collision increases since the orthogonality between the hopping sequence is not guaranteed if the piconets are asynchronous. Previous studies have provided initial steps on the analysis of packet error rate (PER) and throughput performance of multiple co-located Bluetooth piconets [43,66]. However, these previous studies consider neither an interference cancelling receiver nor the capture effect on slowly faded indoor channel.

In this study, we propose an interference cancelling dual decision-feedback (IC-DDF) receiver which is designed to mitigate the interference from multiple Bluetooth piconets by jointly detecting two co-channel signals with a single antenna. The joint detection scheme significantly reduces the packet error rate in the presence of severe packet collisions where most collisions involve only two packets. To estimate and track the channel parameters of two co-channel signals, a simplified recursive least squares (RLS) type adaptive channel parameter estimator is proposed. The computing burden of the covariance update routine in RLS algorithm is largely reduced by adopting a constant covariance matrix. The IC-DDF receiver achieves large gain over the conventional discriminator type receiver especially in a low CIR range. The bit error rate (BER) performance of the IC-DDF receiver is evaluated

by computer simulations for indoor fading channels [82, 150].

Also, we propose a novel system level performance evaluation method for interference cancelling receiver in the presence of heavy packet collisions. PER typically represents the performance of a system in wireless packet communications. In conventional methods, PER is determined by BER performance and error correction coding of the receiver subsystem as well as the characteristics of the propagation channels [25, 154]. Otherwise, the PER computed from purely medium access control(MAC) layer parameters such as probability of packet collision [25, 92]. However, those approaches considering parameters in separate ways can not evaluate the realistic performance of a receiver having interference cancelling capability. In the proposed method, we evaluate the system level performance by integrating the BER performance of the receiver into an interference-traffic driven CIR statistics. This approach properly assess the throughput of overall links in the presence of large packet collisions. Also, a generalized packet collision probability with variable length packets of mixed traffic is derived.

This chapter is organized as follows. Section 3.2 describe the structure of the maximum-likelihood (ML) type IC-DDF receiver which jointly detects two colliding Bluetooth packets. In support of selecting two-user joint detection structure, we showed that the majority of the packet collisions involve only two packets in multiple piconet environments. In Section 3.3, a novel method of computing PER of the IC-DDF receiver in interference dominant channel is derived. To take account into the effect of interference traffic in PER, the pdf of CIR is computed by using interference traffic distribution and path-loss formula for typical indoor radio channel models. Also, the generalized packet collision probabilities of multiple collocated Bluetooth piconets are derived for three different mixed traffic portfolios. The performance of the IC-DDF receiver and the novel PER computation method are evaluated by computer simulation, and the numerical results are discussed in Section 3.4.

3.2 *Signal and Interference Model for Asynchronous SFH Bluetooth Networks*

The Bluetooth system is designed to provide simple and robust short-range high-data-rate physical layer transmission as an alternative to existing various wires for data transmission between computer and communication peripherals, and is designed to operate in 2.4 GHz ISM band. Bluetooth is an ad-hoc network that does not have centralized control channels for medium access and broadcasting purpose. As a result, multiple Bluetooth piconets can be collocated in small area with various types of traffic links as shown in Figure 7. Instead, each Bluetooth piconet avoids interference from each other by randomly hopping over 78 carriers independently and asynchronously. Therefore, when packets from two or more piconets collides, they behaves as CCI to each other with large power very likely.

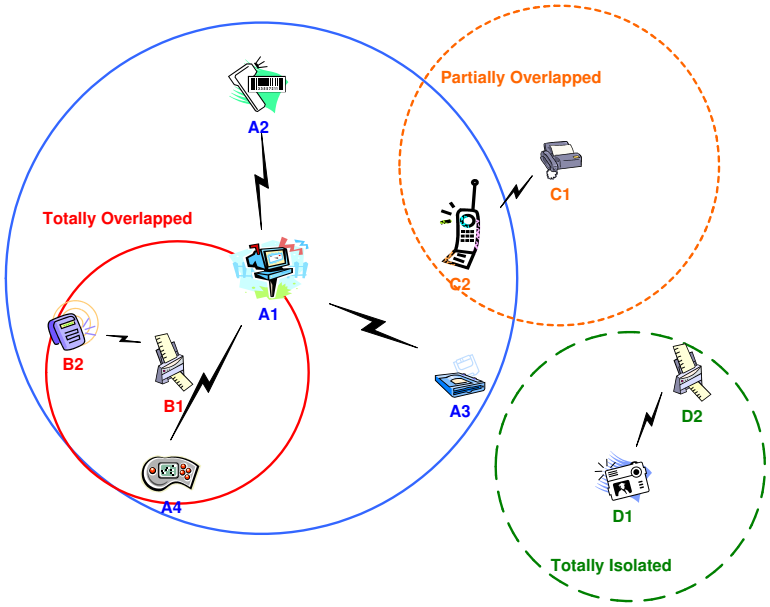

Figure 7: Bluetooth piconet topology.

3.2.1 Signal Model of Bluetooth System

Gaussian filtered FSK (GFSK) modulation gives high immunity to adjacent channel interference (ACI) and narrow channel bandwidth. The Bluetooth passband signal $r_p(t)$ has the form

$$r_p(t) = \sqrt{2P}\cos(\omega_c t + \theta(t)) \tag{6}$$

where P is the signal power, $\omega_c = 2\pi f_c$ is the angular frequency, and

$$\theta(t) = 2\pi h \int_{-\infty}^{t} \sum_{i=-\infty}^{\infty} s_i g(\tau - iT) d\tau \tag{7}$$

where the $s_i \in \{\pm 1\}$ are binary data symbols, h is the modulation index, T is the symbol duration, and $g(t)$ is the response of a Gaussian low-pass filter to a rectangular pulse of duration T. The Gaussian shaping pulse is

$$g(t) = \frac{1}{2T}\left[Q\left(2\pi B_g T \frac{-t}{T\sqrt{\ln 2}}\right) - Q\left(2\pi B_g T \frac{(-t+T)}{T\sqrt{\ln 2}}\right)\right] \tag{8}$$

where $Q(\cdot)$ is the normalized cumulative normal distribution, and $B_g T$ is the normalized 3 dB bandwidth of the Gaussian low-pass filter. In Bluetooth, a small modulation index of $0.28 < h < 0.35$ and a normalized bandwidth of $B_g T = 0.5$ are used. Since the Gaussian shaping pulse is longer than the baud duration, intersymbol interference (ISI) is introduced, but the GFSK pulse also gives the advantage of lower side lobes in the frequency domain than other modulation schemes.

Bluetooth receivers usually employ a low-cost noncoherent frequency discriminator receiver. The frequency discriminator consists of a differentiator followed by an envelope detector, and its output is proportional to baseband signal $r(t)$ [128]. The received complex baseband equivalent signal at the output of the frequency discriminator is

$$\begin{aligned} r(t) &= \sum_{i=-\infty}^{\infty} s_i g(t - iT) h(t - iT - \tau) + n(t) \\ &= \sum_{i=-\infty}^{\infty} a(t) s_i g(t - iT - \tau) + n(t). \end{aligned} \tag{9}$$

where $h(t) = a(t)\delta(t)$ is the channel impulse response with the assumption of flat fading over each subbands. Under the condition of high carrier-to-noise ratio, the additive narrow-band noise, $n(t)$, can be written as

$$n(t) = \frac{1}{2\pi A_c} \frac{dn_Q(t)}{dt} \tag{10}$$

where A_c is the carrier amplitude and $n_Q(t)$ is the quadrature component of complex Gaussian noise having zero mean and power spectral density N_0. The corresponding power

spectral density of $n(t)$ is

$$S_N(f) = \begin{cases} \frac{N_0 f^2}{A_c^2}, & |f| \leq \frac{B}{2} \\ 0, & \text{elsewhere} \end{cases} \tag{11}$$

where B is the bandwidth of an ideal IF filter.

3.2.2 Channel and Co-channel Interference Model

From the results of previous studies, the Rician fading model with K factor ranging from 1.3 to 8.7 and the Doppler frequency f_D less than 10 Hz is fit for the channel measurements data of the stationary or slowly moving pedestrian traffic that is typical of an indoor environment [145]. The delay spread less than 100 ns with the median value under 50 ns implies that the channel coherence bandwidth ranges from 10 to 100 MHz, and each 1-MHz subband of a SFH Bluetooth signal can be assumed to experience flat fading [83, 90].

In asynchronous SFH packet communication systems, a fraction of a packet from one communication link may fall into the time-limited observation window of another communication link. For the simplicity of modelling, only 1 interfering signal is assumed to present, and the desired and interfering packets have lengths L and N symbols, respectively. The no-collision time offset T_{NC} of $JT + \tau$ where $-L + 1 < J < L - 1$ is shown in Figure 8.

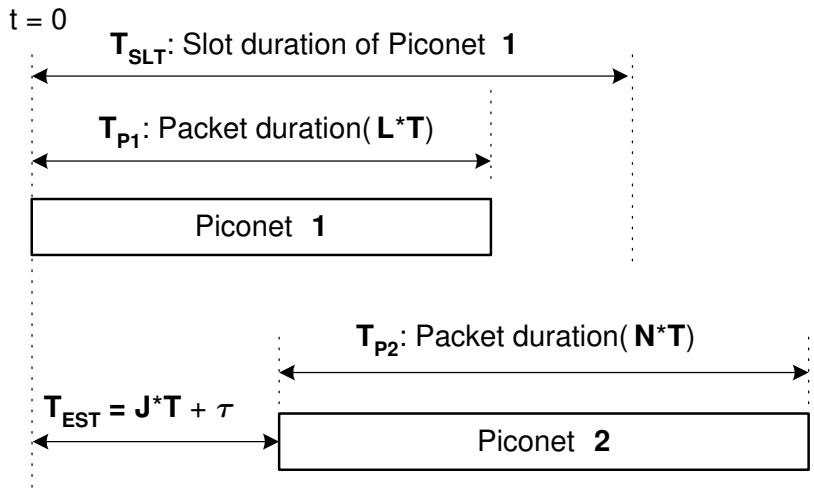

Figure 8: Collision of asynchronous multiple piconets.

With given desired signal's symbol timing information, the received signal sampled at

kth symbol timing epoch is

$$\begin{aligned} r(k) &= \sum_{i=0}^{L-1} s_{1,i} a_1(kT) g((k-i)T) u_{LT}(t) \\ &+ \sum_{i=0}^{N-1} s_{2,i+J} a_2(kT) g((k-i+\tau)T) u_{NT}(t-(J+\tau)T) u_{LT}(t) + n(kT) \end{aligned} \quad (12)$$

where $u_{LT}(t)$ and $u_{NT}(t)$ are unit step functions of length LT and NT, respectively. This can be rewritten in the vector form

$$r(k) = \mathbf{s}_1^T \mathbf{A}_1 \mathbf{g}_{1k} + \mathbf{s}_2^T \mathbf{A}_2 \mathbf{g}_{2k} + n(kT). \quad (13)$$

The $\mathbf{s}_i$ and $\mathbf{g}_{ik}$ are symbol sequences and shaping pulse coefficient vectors of desired (i=1) and interfering (i=2) signals. Also, $\mathbf{A}_1$ and $\mathbf{A}_2$ are diagonal matrices of fading coefficients with length L and N for the desired and interfering signals, respectively. The intra-symbol time offset, τ, between the desired and interfering packet determines the sampling instance of the shaping pulse of the interfering signal.

3.2.3 IC-DDF Maximal Likelihood (ML) Receiver

Interference cancelling receivers with channel parameter estimation algorithms have been proposed to mitigate co-channel interference in TDMA communication systems [54]- [150]. In this study, a frequency discriminator concatenated with an interference cancelling dual decision feedback (IC-DDF) function block is proposed as shown in Figure 9 [87].

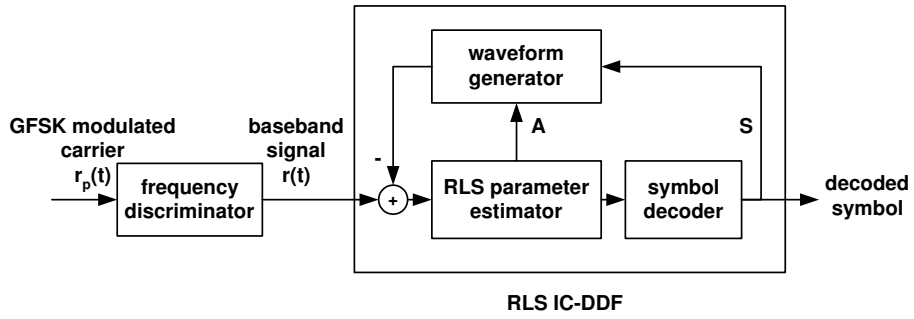

Figure 9: Function blocks of interference cancelling dual decision feedback receiver.

The IC-DDF receiver regenerates an estimate of the received waveform using an estimated data symbols and fading coefficients at every time index. The postcursor part of

estimated signal is subtracted from the received signal to reduce the estimation error in the truncated decision metric for the maximum likelihood receiver. The symbol vector $\mathbf{s}(i) = [s_{1,i}, s_{2,i}]^T$ is estimated at every symbol interval in a ML manner and the diagonal matrix of fading coefficients $\mathbf{A}(k)$ is updated at every symbol interval by using a recursive approach. Assuming that an interfering packet has collided with the desired packet before the kth symbol, the conditional PDF of the received signal $r_{IC}(k)$ at the input to the IC-DDF ML receiver with pth estimated symbol pair, for $p \in \{1, 2, 3, 4\}$, is [150]

$$p(r_{IC}(k)|\mathbf{s}_p(k), \mathbf{A}_p(k)) = \frac{1}{\pi N_o(1 + E_p(k))} \exp\left\{-\frac{1}{N_o(1 + E_p(k))} |e_p(k)|^2\right\} \tag{14}$$

where

$$r_{IC}(k) = r(k) - \sum_{i=0}^{k-1} s_{1,i} a_1(kT) g((k-i)T) - \sum_{i=0}^{k-1} s_{2,i+J} a_2(kT) g((k-i+\tau)T) \tag{15}$$

$$e_p(k) = r_{IC}(k) - \tilde{r}_p(k) \tag{16}$$

$$\tilde{r}_p(k) = \mathbf{s}_p^T(k) \mathbf{A}_p(k) \mathbf{g}_0 \tag{17}$$

$$E_p(k) = \mathbf{s}_p^T(k) \mathbf{P}_p(k|k-1) \mathbf{s}_p(k). \tag{18}$$

The variables in (14) to (18) are listed in Table 3. The normalized covariance matrix of $\mathbf{a}_p(k)$, $\mathbf{P}_p(k|k-1)$, is

$$\mathbf{P}_p(k|k-1) = (\mathbf{A}_p(k) - \langle \mathbf{A}(k|k-1) \rangle) \cdot (\mathbf{A}_p(k) - \langle \mathbf{A}(k|k-1) \rangle)^T / N_o \tag{19}$$

where $\langle \mathbf{A}(k|k-1) \rangle$ is an *a priori* average of the fading coefficients from the 0 to the $(k-1)$th symbols given $\mathbf{s}(k-1)$ and $r_{IC}(k-1)$. With the modified received signal $r_{IC}(k)$, the estimation error $e_p(k)$ is free from the energy of the previous $k-1$ symbols if the estimation of previous symbols and fading coefficients are correct. The equivalent log-likelihood decision metric for IC-DDF ML estimator is

$$\mu(\mathbf{s}_p(k)) = -|e_p(k)|^2 . \tag{20}$$

Table 3: Variables for ML IC-DDF receiver

Variable	Description
$\mathbf{s}_p(k) = [s_{1p,k}, s_{2p,k}]^T$	the pth estimated symbol pair vector at time index k
$\mathbf{A}_p(k) = \begin{bmatrix} a_{1p}(k) & 0 \\ 0 & a_{2p}(k) \end{bmatrix}$	diagonal matrix of fading coefficients for $\mathbf{s}_p(k)$
$\mathbf{g}_0 = [g(0), g(\tau)]^T$	shaping pulse coefficients sample vector for $\mathbf{s}_p(k)$
$e_p(k)$	estimation error for $\mathbf{s}_p(k)$
$1 + E_p(k)$	normalized covariance of $e_p(k)$

3.2.4 Simplified RLS Channel Estimation

To estimate symbols and generate a replica of the received signal for the IC-DDF receiver, the fading coefficient matrix, $\mathbf{A}(k)$, must be estimated precisely. Fukawa *et al.* [54] used Recursive Least Squares (RLS) method to estimate the fading coefficient matrix. In this study, with random walk model, $\mathbf{A}(k)$ at time index k given $\mathbf{A}(k-1)$ is updated by constant covariance matrix $\mathbf{P}_0$, estimation error $e(k)$ and estimated symbols $\mathbf{s}(k)$

$$\mathbf{A}(k) = \mathbf{A}(k-1) + \mathbf{P}_0 \mathbf{s}(k) e(k). \tag{21}$$

$\mathbf{P}_0$ is calculated from the no-collision section T_{NC}, available at either the beginning or end of the packet as shown in Figure 8.

$$\mathbf{P}_0 = \delta^{-1} \begin{bmatrix} P_{NC} & 0 \\ 0 & \frac{1}{\lambda_0} P_{NC} \end{bmatrix} \tag{22}$$

where λ_0 is the estimated CIR, δ is a small positive integer, and P_{NC} is the normalized constant variance of the fading coefficients in T_{NC}, given by

$$P_{NC} = \langle (\mathbf{a}_{NC} - \langle \mathbf{a}_{NC} \rangle)^2 \rangle / N_o. \tag{23}$$

The computation of the constant covariance matrix $\mathbf{P}_0$ requires neither complex computation such as matrix inversions nor updates at every symbol interval.

3.3 Analysis of System Level Performance

The PER and link throughput associated with the PER have been considered as the performance measure of the packet communication systems. The previous studies have been

focused on systematic approach to measure PER under different channel impairments of multipath fading and co-channel interference [67, 92, 149, 154].

However, all those analysis based on the BER data derived from conventional receiver which has no co-channel interference cancellation capability. In this study, PER is derived by integrating BER of interference cancelling receiver with statistics of CIR as well as considering the capture effect in calculation of packet collision probability.

3.3.1 Packet Error Probability

When the multiple packets are transmitted through shared medium, the probability of packet error is defined as follows.

$$Pr(e) = Pr(e|c)Pr(c) + Pr(e|nc)Pr(nc) \tag{24}$$

where $Pr(e|c)$ is the conditional probability of packet error given collision of probability $Pr(c)$, and $Pr(e|nc)$ the conditional probability of packet error given no packet collision. Because the $Pr(e|nc)$ is very smaller than $Pr(e|c)$ in high signal-to-noise ratio condition which is very likely on short distance communication link, $Pr(e|nc)$ is assumed zero.

With given CIR and the BER of interference cancelling receiver associated with it, the PER depends on the length of the collision section in a packet, l and forward error correction (FEC) function of the packet. Thus, the probability of packet error in (24) can be derived from double integration of conditional probability of packet error (CPPE) with $l = m$ and $\Lambda = \lambda$

$$E[Pr(e)] = Pr(c) \int_{R_l} \int_{R_\Lambda} Pr(e|\lambda, m) f_l(m|c) f_\Lambda(\lambda) d\lambda dm \tag{25}$$

where $f_\Lambda(\lambda)$ and $f_l(m|c)$ are the PDF of the average received CIR and the conditional PDF of collision length given collision, respectively. Since the time offset T_{NC} is uniformly distributed over T_{SLTS}, $f_l(m|c)$ is

$$f_l(m|c) = \frac{1}{T_{SLTS}} \quad \text{for} \quad m \in [0, T_{SLTS}]. \tag{26}$$

The PDF of CIR, $f_\Lambda(\lambda)$ is derived from geometric arguments. Since the CIR is a function of the path loss statistics and the relative distances from the intended receiver to the desired

and interfering transmitters, $f_\Lambda(\lambda)$ can be written as

$$f_\Lambda(\lambda) = \int_{R_{r_d}} f_\Lambda(\lambda|\sigma) f_{r_d}(\sigma) d\sigma \tag{27}$$

where $f_{r_d}(\sigma)$ is the PDF of the distance from the desired transmitter to the receiver,r_d, and $f_\Lambda(\lambda|\sigma)$ is the conditional PDF of CIR given r_d. Assuming that the intended receiver is located at the center of the cell and the desired and interfering transmitters are uniformly distributed over the piconet, $f_{r_d}(\sigma)$ is derived by following method. The probability that desired transmitter is located in the annular ring defined by $r_i < \sigma < r_o$ is

$$Pr(r_i < \sigma < r_o) \triangleq \frac{\text{area of } r_i < \sigma < r_o}{\text{total cell area}} = \frac{r_o^2 - r_i^2}{R^2} \tag{28}$$

where R is the radius of a piconet cell. The path-loss equation from a previous study used in derivation of $f_\Lambda(\lambda|\sigma)$ [83]. The received power at distance d is

$$P_{RX}(d) = P_0 + 10a \log_{10}(d). \tag{29}$$

where d is in meter, P_0 is the path loss at 1 m distance, and a is the path loss exponent. The measured value of P_0 is 43.1 dB at 2.4 GHz, and the measured values of a are 1.86 and 3.33 for LOS (line-of-sight) and OBS (obstructed) channels, respectively. Figure 10 shows the cumulative distribution functions (CDF) of CIR computed from (27)-(29) with different visibility indices between transmitters and receivers.

An example of distribution of CIR of a typical frequency reuse cellular system is given for comparison. Unlike the Bluetooth piconets, the frequency reuse scheme of conventional cellular systems shifts the distribution to the right. As a result, the average received CIR is located between 10 to 20 dB range. The CPPE given $\Lambda = \lambda$ and $l = m$ is

$$Pr(e|\lambda, m) = 1 - \left[\sum_{i=0}^{N_e} \binom{N_B}{i} (\rho_b(\lambda))^i (1-\rho_b(\lambda))^{N_B - i}\right]^{N_m} (1-\rho_b(\lambda))^{N_R} \tag{30}$$

where $\rho_b(\lambda)$ is the BER at $\Lambda = \lambda$, and N_e is the maximum number of bit errors allowed in one FEC block of length N_B. The length of collision section m and N_B decide the number of FEC blocks, N_m, and residual bits, N_R, in the collision section of a packet

$$N_m = \left\lfloor \frac{m}{N_B} \right\rfloor \tag{31}$$

$$N_R = m - N_B N_m. \tag{32}$$

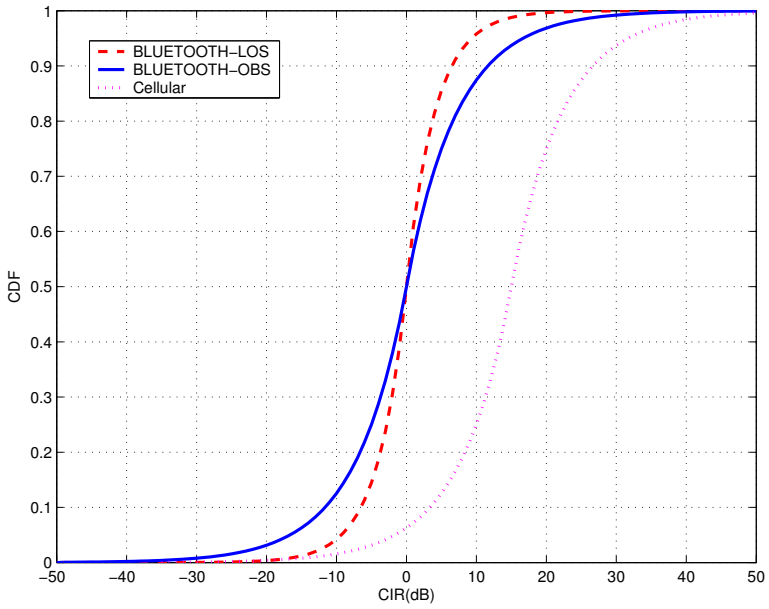

Figure 10: CDF of received CIR .

3.3.2 Packet Collision in Asynchronous Multiple piconets

With N_T active co-located piconets, $Pr(nc|N_T) = 1 - Pr(c|N_T)$ is the probability that a packet does not collide with any other packets where $Pr(c|N_T)$ is the probability that a packet collides with other packets. To simplify the analysis, all N_S SCO piconets and N_A ACL piconets are assumed to have packet lengths T_{SCO} and T_{ACL}, respectively. With this assumption, $Pr(nc|N_S + N_A)$ is

$$Pr(nc|N_S + N_A) = \frac{1}{N_S + N_A} \left(N_S (\rho_{nc}^{S})^{N_S - 1} (\rho_{nc}^{S,A})^{N_A} + N_A (\rho_{nc}^{A})^{N_A - 1} (\rho_{nc}^{S,A})^{N_S} \right) \qquad (33)$$

where ρ_{nc}^{S}, $\rho_{nc}^{S,A}$ and ρ_{nc}^{A} are the probabilities of no packet collision for two piconets of SCO-SCO, SCO-ACL and ACL-ACL links, respectively, as shown in Figure 11(a)-(c). The shaded areas of Figure 11 illustrates collision sections in piconets of different packet sizes and random time offsets.

3.3.2.1 Collision between packets from two SCO piconet links

In recent study, El-Hoiydi derived the packet error rate of SCO piconets which transmit packets in regular intervals [43]. As shown in Figure 11(a), the probability of no packet

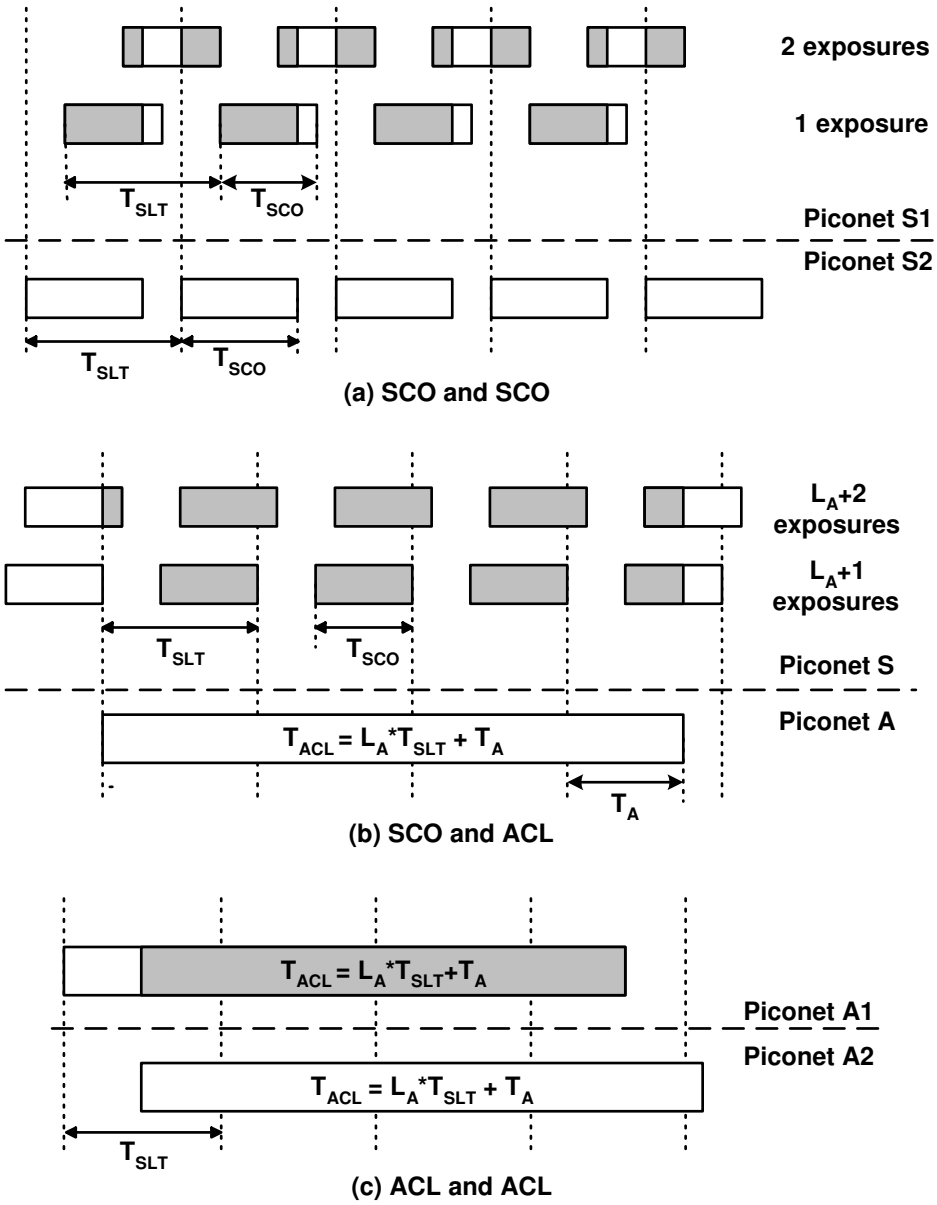

Figure 11: Packet collision diagrams of three different traffic portfolios; (a) SCO and SCO links , (b) SCO and ACL links, and (c) ACL and ACL links.

collision on one SCO link in the presence of another SCO link is

$$\rho_{nc}^{S} = 2(1 - r_s)\left(\frac{78}{79}\right) + (2r_s - 1)\left(\frac{78}{79}\right)^2 \tag{34}$$

where $r_s = T_{SCO}/T_{SLT}$ is the duty cycle of each packet where T_{SLT} and T_{SCO} is the 1-slot duration time of 625μ seconds and packet duration time of SCO link, respectively.

3.3.2.2 Collision between packets from SCO and ACL piconet links

When piconets carry both SCO and ACL traffic, length of ACL packet affects the probability of packet collision. The traffic on the ACL link varies with activity factor ϵ, $0 \leq \epsilon \leq 1$, which is defined as the total time of packet transmission to total time of link transaction session. With ACL packet of length $T_{ACL} = L_A T_{SLT} + T_A$ and SCO packet of length T_{SCO}, the probability of no packet collision is as follows:

$$\rho_{nc}^{S,A} = 2(1 - r_{s,a})\left(\frac{79 - \epsilon}{79}\right)^{L_A+1} + (2r_{s,a} - 1)\left(\frac{79 - \epsilon}{79}\right)^{L_A+2} \tag{35}$$

where $r_{s,a} = T_{SCO}/T_{SLT} = T_A/T_{SLT}$.

3.3.2.3 Collision between packets from two ACL piconet links

ACL links do not transmit packets in regular intervals, but the packet is longer than SCO link packet. To simplify the analysis of the probability of no packet collision of ACL packets, the ACL link is assumed to send its packet in an interval long enough so that a packet from one piconet does not collide with two consecutive packets from the other piconet. If the packets from piconets A1 and A2 have the same length $T_{ACL} = L_A T_{SLT} + T_A$, then probability of no packet collision is as follows:

$$\rho_{nc}^{A} = \left(\frac{79 - \epsilon}{79}\right)^{2L_A+2r_a-1} \tag{36}$$

where $r_a = T_A/T_{SLT}$.

3.3.3 Capture Effect and Multiple Packet Collision

Most receivers capture the stronger of two signals, provided that the ratio of its power to that of the weaker signal exceeds a given threshold, which is called capture ratio, $R = P_d/P_i$, where P_d and P_i are power of desired and interfering signal respectively. R value changes

from 1 to ∞. In this study, the capture effect is used to explain the relationship between the probability of packet collision $Pr(c)$ and number of interference used in the simulation. With N_T actively transmitting piconets, $Pr(c)$ can be rewritten as a function of number of interferers as follows

$$Pr(c) = Pr(c|i=1)Pr(i=1) + \sum_{j=2}^{N_T} Pr(c|i=j)Pr(i=j) \tag{37}$$

where $Pr(c|i=k)$ and $Pr(i=k)$ are the probability of packet collision given k interferers and the probability of presence of k interferers, respectively. When we apply the capture effect on multiple interferers, $Pr(i=1)$ goes to 1 as the capture ratio R approaches to 1, i.e, only one strongest interferer presents at receiver front end of IC-DDF receiver. Thus, it can be claimed that the system level performance analyzed in previous sessions with (33) and given BER statistics is the upper bound of the IC-DDF receiver's performance.

The probability of n different packets from a total of N_T piconets simultaneously hitting one time slot is $\binom{N_T}{n}(1/79)^n(78/79)^{N_T-n}$. The ratio of the probability of a single packet collision to the total packet collision probability can be evaluated as

$$\frac{Pr(c|N_I=1)}{Pr(c|N_I<N_T)} = \frac{\binom{N_T}{1}\left(\frac{1}{79}\right)^1\left(\frac{78}{79}\right)^{N_T-1}}{\sum_{N_I=1}^{N_T-1}\binom{N_T}{N_I}\left(\frac{1}{79}\right)^{N_I}\left(\frac{78}{79}\right)^{N_T-N_I}} \tag{38}$$

where N_I is the number of interfering packets that collides with the desired packet. In Figure 12, the contributions from one ($N_I=1$) and one-plus-two ($N_I=2$) packet collisions are illustrated. The contribution from the single packet collisions to the total packet collision probability is 91% at $N_T=15$, and remains over 82% even at $N_T=35$. Furthermore, the contribution from one-plus-two packet collision is remains dominant even in the region where N_T is greater than 50. When two interfering packets collide with the desired packet, the interfering packets will overlap with each other. In addition, by the capture effect discussed in a previous section, it is likely that the two interfering packets overlapped on the desired packet will be seen as a single interferer. Therefore, only collisions from one interfering packet at a time are considered in the sequel, although the results obtain may be slightly optimistic.

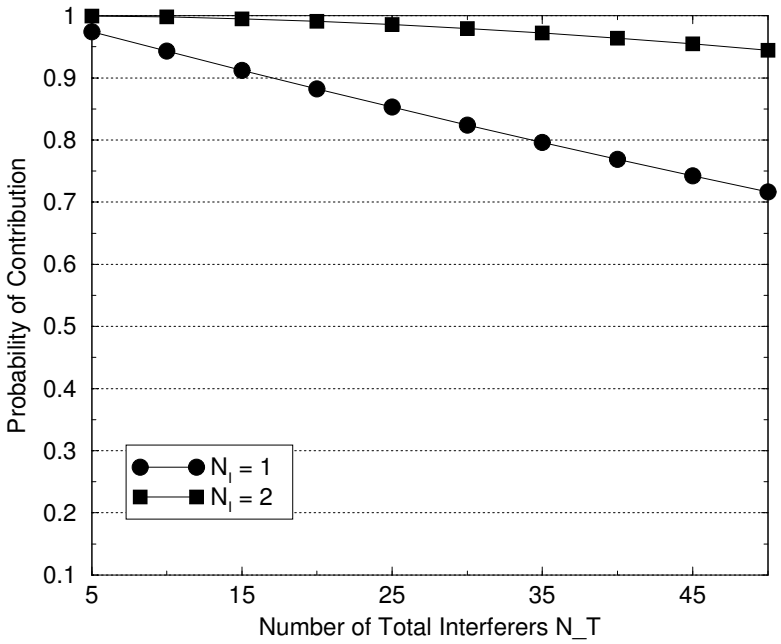

Figure 12: Contributions from one and one-plus-two packet collisions to the total packet collision probability; $N_I = 1$: one packet collision; $N_I = 2$: one-plus-two packet collisions.

3.4 Numerical Results

3.4.1 BER Performance of IC-DDF Receiver

Since the channel changes very slowly compared to baud interval, the change of variance P_{NC} is negligible as the length of T_{NC} changes. Thus, the length of T_{NC} is fixed at 72 symbols for all simulation runs. The intra-symbol time offset τ is known to affect the BER performance of receiver [150]. To minimize the effect of intra-symbol time offset, the BER performance is obtained at every possible time offset τ and averaged to get the overall BER performance. To evaluate the performance of the IC-DDF receiver, computer simulations with different CIR, E_b/N_0 and Doppler frequency f_D are carried out. Table 4 shows the set of conditions for computer simulation. Rayleigh faded signals are generated by Jakes' sum-of-sinusoids method [82].

The BER performance of the IC-DDF receiver for a Rayleigh faded channel with 10 Hz Doppler frequency is compared to that of the conventional frequency discriminator receiver in Figure 13. In the CIR range-of-interest from -12 to 12 dB, a BER of 10^{-2} to 10^{-3} is achieved except at CIR of 0 dB. The exceptionally high BER at 0 dB CIR results from the

Table 4: IC-DDF BER simulation setup

Parameters	Value
Frequency band	2.45 GHz ISM band
Packet type	DM3(1000 bits)
No. of interferers	1
Modulation format	GFSK
Normalized BW(BT)	0.5
Modulation symbol rate	1 Msps
Maximum Doppler frequency(f_D)	10 Hz
Rician coefficient(K)	0 - 8
CIR range	-12 to 12 dB
Modulation index	0.35
Channel model	independent flat fading on 79 1-MHz subband

ambiguity of the ML decision between (1,-1) and (-1,1) pairs. For the CIR range from 2 to 12 dB, the BER has a floor due to channel estimation errors. No significant decrease of BER observed when the E_b/N_o increases from 20 to 30 dB, since the channel estimation error dominates the performance of ML detector. To further illustrate the effect of Doppler frequency on BER performance, Figure 14 plots the BER performance at 5 and 10 Hz Doppler frequencies. Since Bluetooth system experiences normalized Doppler frequency smaller than 10^{-5}, the change in Doppler frequency has little effect on BER performance. Figure 15 shows the BER performance on indoor channels for varying degrees of visibility or LOS conditions between the transmitter and receiver. The BER for high visibility (K=8) is smaller than that for low visibility (K=0) over all range of CIR.

3.4.2 System Level Performance of IC-DDF Receiver

In our example topology, the desired and interfering transmitters are assumed to be uniformly distributed within a 10 m-diameter piconet cell, where the intended receiver is located at the center of the cell. With these assumptions, CIR for a given location of the desired transmitter is calculated by (29). Path loss exponents of 1.86 and 3.33 are used for Rician K factors of 8 and 0, respectively. The packets used in simulation are summarized in Table 5 [6]. The system level performance of the IC-DDF receiver is evaluated by PER and total link throughput with various piconet combinations carrying SCO and ACL link

Table 5: WPAN packets used in system level simulation

Packet	Type	Length	Payload Error Protection	Service type
HV1	SCO	72 + 54 + 240	1/3 FEC, No CRC	64 Kbps Voice
HV2	SCO	72 + 54 + 240	2/3 FEC, No CRC	64 Kbps Voice
HV3	SCO	72 + 54 + 240	No FEC, No CRC	64 Kbps Voice
DM1	ACL	72 + 54 + 240	2/3 FEC, CRC	Data (1 slot)
DH1	ACL	72 + 54 + 240	No FEC, CRC	Data (1 slot)
DM3	ACL	72 + 54 + 2745	2/3 FEC, CRC	Data (5 slots)
DH3	ACL	72 + 54 + 2745	No FEC, CRC	Data (5 slots)

type packets with or without FEC. In the Bluetooth specification, three error correction schemes are defined, namely rate-1/3 FEC, rate-2/3 FEC, and ARQ. A simple 3-times repetition code and a $(15, 10)$ shortened Hamming code with a generator polynomial of $g(D) = (D + 1)(D^4 + D + 1)$ are used for the rate 1/3 and 2/3 FEC codes, respectively. Both codes can correct all single errors in every three and fifteen received symbols , respectively. Therefore, when the received packet contains more than one symbol error in any three or fifteen-symbol block, it is considered erroneous as in (30). For the packets that have no FEC for payload, such as HV3, only the 72-bit header section of HV3 packet is used in packet error detection. Figure 16 plots the PER of the IC-DDF receiver with different piconet links. HV1 packets of the SCO link gain more benefit from the IC-DDF receiver than HV3 packets. This implies that the IC-DDF receiver amplifies the gain achieved by FEC function. This gain increases as the packet length increases (DM3).

In Figure 17, the throughput performance of the IC-DDF receiver with mixed piconet links is plotted. With small portion of ACL traffic (10% ACL, 90% SCO), the throughput approaches that of homogeneous SCO traffic. The IC-DDF receiver gives $60 \sim 70$ % increase in throughput regardless the traffic portfolio. Also, the number of piconets at maximum throughput is increased with the IC-DDF receiver. Assuming that the 30 to 60 piconets would be present at crowded locations such as an airport lounge, the IC-DDF receiver provides substantial gains over a conventional receiver. The effect of the propagation channel between transmitter and receiver on PER performance is analyzed and compared in Figure 18 for OBS and LOS channels. The IC-DDF receiver diminishes the effect of propagation channel on link throughput for both HV2 and DM3 packets.

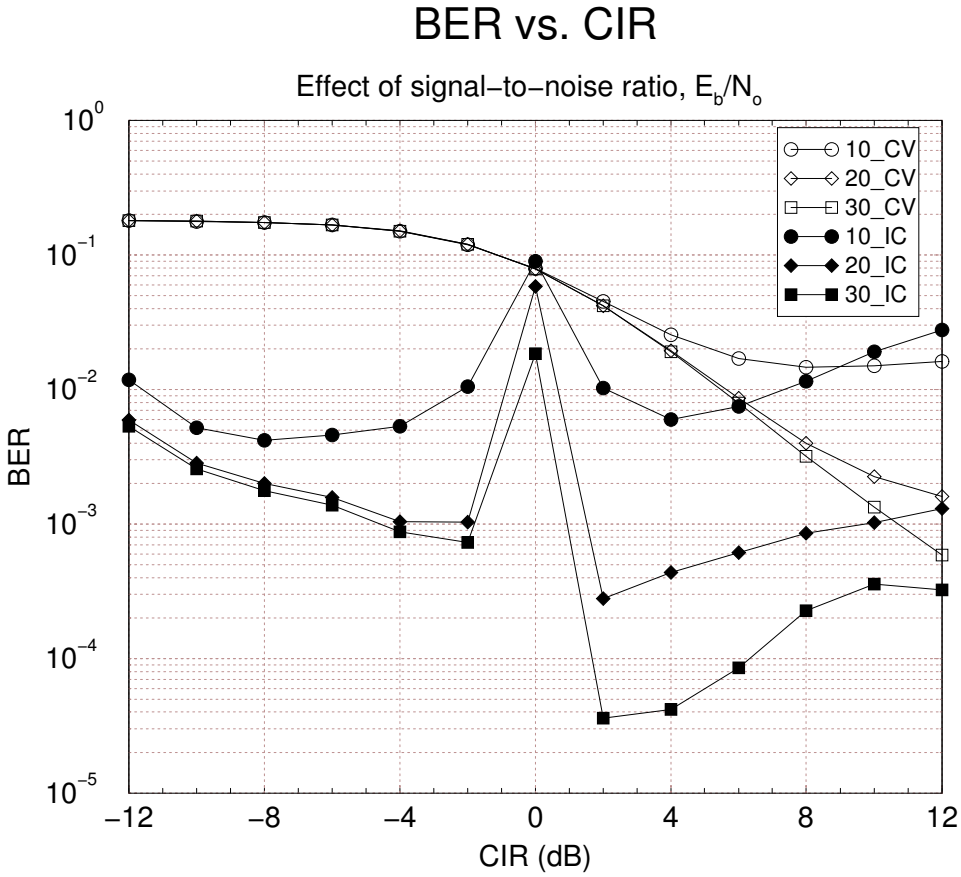

Figure 13: BER performance of the IC-DDF receiver with various signal-to-noise ratio E_b/N_o; Rician factor $K = 0$, Doppler frequency $f_D = 10$ Hz. Legend: xx_yy, xx = E_b/N_o, yy = conventional receiver (CV) or IC-DDF receiver (IC).

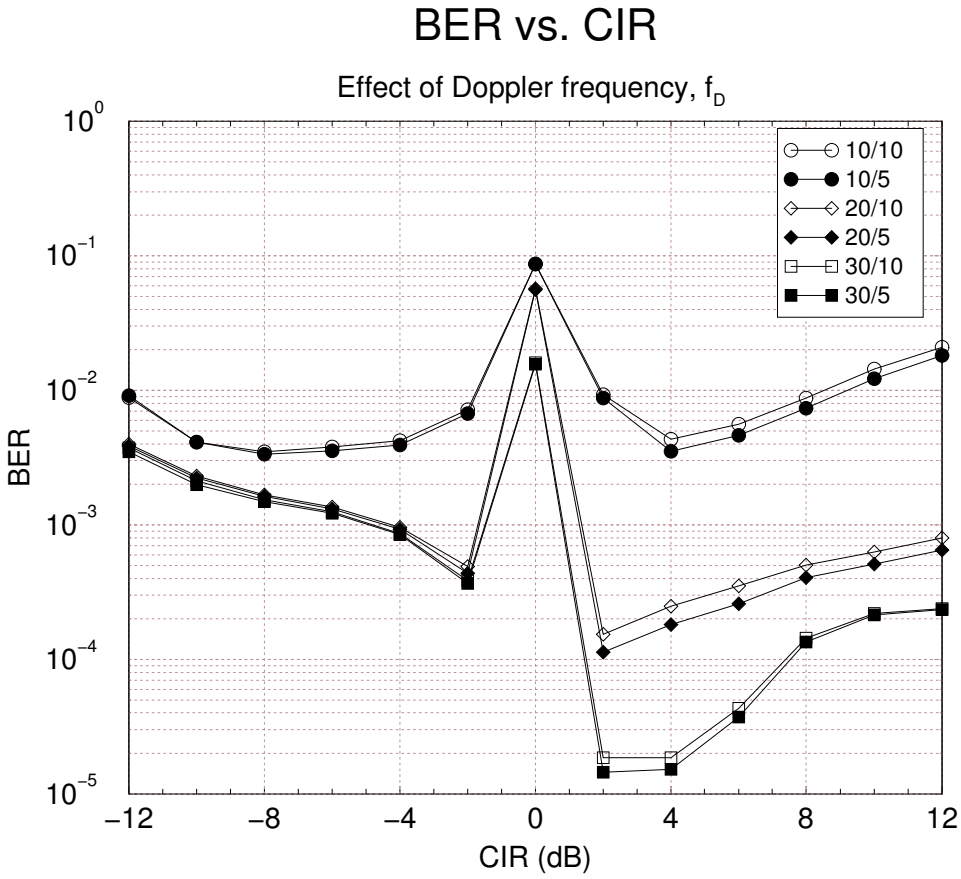

Figure 14: Effect of Doppler frequency f_D on BER performance of the IC-DDF receiver with various E_b/N_0 conditions; Rician factor $K = 2$. Legend: xx/yy, xx = E_b/N_o, yy = f_D.

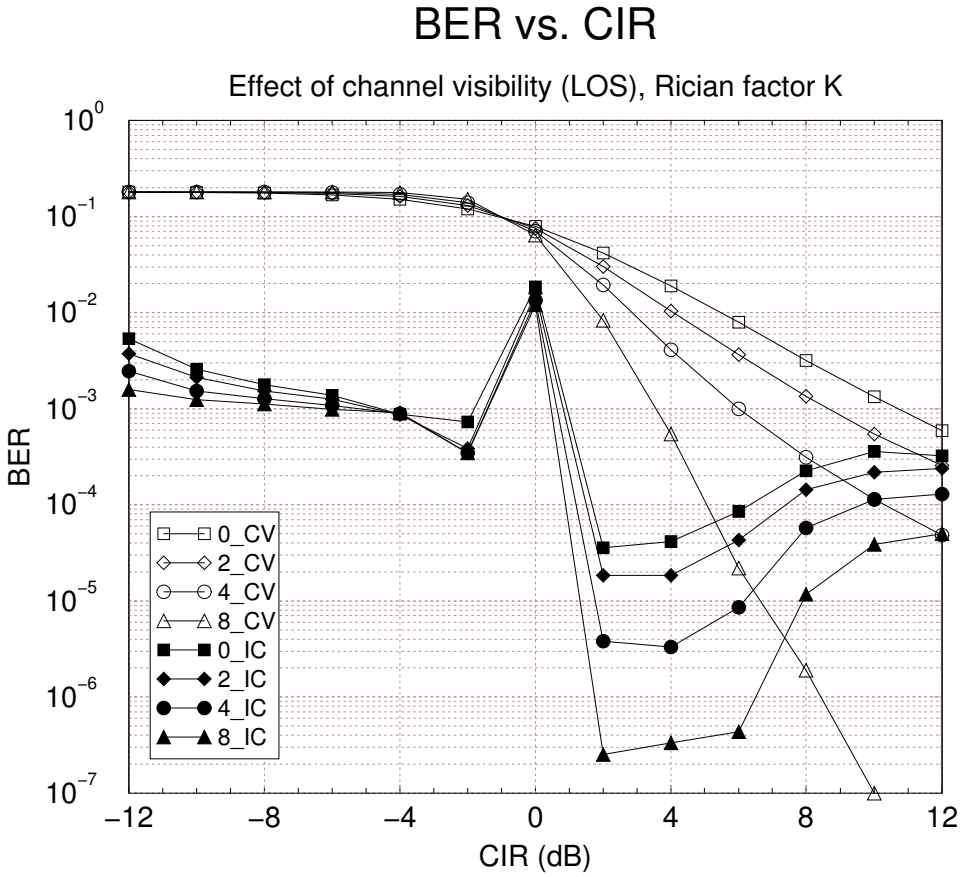

Figure 15: Effect of visibility(LOS) of propagation channel on performance of IC-DDF receiver with various Rician factor K; $E_b/N_o = 30$ dB and $f_D = 10$ Hz. Legend: x_yy, x = Rician factor K, yy = conventional receiver (CV) or IC-DDF receiver (IC).

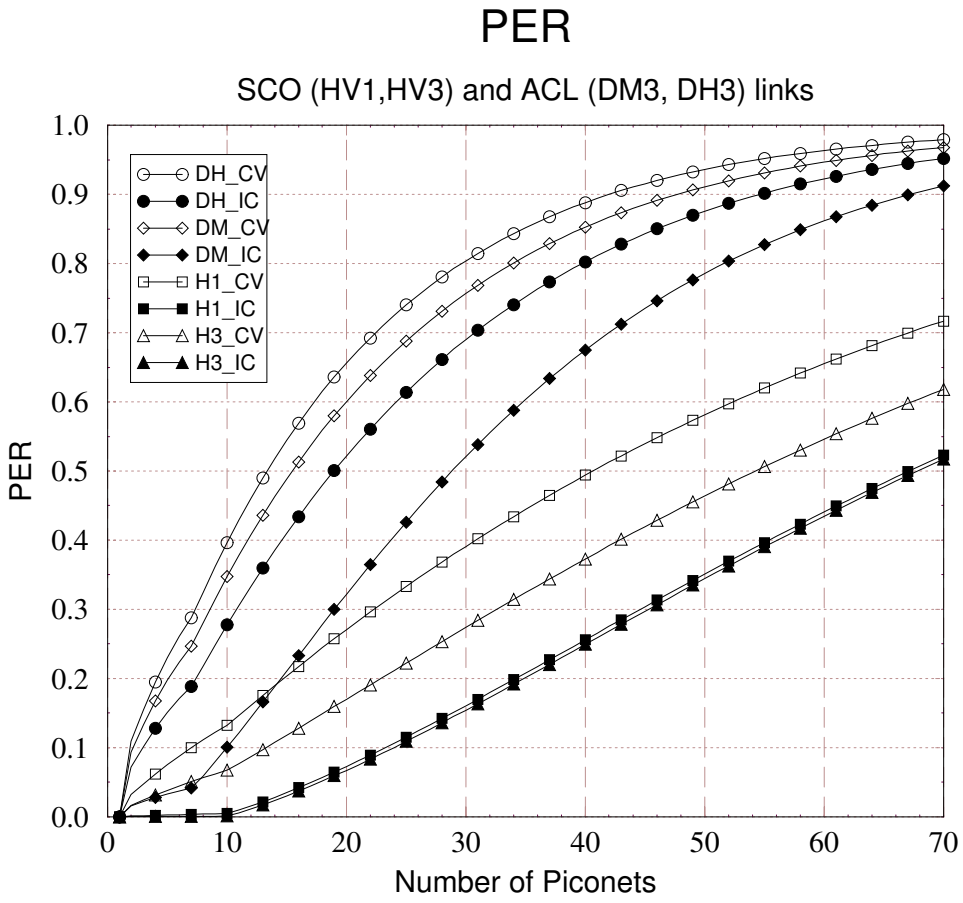

Figure 16: PER performance of the IC-DDF receiver for SCO(HV1,HV3) and ACL(DM3,DH3) piconets; $E_b/N_o = 30$ dB, $K = 0$, $f_D = 10$ Hz and $\epsilon = 0.5$. Legend: xx_yy, xx = DH3 packet (DH), DM3 packet (DM), HV1 packet (H1) or HV3 packet (H3), yy = conventional receiver (CV) or IC-DDF receiver (IC).

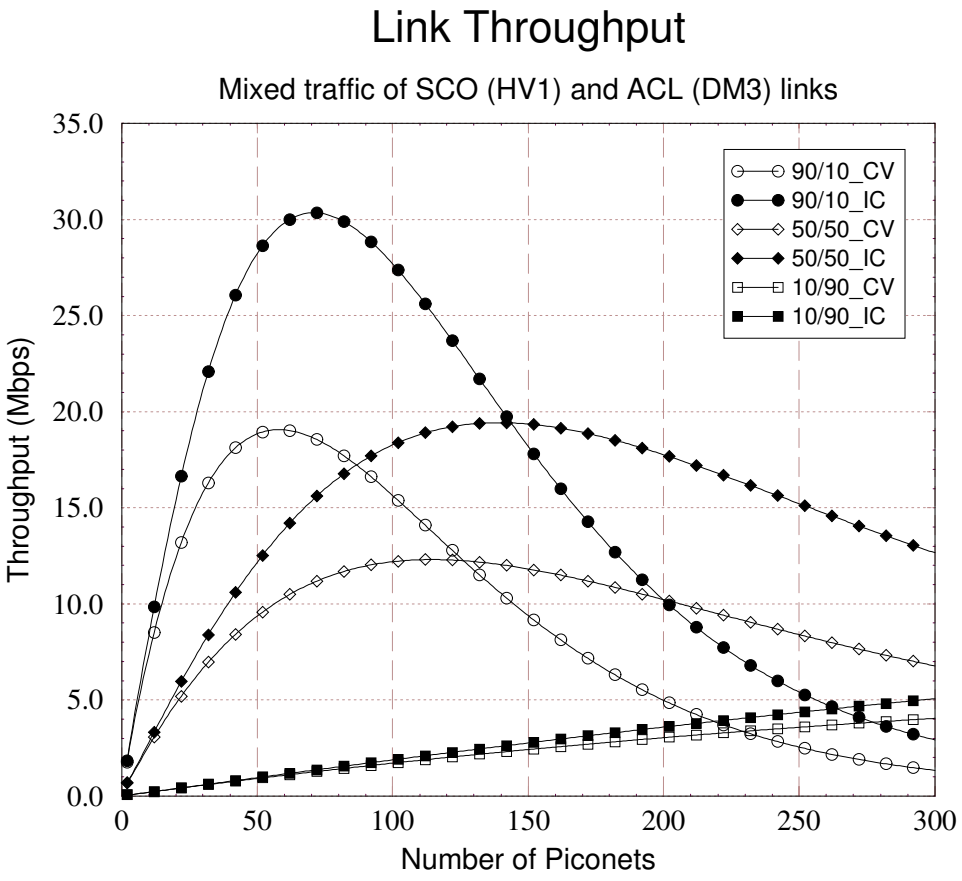

Figure 17: Link throughput performance of the IC-DDF receiver with mixed piconets of HV1(SCO) and DM3(ACL) packets; $E_b/N_o = 30$ dB, $K = 0$, $f_D = 10$ Hz and $\epsilon = 0.1$. Legend: xx/yy_zz, xx = percentage of SCO piconets, yy = percentage of ACL piconets, zz = conventional receiver (CV) or IC-DDF receiver (IC).

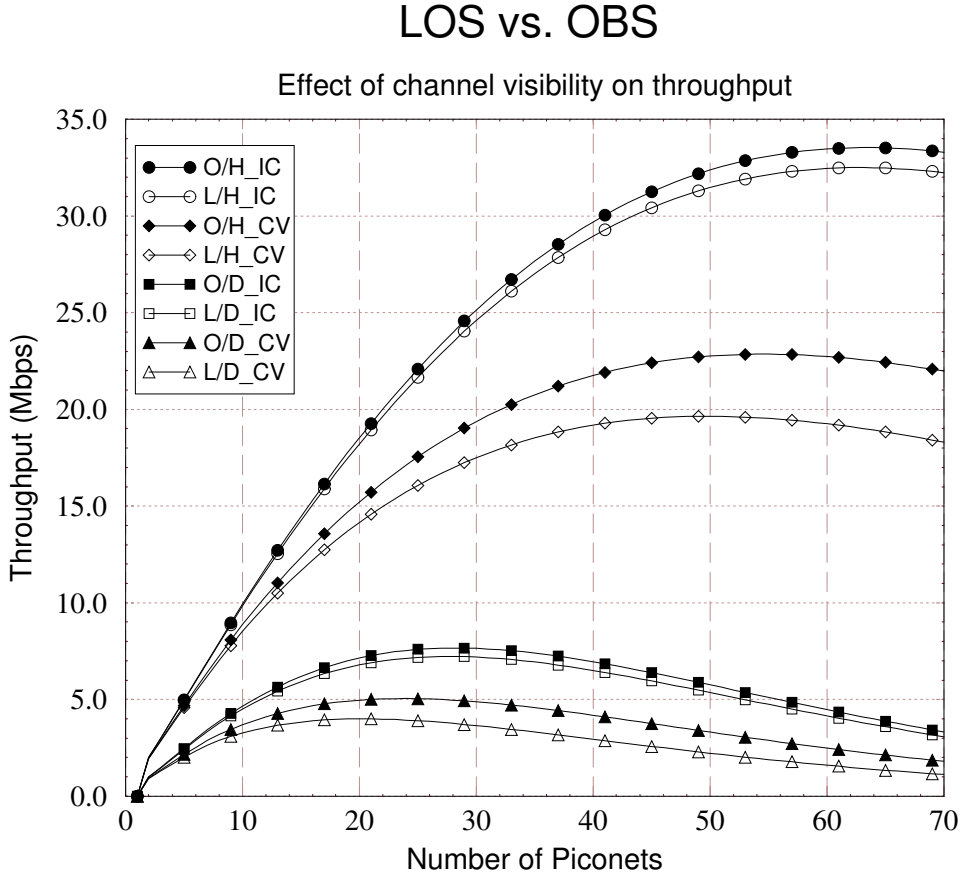

Figure 18: Effect of visibility(LOS) of propagation channel on link throughput of HV2(SCO) and DM3(ACL) packets; $f_D = 10$ Hz, $\epsilon = 0.5$, and $K = 8$ and 0 for LOS(line-of-sight) and OBS(obstructed) channels, respectively. Legend: x/y_zz, x = line-of-sight (L) or obstructed (O), y = HV2 packet (H) or DM3 packet (D), zz = conventional receiver (CV) or IC-DDF receiver (IC).

CHAPTER IV

JOINT DETECTION INTERFERENCE REJECTION COMBINING GSM/EDGE RECEIVER

4.1 Introduction

Co-channel interference (CCI) is the primary impediment in cellular frequency reuse systems. Single antenna interference mitigating receivers that use serial/parallel interference cancellation (SIC/PIC), joint detection (JD), and other multiuser detection (MUD) algorithms have been proposed [93]. Multiple antenna receivers have also been proposed to suppress CCI by using optimal combining [146]. A receiver that combines interference rejection combining (IRC) with maximum likelihood sequence estimation (MLSE) has been proposed for channels exhibiting both CCI and intersymbol interference (ISI) [28]. For channels with long delay spreads, the MLSE decoding is impractical because of increasing complexity, especially for the systems with large signal constellation sets. The delayed decision feedback sequence estimation (DDFSE) scheme is proposed as an alternative solution with reduced complexity at the expense of minute gains [18, 41, 84].

In frequency reuse cellular systems, the received carrier-to-interference ratio is expected to be greater than 0 dB by its network topology, and most interference cancelling receivers are designed to mitigate the CCI weaker than the desired signal. However, when a receiver tries to reach remote BSs for applications such as intelligence or emergency operations, the receiver should be operable in CIR far below the range that conventional receivers are not usually designed to operate in, CIR < 0 dB. Furthermore, multipath fading, non-ideal terrain structures makes decoding of the desired signal more challenging.

This study proposes a soft output fractionally spaced joint detection IRC-DDFSE (JD IRC-DDFSE) receiver. The trellis search technique used in the IRC-DDFSE receiver in [84] is extended to perform joint detection of two co-channel signals, while IRC is used

to reject the remaining co-channel interference. Moreover, the JD IRC-DDFSE receiver generates soft-outputs that are used as inputs to a soft decision channel decoder by using Log-MAP algorithm. This modification permits the receiver to recover signals in very strong CCI, where the received CIR may even be less than 0 dB. The precision of soft-outputs generated by the Log-MAP algorithm in DDFSE function is improved by using the surviving sequence and the covariance matrix estimated from concatenated Viterbi algorithm. Also, the contribution of this study includes a joint least squares (LS) channel estimation which enables the receiver estimate the channel information of the desired signal in low-CIR conditions. Joint channel estimation also reduces the side effect of the timing offset between the co-channel signals.

A narrow beam adaptive antenna (NBAA) array can be used to reduce the number of co-channel signals [15, 81]. In a cellular topology, for example, an NBAA aligned to the line-of-sight (LOS) path from the receiver to the target BS as shown in Figure 19, admits one dominant co-channel signal from the closest tier, plus a few highly attenuated co-channel signals from outer tiers. In contrast, a conventional 120° wide-beam sector antenna receives two strong co-channel signals from the nearest tier. This study shows that the combination of an NBAA with JD IRC-DDFSE is highly effective for mitigating co-channel interference. In fact, this arrangement may provide sufficient interference rejection to allow communication with a distant base station in the presence of a near-by co-channel base station. Such capabilities may be useful for intelligence or emergency operations in cellular networks.

The remainder of this chapter is organized as follows. Section 4.2 introduces the system model with an NBAA array. Section 4.3 details the soft-output fractionally-spaced JD IRC-DDFSE receiver, and presents methods for joint channel estimation technique and soft-output generation. In Section 4.4, the impact of imbalanced CIR observed in receive branches is investigated. Section 4.5 discusses the receiver performance for binary and non-binary 8-PSK modulated systems.

4.2 System Model for Range Extended Reception

4.2.1 Signal Model

The system under consideration can be modelled as a K-input, J-ouptut, channel, where K is the number of co-channel signals and J the number of receiver antenna units. We arbitrarily assign the first user ($k = 1$) as the desired signal while the other users $k = 2, \ldots, K$ are the interfering co-channel signals. The signal at the output of the jth receiver antenna unit is

$$r^{(j)}(t) = \sum_{k=1}^{K} \sum_{\ell=-\infty}^{\infty} x_\ell^{(k)} h^{(k,j)}(t - \ell T - \tau_k) + \eta^{(j)}(t) \ , \tag{39}$$

where $\eta^{(j)}(t)$ is zero-mean complex additive white Gaussian noise process with variance $\sigma_\eta^2 = \frac{1}{2}\mathrm{E}[|\eta^{(j)}(t)|^2] = N_o$ watts/Hz, and $\mathbf{x}^{(k)} = \{x_\ell^{(k)}\}$ is the sequence of complex symbols transmitted by the kth co-channel user. The overall channel response $h^{(k,j)}(t)$ is the convolution of a complex channel impulse response $c^{(k,j)}(t)$ and the transmitting filter $h_a(t)$. For the synchronous GSM network considered in this study, the delay offsets τ_k for all co-channel signals will be at most two symbol intervals [20]. The influence of the delay offsets of 0 to 2 symbol duration will be evaluated by computer simulation in Section IV. Joint channel estimation is performed using the known training symbol sequences (TSS) followed by joint detection.

4.2.2 NBAA Preprocessing

As shown in Figure 19, we consider a cellular topology where a range extended intercept receiver (MS) located in one co-channel BS area (BS7) tries to communicate with a co-channel BS in the outer tier (BS1). There are 3 predominate co-channel BSs, namely BS2, BS3, and BS4, where the angle α between BS2 and BS4 as seen from the intercept receiver is approximately 60°. A practical NBAA array can reject all CCI signals, leaving only one strong source of CCI (BS3) which is located on the LOS path from MS to BS1. In contrast, a conventional 120° wide-beam sector antenna will see at least 2 strong sources of CCI from BSs in the first tier. In addition, both the NBAA array and wide-beam sector antennas will receive additional CCI from the third and higher tiers (for example from BS8 and BS9) but with a very small power level due to path loss attenuation. Finally, for NBAA arrays

the delay spread of the channel impulse responses tends to shorten because of the reduced antenna aperture. This property simplifies the task of equalization, especially in the case of joint detection.

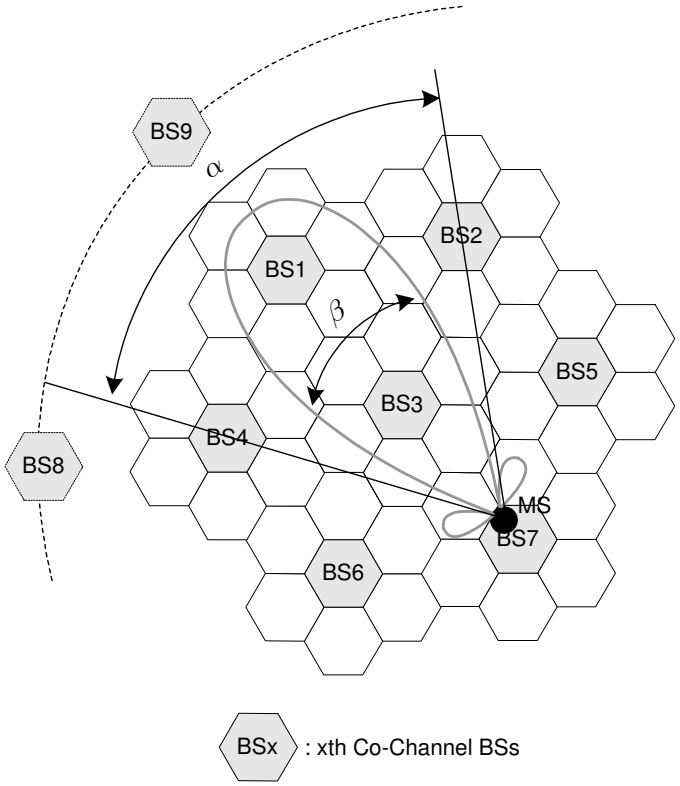

Figure 19: System model with a narrow beam adaptive antenna (NBAA) array.

4.3 Receiver Structure

The proposed fractionally spaced joint detection IRC-DDFSE (JD IRC-DDFSE) is shown in Figure 20 [89].

4.3.1 Fractionally-Spaced Noise Whitening Filtering

The receiver uses a receiver that is matched to the transmitted pulse shape, $h_a(t)$, followed by a rate-$2/T$ sampler and a $T/2$-spaced noise whitening filter. Such front-end

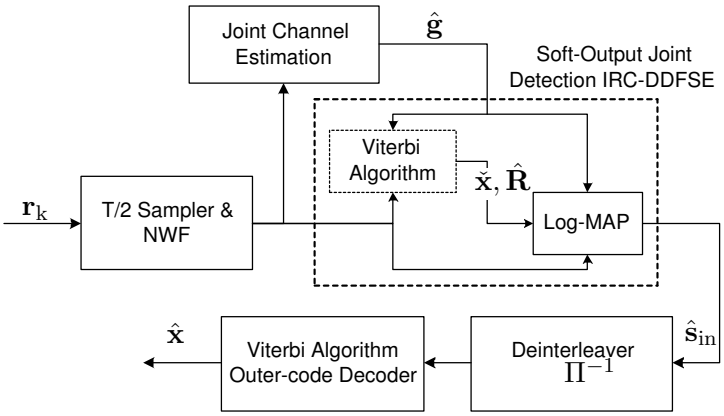

Figure 20: Soft-output JD IRC-DDFSE receiver with joint least squares (LS) channel estimation.

processing is optimal, and the fractional sampling makes the receiver insensitive to sampler timing phase [128]. Let $H_a(z)$ and $C^{(k,j)}(z)$ be the z-transforms of the $T/2$-spaced sample sequences $\mathbf{h}_a$ and $\mathbf{c}^{(k,j)}$, corresponding to $h_a(t)$ and $c^{(k,j)}(t)$, respectively. The z-transform of the autocorrelation function of the noise samples at the output of the receiver filter is given by $N_o F_h(z)$, where $F_h(z) = H_a(z)H_a^*(1/z^*)$. By using the factorization of $F_h(z) = G_h(z)G_h^*(1/z^*)$, the $T/2$-spaced noise whitening filter is obtained as $W(z) = [G_h^*(1/z^*)]^{-1}$ [128]. We choose the stable, anticausal noise whitening filter such that $G_h(z)$ is minimum phase. Then, the overall $T/2$-spaced channel transfer function of the kth user at jth antenna that includes the transmit filter, channel, receiver filter, $T/2$-spaced sampler, and $T/2$-spaced noise-whitening filter is

$$\begin{aligned} G_{\text{eq}}^{(k,j)}(z) &= H_a(z)C^{(k,j)}(z)H_a^*(1/z^*)W(z) \\ &\approx C^{(k,j)}(z)G_h(z), \end{aligned} \tag{40}$$

where the approximation is due to a finite length approximation of the noise whitening filter. For a linearized GMSK pulse $h_a(t)$ of length $L_h+1 = 16$, the noise whitening filter is designed to have larger length of $W+1 = 20$. With the finite length noise whitening filter, the length $L+1$ of overall channel transfer function $G_{\text{eq}}^{(k,j)}(z)$ is $2L_h+L_c+W+1$ where L_c+1 is the length of channel $C^{(k,j)}(z)$. Since the many of the coefficients of $G_{\text{eq}}^{(k,j)}(z)$ are very small and negligible, $G_{\text{eq}}^{(k,j)}(z)$ can be effectively truncated to length $\tilde{L}+1$. For example,

the effective length of the overall $T/2$-spaced channel can be set to 7 symbol durations, i.e., $\tilde{L}+1=14$ for GSM/EDGE as in [59].

4.3.2 Joint Detection IRC-DDFSE

Let $X^{(k)}(z)$ and $V^{(k,j)}(z)$ be the z-transform of the input sequence and received signal from the kth user at jth antenna unit, respectively, and $V^{(k,j)}(z)=G_{\text{eq}}^{(k,j)}(z)X^{(k)}(z)$. Then, the received signal samples at the output of the matched filter on the jth antenna unit are

$$\begin{aligned} r_{2\ell+q}^{(j)} &= \sum_{k=1}^{K} v_{2\ell+q}^{(k,j)} + \eta_{2\ell+q}^{(j)} \\ &= \sum_{k=1}^{K}\left(\sum_{n=0}^{\mu} g_{\text{eq},2n+q}^{(k,j)} x_{\ell-n}^{(k)} + v_{2\ell+q}^{(k,j)+}\right) + \eta_{2\ell+q}^{(j)}, \quad q=0,1 \end{aligned} \tag{41}$$

where $v_{2\ell+q}^{(k,j)+}$ is the signal term from the channel impulse response longer than μ, and where μ is the truncation length used in the DDFSE algorithm [41].

The proposed receiver jointly detects N co-channel signals, while the remaining $K-N$ co-channel signals plus additive white gaussian noise are treated as impairments. Equation (41) can be rewritten as

$$r_{2\ell+q}^{(j)} = \sum_{k=1}^{N}\left(\sum_{n=0}^{\mu} g_{\text{eq},2n+q}^{(k,j)} x_{\ell-n}^{(k)} + v_{2\ell+q}^{(k,j)+}\right) + n_{2\ell+q}^{(j)}, \quad q=0,1 \tag{42}$$

where $n_{2\ell+q}^{(j)}$ is the impairment

$$n_{2\ell+q}^{(j)} = \sum_{k=N+1}^{K}\left(\sum_{n=0}^{L/2} g_{\text{eq},2n+q}^{(k,j)} x_{\ell-n}^{(k)}\right) + \eta_{2\ell+q}^{(j)}, \quad q=0,1\ . \tag{43}$$

The Gaussian noise components $\eta_{2\ell}^{(j)}$ and $\eta_{2\ell+1}^{(j)}$ have zero mean and are uncorrelated in time due to the $T/2$-spaced noise whitening filter. Under the assumption that the residual terms $v_{2\ell+q}^{(k,j)+}$ and the CCI are stationary zero-mean complex Gaussian random processes [28], the impairment vectors $\mathbf{n}_{2\ell+q}=(n_{2\ell+q}^{(1)},\ldots,n_{2\ell+q}^{(J)})^{\mathbf{T}}$ have the joint Gaussian pdfs

$$p(\mathbf{n}_{2\ell+q}) = \frac{1}{\pi^{L}|\mathbf{R}_{2\ell+q}|}\exp\left\{-\mathbf{n}_{2\ell+q}^{\mathbf{H}}\mathbf{R}_{2\ell+q}^{-1}\mathbf{n}_{2\ell+q}\right\} \quad q=0,1 \tag{44}$$

where $\mathbf{R}_{2\ell+q}=\frac{1}{2}\text{E}[\mathbf{n}_{2\ell+q}\mathbf{n}_{2\ell+q}^{\mathbf{H}}]$ is the covariance matrix. In the joint detection Viterbi algorithm, the state vectors at time ℓ are defined as

$$\mathbf{s}_{\ell}^{\mu(i)} = \left(\mathbf{x}_{\ell,\mu}^{(1)^T}, \mathbf{x}_{\ell,\mu}^{(2)^T}, \ldots, \mathbf{x}_{\ell,\mu}^{(N)^T}\right), i=1,\ldots,N_s \tag{45}$$

where $\mathbf{x}_{\ell,\mu}^{(k)} = (x_{\ell-1}^{(k)}, x_{\ell-2}^{(k)}, \ldots, x_{\ell-\mu}^{(k)})^T$ is the kth symbol sequence, and $N_s = M^{\mu N}$ is the number of states in the Viterbi algorithm, corresponding to a signal constellation of size M and reduced channel memory of length μ in DDFSE algorithm. From the above joint Gaussian density functions, and the time independence assumption of the interference impairment, the Viterbi branch metric associated with the state transition $\mathbf{s}_\ell^{\mu(i)} \rightarrow \mathbf{s}_{\ell+1}^{\mu(j)}$ at epoch ℓ is

$$m_\ell(\mathbf{s}_\ell^{\mu(i)} \rightarrow \mathbf{s}_{\ell+1}^{\mu(j)}) = \hat{\mathbf{n}}_{2\ell}^{\mathbf{H}} \mathbf{R}_{2\ell}^{-1} \hat{\mathbf{n}}_{2\ell} + \hat{\mathbf{n}}_{2\ell+1}^{\mathbf{H}} \mathbf{R}_{2\ell+1}^{-1} \hat{\mathbf{n}}_{2\ell+1} \tag{46}$$

where

$$\hat{\mathbf{n}}_{2\ell+q} = (\hat{n}_{2\ell+q}^{(1)}, \ldots, \hat{n}_{2\ell+q}^{(J)})^{\mathbf{T}} \tag{47}$$

are the hypothesis impairment vectors with elements

$$\begin{aligned} \hat{n}_{2\ell+q}^{(j)} &= r_{2\ell+q}^{(j)} - \sum_{k=1}^{N} \Bigg(g_{\mathrm{eq},q}^{(k,j)} x_\ell^{(k)}(\mathbf{s}_\ell^{\mu(i)} \rightarrow \mathbf{s}_{\ell+1}^{\mu(j)}) + \sum_{n=1}^{\mu} g_{\mathrm{eq},2n+q}^{(k,j)} x_{\ell-n}^{(k)}(\mathbf{s}_\ell^{\mu(i)}) \\ &\quad + \sum_{l=\mu+1}^{\hat{L}/2} g_{\mathrm{eq},2l+q}^{(k,j)} \check{x}_{\ell-l}^{(k)}(\varrho_\ell^{\mu(i)}) \Bigg), \quad q = 0, 1. \end{aligned} \tag{48}$$

In (48), $x_\ell^{(k)}(\mathbf{s}_\ell^{\mu(i)} \rightarrow \mathbf{s}_{\ell+1}^{\mu(j)})$ is the input symbol that is uniquely determined by the state transition $(\mathbf{s}_\ell^{\mu(i)} \rightarrow \mathbf{s}_{\ell+1}^{\mu(j)})$, the term $\sum_{n=1}^{\mu} g_{\mathrm{eq},2n+q}^{(k,j)} x_{\ell-n}^{(k)}(\mathbf{s}_\ell^{\mu(i)})$ is uniquely specified by the previous state vector $(\mathbf{s}_\ell^{\mu(i)})$, and $\sum_{l=\mu+1}^{\hat{L}/2} g_{\mathrm{eq},2l+q}^{(k,j)} \check{x}_{\ell-l}^{(k)}(\varrho_\ell^{\mu(i)})$ is the decision feedback term $v_{2\ell+q}^{(k,j)+}$ in (41) and (42) with a reduced equivalent channel length $\hat{L}+1$. The estimated symbol $\check{x}_{\ell-l}^{(k)}(\varrho_\ell^{\mu(i)})$ is the l^{th} component of the surviving sequence $\check{\mathbf{x}}^{(k)}(\varrho_\ell^{\mu(i)})$ of the kth user.

4.3.3 Covariance Matrix $\hat{\mathbf{R}}$

To calculate the impairments term $\hat{n}_{2\ell+q}^{(j)}$ in (48), the surviving sequence $\check{\mathbf{x}}^{(k)}(\varrho_\ell^{\mu(i)})$ entering each state is estimated from the backward recursion in Viterbi algorithm. Also, the impairments vector $\hat{\mathbf{n}}_{2\ell+q}$, generated with the surviving sequence $\check{\mathbf{x}}^{(k)}(\varrho_\ell^{\mu(i)})$, is used in estimation of the covariance matrix $\hat{\mathbf{R}}_{2\ell+q}$. After obtaining initial estimates of $\hat{\mathbf{R}}_{2\ell}$ and $\hat{\mathbf{R}}_{2\ell+1}$ with the known TSS sequences, the covariance matirx is tracked and updated at every baud interval. At epoch ℓ, the covariance matrix is

$$\hat{\mathbf{R}}_{2\ell+q} = \frac{1}{N} \sum_{n=0}^{N-1} \hat{\mathbf{n}}_{2(\ell-n)+q} \hat{\mathbf{n}}_{2(\ell-n)+q}^{\mathrm{H}}, \quad q = 0, 1 \tag{49}$$

where $N = 16$ is the window size, and $\hat{\mathbf{n}}_{2(\ell-n)+q}$ is the impairments vector at epoch $\ell - n$. Note that the surviving sequence and the covariance matrix estimated from the Viterbi algorithm are used in the generation of the soft output in Log-MAP algorithm as shown in Fig 20. Each state and the corresponding surviving sequence estimated in the Viterbi algorithm are one-to-one mapped into the Log-MAP algorithm so that the decision metric in (52) for Log-MAP algorithm can be calculated without any loss in decision feedback term. Also, the covariance matrix generated from the Viterbi algorithm in (49) is used in the Log-MAP algorithm in (52) since the covariance matrix is generated with the surviving sequence of decision feedback term which is not available from the Log-MAP algorithm.

4.3.4 Soft Outputs

Soft outputs are generated by using a Log-MAP algorithm in a JD IRC-DDFSE [21]. Define the ℓth symbol mapping function $x(\ell) = f(\mathbf{b}(\ell))$, where the output symbol $x(\ell)$ is selected from a $M = 2^U$ element signal constellation depending on the binary input sequence, $\mathbf{b}(\ell) = [b_0(\ell), \ldots, b_{U-1}(\ell)], b_i(\ell) \in 0, 1$. With this relationship, the log-likelihood ratio (LLR) of bit $b_i(\ell)$ is

$$\lambda(b_i(\ell)) = \log \frac{\sum_{b_i(\ell)=1|x(\ell)} p(x(\ell)|\mathbf{r})}{\sum_{b_i(\ell)=0|x(\ell)} p(x(\ell)|\mathbf{r})}, \tag{50}$$

where $p(x(\ell)|\mathbf{r})$ is the conditional *a posteriori* probability of the symbol $x(\ell)$ given the entire observation vector $\mathbf{r}$. The probability $p(x(\ell)|\mathbf{r})$ from the JD IRC-DDFSE receiver is defined as

$$\begin{aligned} p(x(\ell)|\mathbf{r}) &= \sum_{(\mathbf{s}_\ell \to \mathbf{s}_{\ell+1}) \in S(x(\ell))} p(\mathbf{s}_\ell, \mathbf{s}_{\ell+1}|\mathbf{r}) \\ &= \sum_{(\mathbf{s}_\ell \to \mathbf{s}_{\ell+1}) \in S(x(\ell))} p(\mathbf{s}_\ell, \mathbf{r}_{l<\ell}) p(\mathbf{s}_{\ell+1}, \mathbf{r}_\ell|\mathbf{s}_\ell) p(\mathbf{r}_{l>\ell}|\mathbf{s}_{\ell+1})/p(\mathbf{r}). \end{aligned} \tag{51}$$

where $S(x(\ell))$ is the set of all state transition pairs $\mathbf{s}_\ell \to \mathbf{s}_{\ell+1}$ having input symbol $x(\ell)$. In (51), $p(\mathbf{s}_{\ell+1}, \mathbf{r}_\ell|\mathbf{s}_\ell)$ is calculated from the decision metric of the JD IRC-DDFSE receiver as

$$p(\mathbf{s}_{\ell+1}, \mathbf{r}_\ell|\mathbf{s}_\ell) = \exp\left(- \mid \hat{\mathbf{n}}_{2\ell}^{\mathbf{H}} \hat{\mathbf{R}}_{2\ell}^{-1} \hat{\mathbf{n}}_{2\ell} + \hat{\mathbf{n}}_{2\ell+1}^{\mathbf{H}} \hat{\mathbf{R}}_{2\ell+1}^{-1} \hat{\mathbf{n}}_{2\ell+1} \mid\right) \tag{52}$$

In the same manner, the terms from past and future observations are recursively updated during the forward and backward processing, respectively, as

$$p(\mathbf{s}_{\ell+1}, \mathbf{r}_{l<\ell+1}) = \sum_{\mathbf{s}_\ell \in Q} p(\mathbf{s}_\ell, \mathbf{r}_{l<\ell}) p(\mathbf{s}_{\ell+1}, \mathbf{r}_\ell | \mathbf{s}_\ell) \quad (53)$$

$$p(\mathbf{r}_{l>\ell-1} | \mathbf{s}_\ell) = \sum_{\mathbf{s}_{\ell+1} \in Q} p(\mathbf{r}_\ell, \mathbf{s}_{\ell+1} | \mathbf{s}_\ell) p(\mathbf{r}_{l>\ell} | \mathbf{s}_{\ell+1}) \quad (54)$$

where Q is the set of all possible states. The LLRs of the code bit sequence from the IRC-DDFSE receiver are reordered by a block deinterleaver (GSM interleaver) and forwarded to the outer Viterbi decoder.

4.3.5 Joint Channel Estimation

The JD IRC-DDFSE receiver requires an accurate estimate of overall channel impulse response, $G_{\text{eq}}(z)$ defined in (40). In GSM/EDGE cellular systems, the channel is estimated by using the training sequence that is inserted into every transmitted data burst as shown in Figure 21. For a joint detection receiver, joint channel estimation is necessary because of the cross-correlation of the training sequences of the co-channel signals [118].

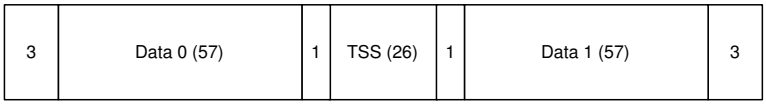

Figure 21: GSM/EDGE burst structure

Joint channel estimation is conducted at every antenna independently. We assume that the length of the equivalent channel impulse responses of all the participating co-channel signals are equal. The length of the equivalent channel impulse response $\hat{L}+1$ should be chosen appropriately so that the receiver is less sensitive to the channel variation. We set $\hat{L}+1 = 6$ since the BER increase for all three channel models after 6 as shown in Fig 22.

For the jth receiver antenna unit, define the channel impulse response corresponding to the kth signal, the received signal vector, and received impairment vector as $\mathbf{G}_{\text{eq},q}^{(k,j)} = [g_{\text{eq},q}^{(k,j)}, \ldots, g_{\text{eq},\hat{L}+q}^{(k,j)}]^T$, $\mathbf{v}_q^{(j)} = (v_q^{(j)}, \ldots, v_{2P+q}^{(j)})^T$, and $\mathbf{n}_q^{(j)} = (n_q^{(j)}, \ldots, n_{2P+q}^{(j)})^T$, $q \in \{0, 1\}$, respectively. In the GSM/EDGE system, one of 8 different 26-symbol midamble training

symbol sequences (TSS) are inserted into each burst. For the co-channel signals with D-symbol interval delay offset and equivalent channels of length $\hat{L}+1 = 6$, $24-D$ TSS symbols and $2(P+1-D) = 48-2D$, $T/2$-spaced, received signal vectors are used to insure that the known training sequences are involved in the channel estimation process.

The received samples during the training sequence at jth antenna are

$$\mathbf{v}_q^{(j)} = \mathbf{X}\mathbf{G}_{\text{eq},q}^{(j)} + \mathbf{n}_q^{(j)}, \;\; q = 0, 1 \tag{55}$$

where $\mathbf{G}_{\text{eq},q}^{(j)} = (\mathbf{G}_{\text{eq},q}^{(1,j)^T}, \ldots, \mathbf{G}_{\text{eq},q}^{(N,j)^T})^T$ is a joint channel impulse response vector, and $\mathbf{X} = (\mathbf{X}^{(1)}, \ldots, \mathbf{X}^{(N)})$ is the transmitted training sequence matrix with elements

$$\mathbf{X}^{(k)} = \begin{bmatrix} x_0^{(k)} & \cdots & x_{-(\hat{L}-1)/2}^{(k)} \\ x_1^{(k)} & \cdots & x_{-(\hat{L}-1)/2+1}^{(k)} \\ \vdots & \ddots & \vdots \\ x_P^{(k)} & \cdots & x_{-(\hat{L}-1)/2+P}^{(k)} \end{bmatrix} . \tag{56}$$

Under our time independence assumption, $\mathbf{n}_q^{(j)}$, $q \in \{0, 1\}$, is a white Gaussian noise vector, and the least squares solution to (55) is [75]

$$\hat{\mathbf{G}}_{\text{eq,LS},q}^{(j)} = (\mathbf{X}^H\mathbf{X})^{-1}\mathbf{X}^H\mathbf{v}_q^{(j)}, \;\; q = 0, 1 \;\; . \tag{57}$$

4.4 Imbalanced CIRs at Antenna Branches

In general, the received CIRs are assumed equal at all antenna branches. However, the crowded high-rise buildings and narrow streets fertilize the construction of virtual waveguides for radio wave propagation in urban cities. In those radio propagation environments, average power of received signals at antenna branches may not equal. Mallik *et al*'s study shows that the imbalance of Gaussian noise across antenna branches degrades the performance of equal gain combining (EGC) in correlated Rayleigh faded channels [103]. Also, another study shows that optimal and selective combining receivers with linear/nonlinear equalizer achieves minimum BER when all antenna branches have an equal received SNRs [99].

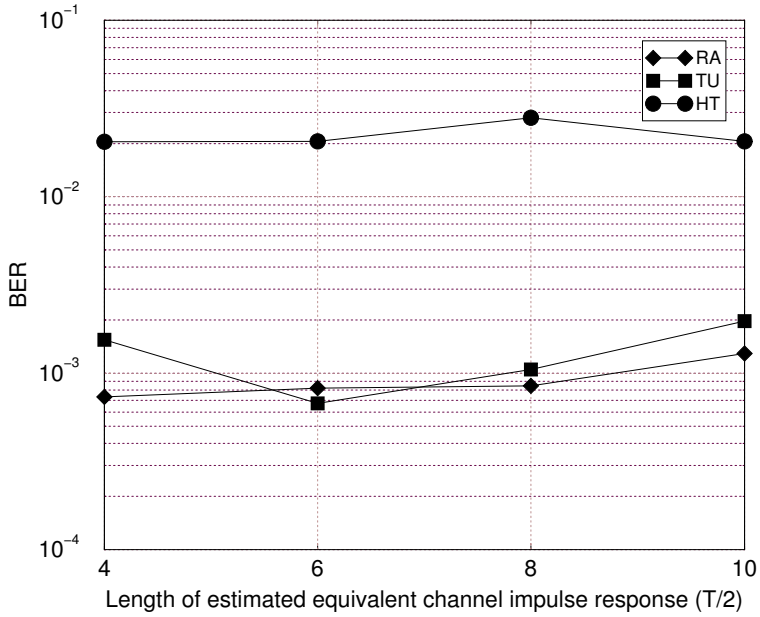

Figure 22: Effect of equivalent channel impulse response length in JD IRC-DDFSE receiver for GSM system; $J = 2$, $E_b/N_0 = 30$ dB, CIR $= 0$ dB, Legend: RA (RA120), TU (TU50) or HT (HT120).

Unlike the EGC where the decision metric directly decided by the imbalanced CIR at antenna branches, the performance of the joint detection IRC-DDFSE receiver is depends on the precise channel estimation. Therefore, the effect of the imbalanced CIR on the receiver performance can be investigated from the viewpoint of joint channel estimation in imbalanced CIR conditions.

The received signal at jth antenna in (55) can be rewritten as

$$\begin{aligned} \mathbf{v}_q^{(j)} &= \mathbf{X}\mathbf{G}_{\mathrm{eq},q}^{(j)} + \mathbf{n}_q^{(j)}, \\ &= \mathbf{X}^{(1)}\mathbf{G}_{\mathrm{eq},q}^{(1,j)^T} + \ldots + \mathbf{X}^{(N)}\mathbf{G}_{\mathrm{eq},q}^{(N,j)^T} + \mathbf{n}_q^{(j)} \quad q = 0, 1. \end{aligned} \tag{58}$$

With LS joint channel estimation and the assumption of orthogonality between the training sequences of signal from different users, $\mathbf{X}^{(m)^H}\mathbf{X}^{(l)} = 0, m \neq l$, the channel estimation error of kth user at jth antenna can be defined as

$$\begin{aligned} \mathcal{E}_{\mathrm{eq},q}^{(k,j)} &= \mathbf{G}_{\mathrm{eq},q}^{(k,j)} - \hat{\mathbf{G}}_{\mathrm{eq,LS},q}^{(k,j)} \\ &= (\mathbf{X}^{(k)^H}\mathbf{X}^{(k)})^{-1}\mathbf{X}^{(k)^H}\mathbf{n}_q^{(j)} \quad q = 0, . \end{aligned} \tag{59}$$

Alternatively, an equivalent channel impulse response of kth user at jth antenna can be

represented as

$$\mathbf{G}_{\mathrm{eq},q}^{(k,j)} = \sqrt{P_{k,j}}\mathbf{h}_{\mathrm{eq},q}^{(k,j)} \quad q = 0, \tag{60}$$

where $\sqrt{P_{k,j}}$ and $\mathbf{h}_{\mathrm{eq},q}^{(k,j)}$ are the average received power and the normalized equivalent channel impulse response with elements of $E[|h_{\mathrm{eq},q}^{(k,j)}|^2] = 1$. Consequently, the channel estimation error of the signal of kth user at jth branch depends on the ratio of the power of the kth user's signal $P_{k,j}$ to the power of the noise at jth antenna branch $\sigma_{n_j}^2$, $\mathcal{E}_{\mathrm{eq},q}^{(k,j)} \propto P_{k,j}/\sigma_{n_j}^2$.

For the comparison of the performance of the proposed receiver in balanced and imbalanced CIR conditions at receivers with two antenna branches, we assumed that the power of the desired signal is equally allocated over all antenna branches, and the receiver expects imbalanced channel estimation errors across antenna branches due to the imbalanced interfering signal powers across antenna branches.

4.5 Numerical Results

4.5.1 Simulation Setup

The performance of the JD IRC-DDFSE receiver has been tested for the downlinks of GSM (Group Special Mobile) and EDGE (Enhanced Data rate for GSM Evolution) systems for binary and non-binary (8-psk) systems, respectively. Both GSM and EDGE use Gaussian shaping filter so that the sidelobe of the transmitted signal is fairly suppressed with fairly small penalty in bandwidth increase. Grey-coded 8-PSK EDGE symbols gets $3/8\pi$ cumulative phase shift before complex filtering to avoid abrupt phase transitions through origin as shown in Figure 23. Table 6 shows the summary of the radio interfaces of GSM/EDGE systems [3, 4].

EDGE uses existing GSM radio bands to offer wireless multimedia IP-based services and applications at theoretical maximum speeds of 384 kbps with a bit-rate of 48 kbps per timeslot and up to 69.2 kbps per timeslot in good radio conditions. It uses the same TDMA frame structure, logical channels and 200 kHz carrier bandwidth as today's GSM networks.

Through the simulations, a speech channel at full rate (TCH/FS) is selected so that the BER and FER performance of the proposed receiver can be evaluated after channel decoding. One frame of the TCH/FS consists of a 378-bit rate-1/2 convolutionally encoded

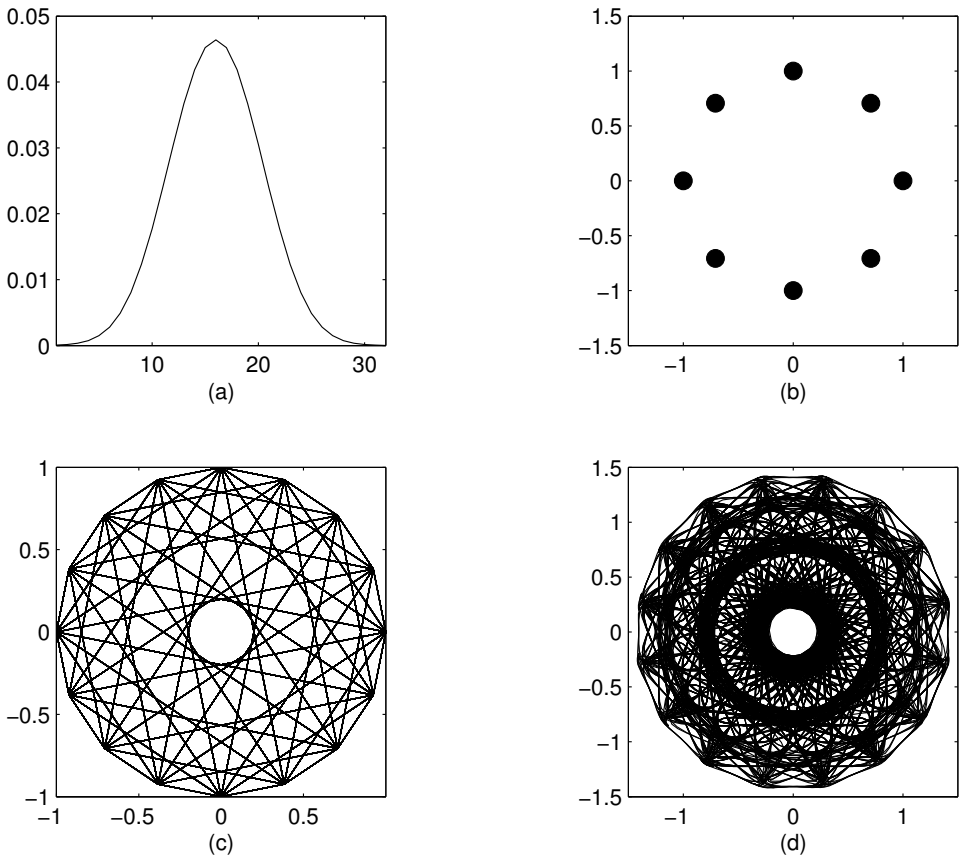

Figure 23: Constellation of the complex equivalent 8-PSK baseband signal of EDGE: (a) Gaussian shaping pulse, (b) Main pulse of Linearized GMSK pulse, (c) $3/8\pi$ cumulative phase shifted signal constellation of before complex filtering, and (d) Signal constellation after LGMSK complex filtering.

Table 6: Radio interface of GSM/EDGE

Parameters	Value
Frequency band	890-915 MHz (Up), 935-960 MHz (Down)
Multiple Access	FD/TDMA
Channel Spacing	200 KHz/channel
No. of timeslots	8/channel
Modulation format	GMSK (GSM)/8-PSK (EDGE)
Modulation index	h = 0.5
Normalized Bandwidth	BT = 0.3

information payload followed by 78 parity bits. The 456 bits are interleaved, reordered and transmitted in 8 bursts [2]. From the 8 TSSs used in GSM/EDGE systems, TSS0 and TSS1 are selected for two joint detected co-channel signals since they have a relatively large cross-correlation compared to other sequence pairs, and represent a worst case condition. The beam widths and number of equal power co-channel interferers in the closest tier are assumed 30° and one, and 120° and two for the case of NBAA arrays and conventional wide-beam sector antennas, respectively. Also, two additional CCI signals from outer tier are included. Timing and frequency synchronization is assumed.

In computer simulations, the typical rural (RA120), typical urban (TU50) and hilly terrain (HT120) models of the COST207 channel models with delay profiles at 120, 50 and 120 km/hr mobile speed, respectively, are used. The delay profile of the channel models are summarized in Table 7. The DDFSE algorithm uses 4 and 64-states ($\mu = 1$) for joint detection of two co-channel signals in GSM and EDGE systems, respectively.

Table 7: COST207 channel models

	Channel Model			Channel Model		
	RA	TU	HT	RA	TU	HT
Tap No.	Relative Time (μsec)			Avg. Relative Power (dB)		
1	0.0	0.0	0.0	0.0	-3.0	-10.0
2	0.1	0.2	0.1	-4.0	0.0	-8.0
3	0.2	0.5	0.3	-8.0	-2.0	-6.0
4	0.3	1.6	0.5	-12.0	-6.0	-4.0
5	0.4	2.3	0.7	-16.0	-8.0	0.0
6	0.5	5.0	1.0	-20.0	-10.0	0.0
7			1.3			-4.0
8			15.0			-8.0
9			15.2			-9.0
10			15.7			-10.0
11			17.2			-12.0
12			20.0			-14.0

4.5.2 BER and FER Performance

Figure 24 compares the BER performance of the proposed receiver to a conventional single user detection receiver with an NBAA array configuration. A CIR gain of approximately 10 to 15 and 1 to 3 dB is achieved over the conventional receiver for GSM and EDGE systems, respectively, at a decoded BER of 10^{-2}. Note that the joint detection structure achieves higher gain in a low CIR range than in a high CIR range. In highly dispersive channels (TU50,HT120), only a fraction of signal energy is considered in the channel taps used in DDFSE function. Therefore, the detection can be easily impaired by a small amount of noise-plus-interference and the diversity gain fades especially when the channel taps are in deep fade.

Figure 25 illustrates that the joint detection receiver is highly effective when it have NBAA preprocessor. The increased number of interfering signals receiving at conventional sector antenna configuration fairly degrades the BER performance of the proposed receiver. Also, by its nature, the narrow beam pattern of NBAA reduces the length of channel impulse response of the desired signal and escalates the gain from DDFSE structure even in highly dispersive channel conditions.

For services that use block-by-block CRC-check and retransmission schemes, the FER is widely accepted as a performance measurement since most QoS specifications are in terms of the FER. At 10% FER criterion, the joint detection technique yields 2 to 12 and 1 to 6 dB CIR gains over a conventional receiver for GSM and EDGE, respectively, as shown in Figure 26. The FER of a communication link depends on the received BER and the channel coding technique employed. Therefore, the achieved FER will be lowered in case of data packets normally protected by stronger channel coding than speech packets such as TCH/FS.

In synchronized networks, the delay offset is expected to be smaller than 3 symbol durations. Figure 27 illustrates that delay offset between the two co-channel signal bursts which are jointly detected has a relatively minor effect on BER performance in synchronized networks. Fractionally spaced structure of the receiver as well as the joint channel estimation diminishes the impairments from the delay offset on BER performance.

4.5.3 Performance Variation with Imbalanced CIR

For the imbalanced CIR conditions, the simulation results show that the performance of the receiver is optimal in balanced CIR conditions, and the BER performance gap between balanced and imbalanced conditions tends to increase as the average received CIR increases as shown in Figure 28. In contrast, the single detection receiver is virtually unaffected by the imbalanced conditions as shown in Figure 29. The performance loss of the joint detection receiver from imbalanced CIR conditions can be explained by the nature of joint channel estimation. In general, the channel estimation error of the interfering signal in joint detection receivers results in error floor in the BER of the desired signal in high CIR region. For the proposed receiver in imbalanced CIR conditions, an interfering signal arriving at one antenna branch experiences higher CIR and suffers larger channel estimation error than the other one arriving at antenna branch of lower CIR. This large error contributes to the decision metric, especially in high CIR regions. The desired signal experiences similar asymmetric channel estimation errors in low CIR region. However, the outcome of an equal amount of channel estimation error in a low BER range is more critical than that in a high BER range.

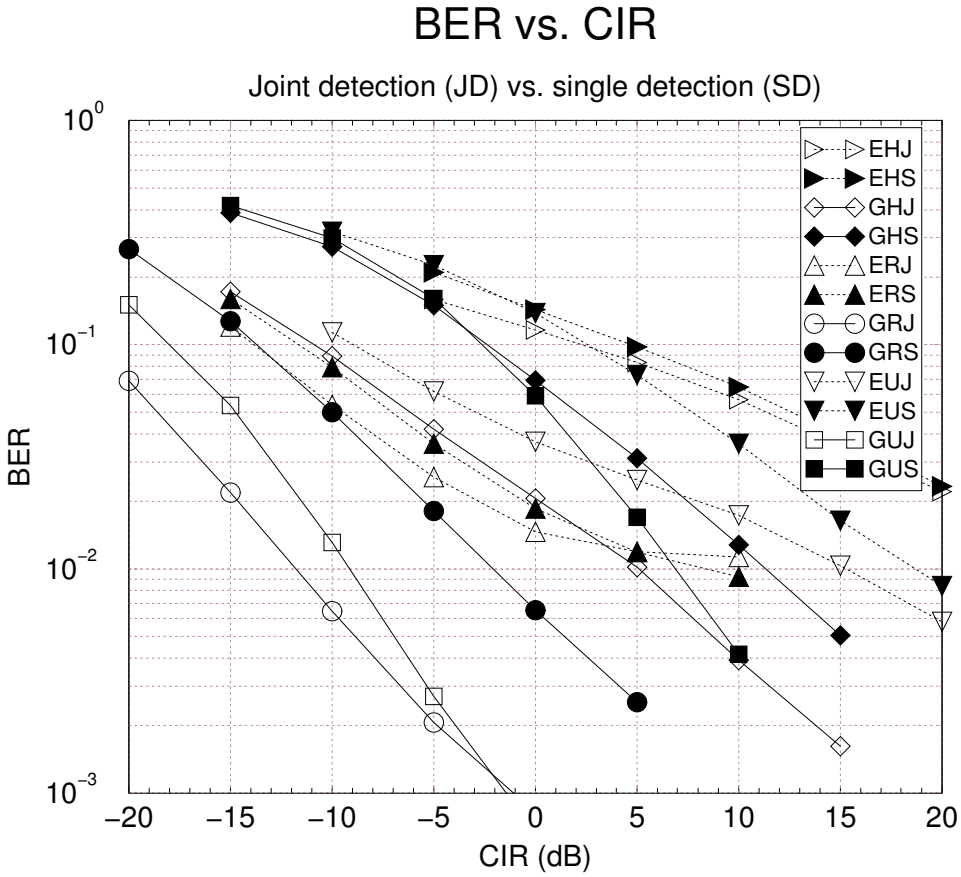

Figure 24: BER performance of the JD IRC-DDFSE receiver compared to single detection; $J = 2$, $E_b/N_0 = 30$ dB, Legend: xyz, x = G (GSM) or E (EDGE), y = R (RA120), U (TU50) or H (HT120), z = J (Joint detection) or S (Single detection).

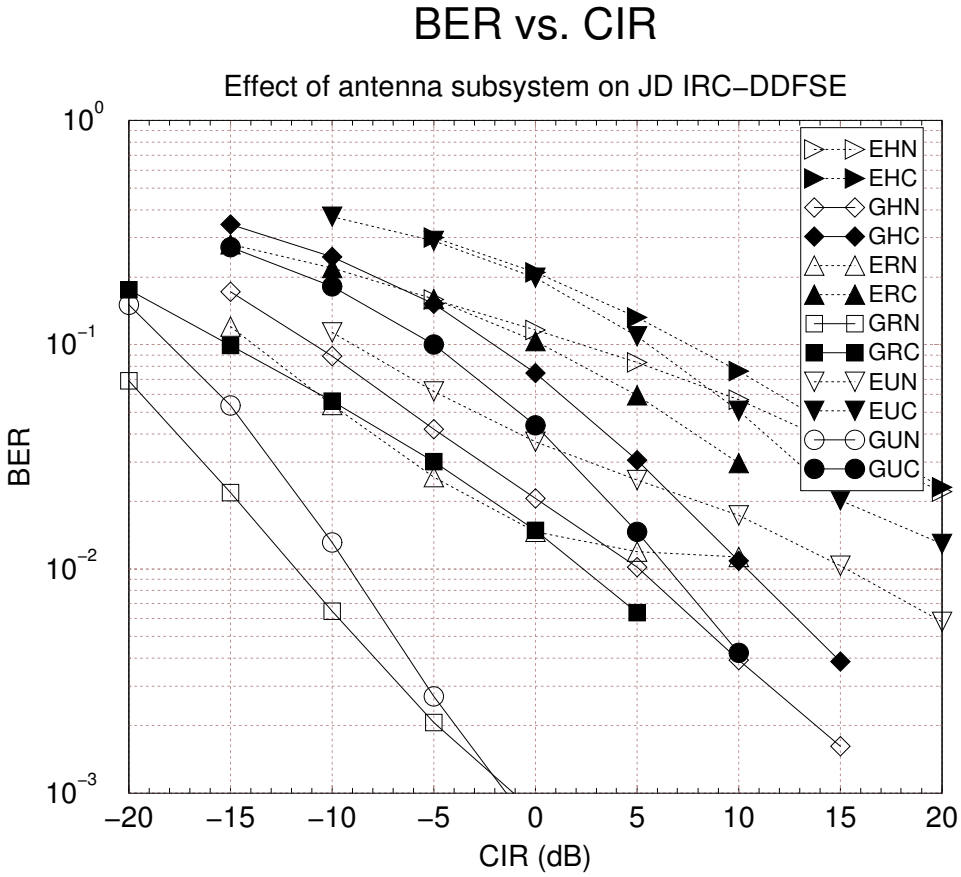

Figure 25: BER performance of the JD IRC-DDFSE receiver with different antenna subsystem models; $J = 2$, $E_b/N_0 = 30$ dB, Legend: xyz, x = G (GSM) or E (EDGE), y = R (RA120), U (TU50) or H (HT120), z = N (NBAA array) or C (Conventional antenna).

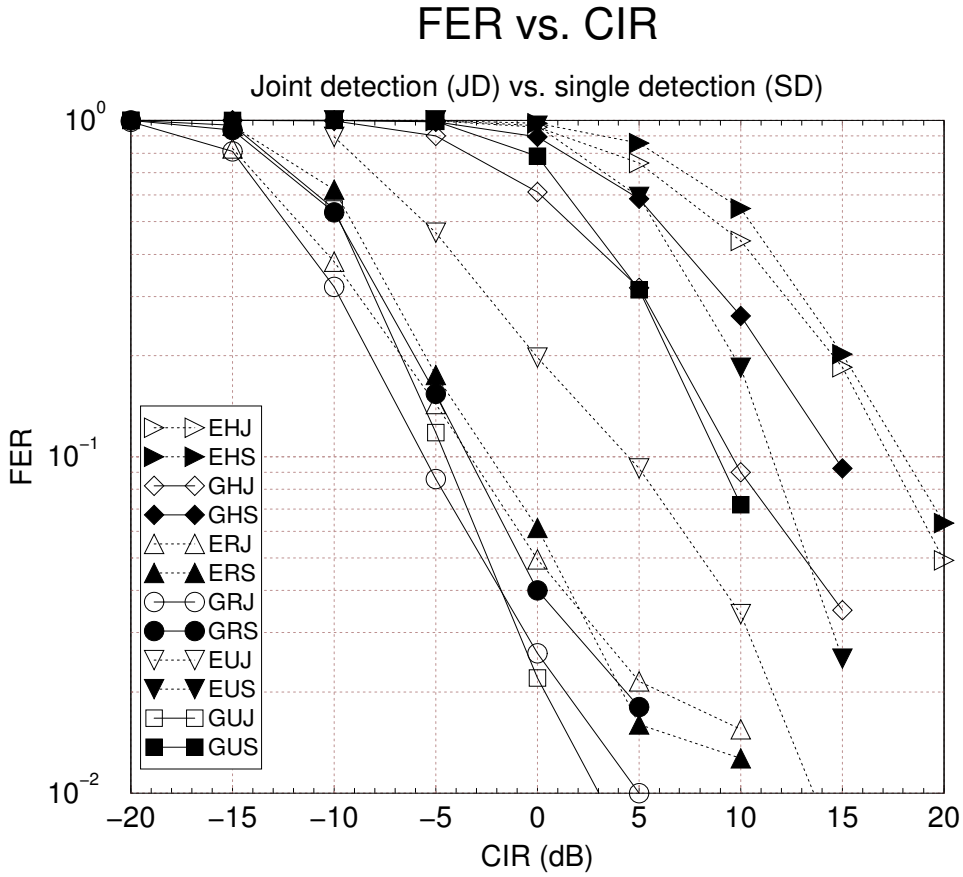

Figure 26: FER performance of the soft output JD IRC-DDFSE receiver; $J = 2$, $E_b/N_0 =$ 30 dB, Legend: xyz, x = G (GSM) or E (EDGE), y = R (RA120), U (TU50) or H (HT120), z = J (Joint detection) or S (Single detection).

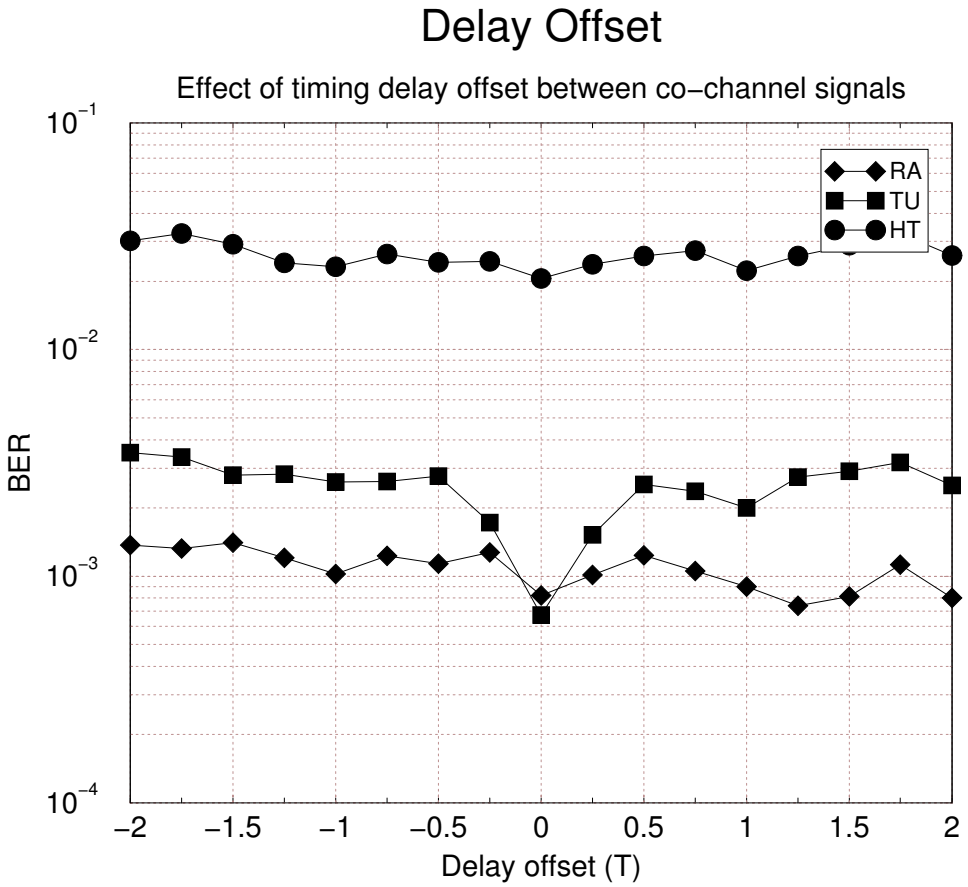

Figure 27: Effect of the timing offset between two jointly detected co-channel signals for GSM system; $J = 2$, $E_b/N_0 = 30$ dB, $CIR = 0$ dB, Legend: RA (RA120), TU (TU50) or HT (HT120).

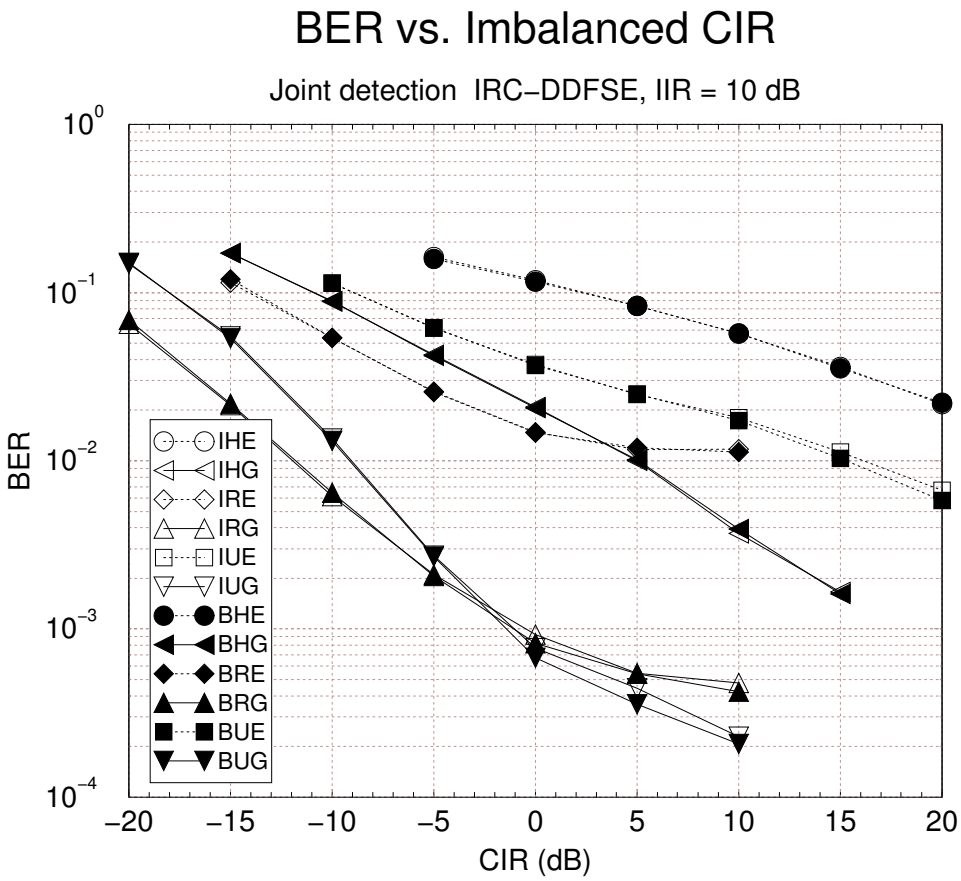

Figure 28: Effect of imbalanced CIR on JD IRC-DDFSE receiver; $J = 2$, $E_b/N_0 = 30$ dB, $IIR = 10$ dB, Legend: xyz, x = I (Imbalanced) or B (Balanced), y = R (RA120), U (TU50) or H (HT120), z = E (EDGE) or G (GSM).

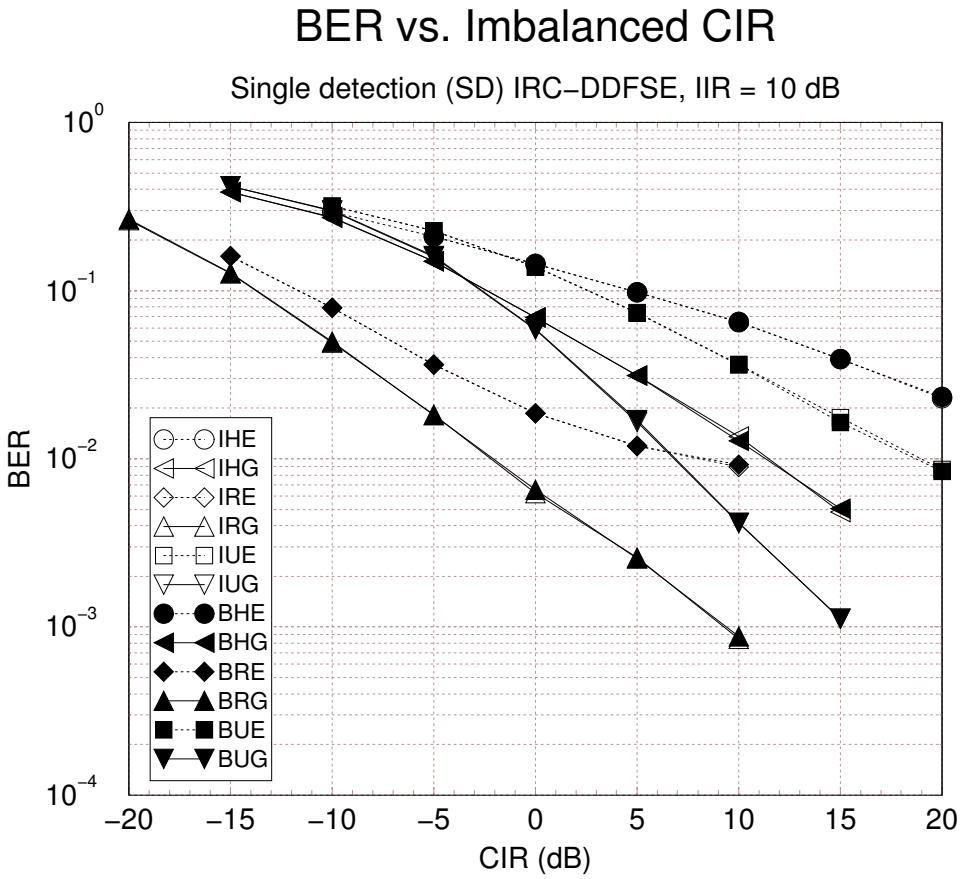

Figure 29: Effect of imbalanced CIR on conventional single detection IRC-DDFSE receiver; $J = 2$, $E_b/N_0 = 30$ dB, $IIR = 10$ dB, Legend: xyz, x = I (Imbalanced) or B (Balanced), y = R (RA120), U (TU50) or H (HT120), z = E (EDGE) or G (GSM).

CHAPTER V

INTERFERENCE MITIGATION IN MIMO SYSTEMS BY SUBSET ANTENNA TRANSMISSION

5.1 Introduction

The capacity of a multiple-input multiple-output (MIMO) system depends on the number of transmit/receive antennas, the correlation between the channel coefficients of individual paths, and the method for allocating the power over the transmit antennas [147]. If channel state information (CSI) is available at the transmitter, power allocation by a water-filling algorithm is known to optimize capacity for AWGN channels. Likewise, if CSI is not available, equal power distribution is optimum for AWGN channels. However, if co-channel interference (CCI) is present, these techniques no longer optimize capacity.

Previous studies on the techniques of power allocation in MIMO systems have focused on the characteristics of the propagation channel matrix. In [106], a game theoretic approach is introduced to verify the optimality of water-filing and equal-power methods in with- and without-CSI at transmitter cases, respectively. On the other hand, the observation of non-uniform eignemodes and associated eigenvalues of channel matrices prompted other approaches that use non-equal power distribution over selected subset of transmit antennas [22,111]. To maximize the information channel capacity, adaptive modulation on eigenmodes and adaptive bit loading techniques with minimum mean square error (MMSE) criterion are introduced with non-uniform power loading [61,74]. Also, various transmit/receive antenna selection techniques for ZF and MMSE receivers have been proposed to maximize received SINR and channel capacity by using decision metric computed from the channel matrix [57,69,70].

CCI by nature is colored noise with non-zero off-diagonal terms in its covariance matrix. These correlations spoil the optimality of water-filing method when CSI of CCI is not

available at transmitters [48, 126]. The recent work by Blum [26] has taken an initial step on the problem of power allocation in the presence of CCI, by switching between two power allocation strategies; i) transmitting equal-power over all antennas, and ii) transmitting all-power over one antenna. Another approach uses MIMO multiuser detection to process the co-channel signals [64, 153]. However, Blum's approach suffers from a large capacity loss as the number of transmit antennas increases, while the approach of Goldsmith *et al.* is only feasible when full CSI of all co-channel signals is available [64].

This study investigates the performance of an adaptive practical power distribution scheme by using subset antenna transmission (SAT) for MIMO systems. The introduction of the SAT scheme is motivated by the observation of reduced eigenmodes in severely perturbed MIMO channels [120]. In the SAT scheme, the transmit power is distributed equally across subset of the transmit antennas. The subset is determined from criteria generated from CSI of the desired signal, while CSI of the CCI is not needed. This simplicity makes the SAT scheme beneficial in most practical systems where the CSI of CCI is not available. The capacity gain from the increased transmit power per antenna with SAT is evaluated by computer simulations with V-BLAST systems. Also, we investigated the performance of the space-time diversity coding (STDC) scheme in terms of interference mitigation for comparison. While the STDC exploits the gain from spatial and temporal diversity at the cost of increased redundancy, the SAT scheme use only the property of spatial multiplexing of MIMO systems.

The remainder of this chapter is organized as follows: Section 5.2 provides system and channel models of MIMO systems in the presence of CCI and noise. Section 5.3 introduces phenomena of reduced eigenmodes in terms of the condition number and the effective eigenmodes of the channel matrix. In Section 5.4, the capacity gain from adaptive power allocation with SAT is characterized. Section 5.5 presents an application of the SAT scheme to a 4×4 V-BLAST MIMO system. Section 5.6 probes the capability of a space-time diversity coding scheme in terms of CCI mitigation in MIMO systems. Section 5.7 discusses the performance of the proposed power allocation schemes evaluated on 4×4 and 2×2 MIMO systems by computer simulations.

5.2 Channel Capacity with Equivalent Channel Matrix

5.2.1 System and Channel Models

The system under consideration has a single-user link of interest affected by CCI from another user. The user of interest and interfering user have M transmit and N receive antennas, respectively. In a flat faded MIMO system, the received signal vector $\mathbf{y}_{N\times 1}$ is

$$\begin{aligned} \mathbf{y} &= \sqrt{P_T}\mathbf{H}\mathbf{s} + \sqrt{P_I}\mathbf{H}_I\mathbf{s}_I + \mathbf{w} \\ &= \mathbf{H}\mathbf{s} + \mathbf{n} \end{aligned} \tag{61}$$

where $\mathbf{H}_{N\times M}$, $\mathbf{s}_{M\times 1}$ and P_T are the MIMO channel matrix and transmitted signal vector and power of the user of interest, respectively, $\mathbf{H}_{I\ N\times M}$, $\mathbf{s}_I$ and P_I are the channel matrix, transmit signal, and power of the interfering signal, respectively, and $\mathbf{w}_{N\times 1}$ is the thermal noise with covariance matrix $\mathrm{E}\{\mathbf{w}\mathbf{w}^{\mathbf{H}}\} = \sigma^2\mathbf{I}_N$ where H denotes conjugate transpose. The vector $\mathbf{n}_{N\times 1}$ is the interference-plus-noise vector.

The channel matrices $\mathbf{H}$ and $\mathbf{H}_I$ are mutually independent, and assumed to be quasi-static. The elements in $\mathbf{H}$ and $\mathbf{H}_I$ are independent identically distributed (i.i.d.) zero-mean complex Gaussian random variables with unit variance. Also, the signal of the user of interest, interferer's signal and the thermal noise, $\mathbf{s}$, $\mathbf{s}_I$, and $\mathbf{w}$, respectively, are mutually independent. The spatial covariance matrix of interference-plus-noise is $\mathbf{K}^n = \mathrm{E}\{\mathbf{n}\mathbf{n}^H\}$. The covariance matrix of the user of interest is $\mathbf{\Phi} = \mathrm{E}\{\mathbf{s}\mathbf{s}^H\}$. The covariance matrix of the received signal component of the user of interest is $\mathbf{K}^d = \mathbf{H}\mathbf{\Phi}\mathbf{H}^H$.

5.2.2 Mutual Information

Assuming the interference has a Gaussian distribution, the optimal input distribution of $\mathbf{s}$ is Gaussian [34, 134]. The mutual information between the channel input $\mathbf{s}$ and output $\mathbf{y}$ is

$$\begin{aligned}
\mathcal{I} &= \log_2 \det(\mathbf{K}^d + \mathbf{K}^n) - \log_2 \det(\mathbf{K}^n) \\
&= \log_2 \det(\mathbf{K}^d (\mathbf{K}^n)^{-1} + \mathbf{I}_N) \\
&= \log_2 \det(\mathbf{H}\mathbf{\Phi}\mathbf{H}^H (\mathbf{K}^n)^{-1} + I_N) \\
&= \log_2 \det(((\mathbf{K}^n)^{-1/2}\mathbf{H})\mathbf{\Phi}((\mathbf{K}^n)^{-1/2}\mathbf{H})^H + \mathbf{I}_N) \\
&= \log_2 \det(((\mathbf{K}^n)^{-1/2}\mathbf{H})^H((\mathbf{K}^n)^{-1/2}\mathbf{H})\mathbf{\Phi} + \mathbf{I}_M) \\
&= \log_2 \det(\hat{\mathbf{H}}^H\hat{\mathbf{H}}\mathbf{\Phi} + \mathbf{I}_M) \qquad (62)
\end{aligned}$$

where the determinant identity $\det(\mathbf{AB} + \mathbf{I}) = \det(\mathbf{BA} + \mathbf{I})$ is used in the fifth equality. Eq. (62) represents the mutual information of the equivalent channel $\hat{\mathbf{H}} = (\mathbf{K}^n)^{-1/2}\mathbf{H}$.

5.2.3 CSI Available at Transmitter

When CSI of the equivalent channel $\hat{\mathbf{H}}$ is available at the transmitter, the channel capacity is achieved by a water-filling solution, where $\mathbf{\Phi}$ is chosen to maximize the mutual information subject to the power constraint $\mathrm{tr}(\mathbf{\Phi}) \leq \mathrm{P_T}$. Since $\hat{\mathbf{H}}^H\hat{\mathbf{H}}$ is Hermitian, it can be diagonalized, i.e., $\hat{\mathbf{H}}^H\hat{\mathbf{H}} = \mathbf{U}\mathbf{\Lambda}\mathbf{U}^H$, with unitary matrix $\mathbf{U}$ and non-negative diagonal matrix $\mathbf{\Lambda} = \mathrm{diag}(\lambda_1, \ldots, \lambda_M)$. The mutual information in (62) can be rewritten as

$$\begin{aligned}
\mathcal{I} &= \log_2 \det(\mathbf{U}\mathbf{\Lambda}\mathbf{U}^H\mathbf{\Phi} + \mathbf{I}_M) \\
&= \log_2 \det(\mathbf{\Lambda}^{1/2}\mathbf{U}^H\mathbf{\Phi}\mathbf{U}\mathbf{\Lambda}^{1/2} + \mathbf{I}_M). \qquad (63)
\end{aligned}$$

Since $\mathbf{U}^H\mathbf{\Phi}\mathbf{U}$ is positive definite if and only if $\mathbf{\Phi}$ is, and $\mathrm{tr}(\mathbf{U}^{\mathrm{H}}\mathbf{\Phi}\mathbf{U}) = \mathrm{tr}(\mathbf{\Phi})$, the channel capacity is achieved when $\mathbf{U}^H\mathbf{\Phi}\mathbf{U}$ is diagonal

$$\mathbf{U}^H\mathbf{\Phi}\mathbf{U} = \mathrm{diag}(p_1, \ldots, p_M). \qquad (64)$$

The optimal diagonal entries of $\mathbf{U}^H\mathbf{\Phi}\mathbf{U}$ can be found via the water-filling process

$$p_i = (\mu - \lambda_i^{-1})^+, i = 1, \ldots, M \qquad (65)$$

where μ is chosen to satisfy the sum constraint $\sum_i p_i = P_T$, and $(\cdot)^+$ is zero when the argument is negative. The corresponding channel capacity is

$$\mathcal{C} = \max_{\{p_i\}} \mathcal{I} = \sum_{i=1}^{M} \log_2(1 + p_i \lambda_i). \tag{66}$$

5.2.4 CSI not Available at Transmitter

If CSI is not available at the transmitter, the optimal transmit covariance is $\mathbf{\Phi} = (P_T/M)\mathbf{I}_M$, and the channel capacity is

$$\mathcal{C} = \log_2 \det \left(\frac{P_T}{M} \hat{\mathbf{H}} \hat{\mathbf{H}}^H + \mathbf{I}_N \right). \tag{67}$$

In a noise-limited or white-interference conditions, $\mathbf{K}^n = \sigma^2 \mathbf{I}$ and the capacity is

$$\mathcal{C} = \log_2 \det \left(\frac{P_T}{\sigma^2 M} \mathbf{H} \mathbf{H}^H + \mathbf{I}_N \right). \tag{68}$$

5.3 Eigenmodes, Condition Number and Power Allocation

5.3.1 Eigenmodes of Channel Matrix

The channel matrix $\mathbf{H}^{\in N \times M}$ linking the transmitter and the receiver can be represented in terms of a singular value decomposition (SVD): $\mathbf{H} = \mathbf{U}\mathbf{\Lambda}\mathbf{V}^H$, where $\mathbf{U}^{\in N \times N}$ and $\mathbf{V}^{\in M \times M}$ are complex unitary matrices, and $\mathbf{\Lambda}^{\in N \times M} = \text{diag}(\sqrt{\lambda_1}, \ldots, \sqrt{\lambda_r}, 0, \ldots, 0)$ is a diagonal matrix, where the nonzero diagonal elements are the square roots of the eigenvalues of the channel covariance matrix $\mathbf{K} = \mathbf{H}\mathbf{H}^H$. The number of nonzero eigenvalues is equal to the rank of the covariance matrix, $r \leq \min\{M, N\}$. With orthogonal SVD, the $N \times M$ MIMO channel can be decomposed into r independent single-input single-output (SISO) channels, called *eigenmodes* or *eigenchannels*, where the received signal on the ith channel is $y_i = \sqrt{\lambda_i} s_i + n_i$. Each eigenvalue represents the amount of power that is transferred through the channel into the direction coordinated by the corresponding eigenvector. Of course the eigenvalues are unequal for a random realization of $\mathbf{H}$. When a subset of eigenvalues of a matrix are negligible in magnitude compared to the others, the matrix transformation can be well approximated by the set of eigenvalues of significant magnitudes and the corresponding eigenvectors [105]. In such a case, the condition number of the channel matrix is a useful indicator of unequal eigenmodes.

5.3.2 Condition Number

The condition number of matrix $\mathbf{A}$ is defined as [78]

$$\kappa(\mathbf{A}) = \rho(\mathbf{A})\rho(\mathbf{A}^{-1}) = |\lambda_{max}(\mathbf{A})/\lambda_{min}(\mathbf{A})| \tag{69}$$

where $\rho(\mathbf{A}) \equiv \max\{|\lambda| : \ \lambda \text{ is an eigenvalue of } \mathbf{A}\}$ is the *spectral radius* of a matrix $\mathbf{A}$. Condition number often used to measure the invertibility of a matrix, i.e., a matrix having a larger condition number is more likely to be singular than one having a smaller condition number. A large condition number generally indicates the presence of a dominant eigenmode in a given matrix as well. Figure 30 shows the probability density function (pdf) of the condition number with different signal-to-interference ratio (SIR), P_T/P_I, conditions at a signal-to-noise ratio (SNR) P_T/σ^2 of 30 dB. Each pdf is obtained from $10,000$ independent channel realizations. Observe that the mean value of condition number increases/decrease as the SIR increases/decreases. This means that the MIMO channel is likely to be dominated by smaller number of eigenmodes as the SIR decreases.

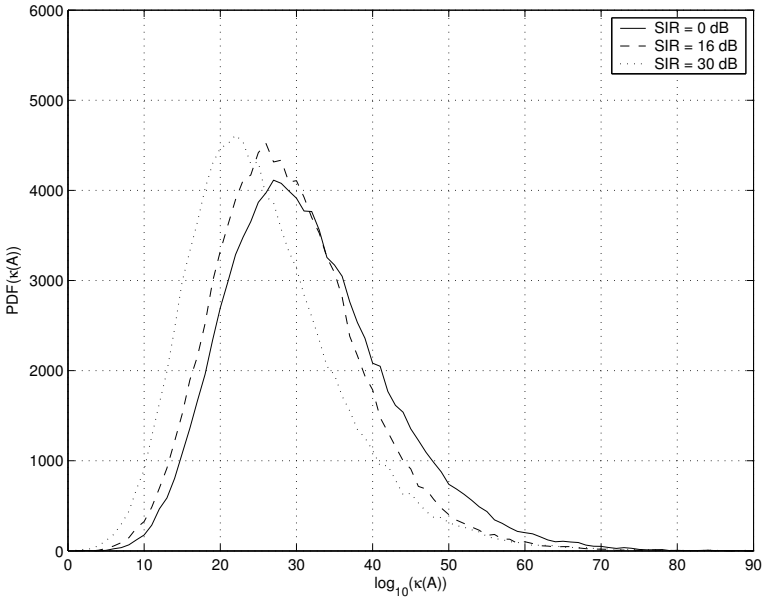

Figure 30: A pdf of condition number as a function of received signal-to-interference ratio (SIR) at SNR = 30 dB.

5.3.3 Effective Eigenmodes

The dominance of the largest eigenmode in the low SIR regime is intensified by the nature of the water-filling algorithm. Elimination of all but the few largest eigenmodes in the low SNR regime has been observed previously [74,134], and is apparent in Figure 31 as well. In Figure 31(a), ill-conditioned (large $\kappa(\mathbf{A})$) channel matrix pour most of the power into the small deepest buckets (eigenmodes) as the transmit power reduces from P_H to P_L. However, the channel matrix $\mathbf{A}$ is well-conditioned (small $\kappa(\mathbf{A})$), and most of the eigenmodes are carrying information with corresponding allocated transmit power even with reduced total power level (Figure 31(b)).

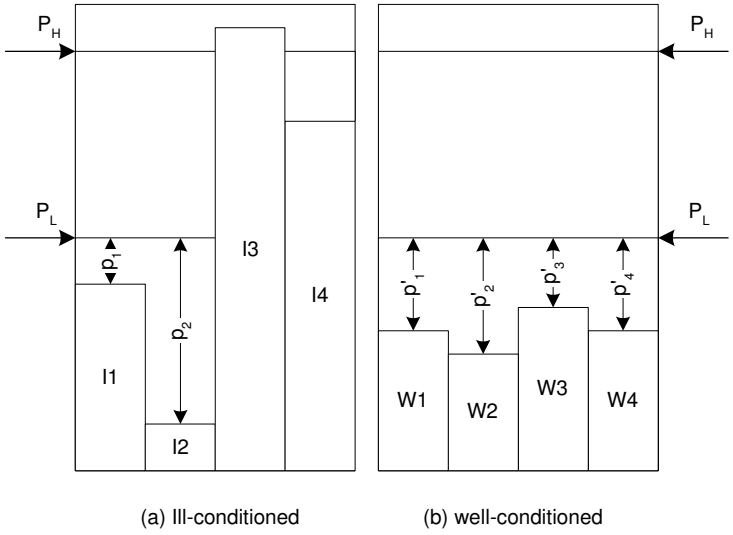

Figure 31: Power allocation in water-filling method: (a) ill-conditioned (large $\kappa(\mathbf{A})$), (b) well-conditioned (large $\kappa(\mathbf{A})$). P_L, and P_H are power level for low and high SIR conditions.

Let us define the number of effective eigenmodes η as

$$\eta = E\{\#\text{ of eigenmodes } \lambda_i \text{where } p_i \neq 0 \mid \gamma\}. \tag{70}$$

Figure 32 plots the number of effective eigenmodes η in a 4×4 MIMO system against the SIR and SNR. As predicted above, the number of effective eigenmodes decreases from four to one as the SNR and SIR decreases. When CSI is available at transmitter, the water-filling method achieves capacity by properly controlling the fraction of power assigned to each eigenmode. However, if CSI of the equivalent channel $\hat{\mathbf{H}}$ is not available at the transmitter

and all transmit antennas are assigned equal power, a capacity loss arises from the unequal eigenmodes. Therefore, we need to improve the equal-power algorithm in this case.

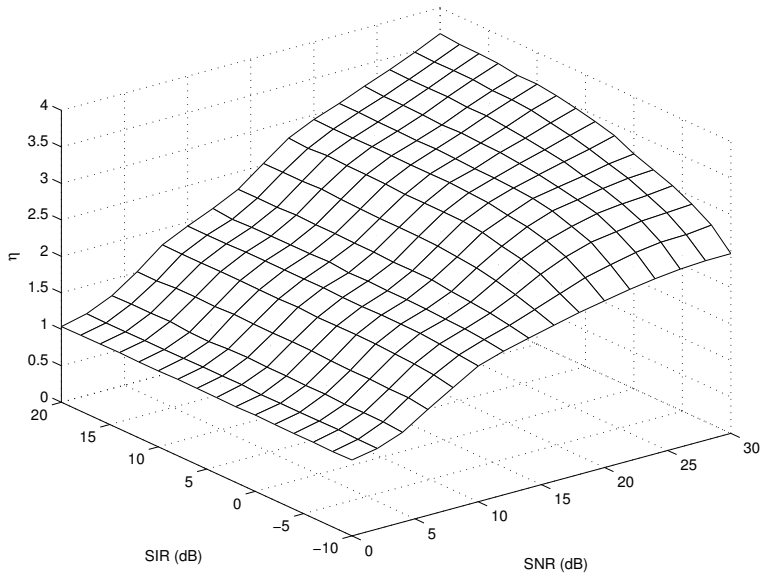

Figure 32: Average number of effective eigenmodes: Both transmitter and receiver are equipped with four antennas, $M = N = 4$.

5.4 Subset Antenna Transmission

Under ideal conditions where the CSI of desired and interfering signals are available at transmitters, the water-filling method achieves capacity regardless the received SIR and the condition number of the equivalent channel matrix $\hat{\mathbf{H}}$. However, in many practical systems, CSI of interfering signal is not available at the transmitter. In such cases, an equal power distribution across the transmit antennas is the most feasible power allocation strategy. The SAT method uses an equal-power distribution as well, but only uses a subset containing $\hat{M}$ of the M antennas.

5.4.1 Capacity with Subset Antenna Transmission

The capacity of a MIMO system employing the equal-power distribution scheme over M transmit antennas is [52]

$$\begin{aligned} \mathcal{C}_M &= \log_2 \det\left(\frac{P_T}{M}\hat{\mathbf{H}}\hat{\mathbf{H}}^H + \mathbf{I}\right) \\ &= \sum_{i=1}^{M} \log_2\left(\frac{P_T}{M}\lambda_i + 1\right) \end{aligned} \tag{71}$$

where $\lambda_1 > \ldots > \lambda_M$ are eigenvalues of covariance matrix $\hat{\mathbf{H}}\hat{\mathbf{H}}^H$ and P_T is the total transmit power.

For an SAT scheme with $\hat{M} < M$ antennas, the capacity can be redefined as

$$\mathcal{C}_{SAT} = \sum_{i=1}^{\hat{M}} \log_2\left(\frac{P_T}{\hat{M}}\tilde{\lambda}_i + 1\right) \tag{72}$$

where $\tilde{\lambda}_1 > \ldots > \tilde{\lambda}_{\hat{M}}$ are eigenvalues of covariance matrix $\tilde{\mathbf{H}}\tilde{\mathbf{H}}^H$ generated by the channel matrix between selected transmit antennas and all receive antennas $\tilde{\mathbf{H}}$. With transmit power P_T equally allocated over all (M) and a subset $(\hat{M})$ transmit antennas, the capacity gap between two schemes is depends on by the two factors - increase in transmit power and changed eigenvalues. Initial observation on this property can be found in Sandhu *et al.*'s study [120].

- *Example*: Uncoupled channels

For ideal uncoupled channels, only the diagonal elements of channel matrix has non-zero values, and it results in M orthogonal parallel SISO channels. Under this ideal condition, eigenvalues of $\tilde{\mathbf{H}}\tilde{\mathbf{H}}^H$ is a subset of the eigenvalues of $\hat{\mathbf{H}}\hat{\mathbf{H}}^H$. Since capacity increases by one as the transmit power doubles in high SIR/SNR regions, the channel capacity of the SAT scheme with $\hat{M} = M/2$ can be rewritten as

$$\mathcal{C}_{SAT} < \sum_{i=1}^{\hat{M}} \log_2\left(\frac{P_T}{M}\lambda_i + 1\right) + \hat{M}. \tag{73}$$

Thus, the difference in channel capacity $\Delta\mathcal{C}$ is

$$\begin{aligned} \Delta\mathcal{C} &= \mathcal{C}_{SAT} - \mathcal{C}_M \\ &< \hat{M} - \sum_{i=\hat{M}+1}^{M} \log_2\left(\frac{P_T}{M}\lambda_i + 1\right). \end{aligned} \tag{74}$$

5.4.2 Subset Antenna Selection

The selection of the antenna subset is an important factor that changes the capacity of the proposed power allocation technique with SAT. The size of subset antenna set, $\hat{M}$, can be specified by determining the average number of effective eigenmodes through computer simulation. Without loss of generality, we assume that only the CSI of the desired signal is available at the transmitter and receiver in the presence of unknown CCI. With this condition, we employed norm-based and crosscorrelation-based antenna selection criteria computed from the CSI of the desired signal in the computer simulations for their simplicity and practicality. Since the research on the antenna selection criteria is beyond the scope of this study and we focused on the capacity gain from increased power per selected transmit antennas, more complex but capacity maximizing selection techniques which were proposed in previous studies [57, 69, 70] are not considered in this study.

5.4.2.1 Maximum Modulus

This norm-based techniques chooses $\hat{M}$ antennas having the largest modulus of the channel coefficient vector, $\mathcal{M}_i$, for transmission, where

$$\mathcal{M}_i = \sqrt{\sum_{j=1}^{N} h_{ij} h_{ij}^H}, \quad 1 \leq i \leq M \tag{75}$$

where h_{ij} is the channel coefficient from ith transmit to jth receive antenna.

5.4.2.2 Minimum Cross-correlation

Another method for choosing the optimal antenna subset is to selecting antennas having the minimum cross-correlation

$$\mathcal{R}_{ij} = \sum_{k=1}^{N} h_{ik} h_{jk}^H, \quad i \neq j. \tag{76}$$

5.4.2.3 Random Selection

A randomly selected $\hat{M}$ antenna subset can be a last resort for the worst case, where even the CSI of desired signal may not available at the transmitter.

Table 8: SAT antenna selection criteria and corresponding capacities

	Ant. Sel.	Capacity
EP1R	1 Random	$\log_2 \det(P_T \hat{\mathbf{H}}_{r1} \hat{\mathbf{H}}_{r1}^H + \mathbf{I}_N)$
EP1M	1 Max $\mathcal{M}_i$	$\log_2 \det(P_T \hat{\mathbf{H}}_{m1} \hat{\mathbf{H}}_{m1}^H + \mathbf{I}_N)$
EP2R	2 Random	$\log_2 \det(\frac{P_T}{\hat{M}} \hat{\mathbf{H}}_{r2} \hat{\mathbf{H}}_{r2}^H + \mathbf{I}_N)$
EP2M	2 Max $\mathcal{M}_i s$	$\log_2 \det(\frac{P_T}{\hat{M}} \hat{\mathbf{H}}_{m2} \hat{\mathbf{H}}_{m2}^H + \mathbf{I}_N)$
EP2C	2 Min $\mathcal{R}_i s$	$\log_2 \det(\frac{P_T}{\hat{M}} \hat{\mathbf{H}}_{c2} \hat{\mathbf{H}}_{c2}^H + \mathbf{I}_N)$
EP4	All 4	$\log_2 \det(\frac{P_T}{M} \hat{\mathbf{H}} \hat{\mathbf{H}}^H + \mathbf{I}_N)$

5.4.3 Theoretical Capacity by Computer Simulations

The computer simulations by Monte Carlo method is provided to evaluate the performance of the SAT method in theoretical viewpoint. The MIMO system for simulations has 4×4 antennas, and the SAT scheme uses two ($\hat{M} = 2$) antennas for transmission. The subset selection criteria and their capacity is listed in Table 8.

5.5 SAT in V-BLAST Type Receiver

5.5.1 V-BLAST Architecture

To achieve the higher capacity predicted by previous studies using MIMO schemes, the architectures known as vertically layered BLAST (D/V-BLAST) are proposed [51, 147]. The data stream is demultiplexed into M substreams, and each substream is encoded into constellation symbols and fed into a transmitter directly connected into its corresponding transmit antenna in $M \times N$ V-BLAST MIMO systems.

The encoding process is a simple bits-to-symbol mapping, and all substreams are mapped independently. The total transmit power is equally divided into M transmitters. The channel matrix H is assumed to remain constant, i.e., quasi-stationary, during the transmission of a whole data block. The independent transmission of data streams across the transmit antennas enables the receiver decodes each symbol of data streams in an arbitrary order. As V-BLAST does not use orthogonality in transmitters, the capacity of the V-BLAST scheme is achieved only from the richness of channels. The co-channel signals transmitted from different antennas are decorrelated to each other by exploiting the propagation environment

itself.

5.5.2 Decoding Process of V-BLAST

The detection process of the V-BLAST scheme estimates the transmitted symbols $\mathbf{s}$ given received signal vector $\mathbf{y}$ and channel matrix $\mathbf{H}$ in

$$\mathbf{y} = \mathbf{H}\mathbf{s} + \mathbf{n}. \tag{77}$$

For the SAT scheme, the $\hat{M}$ elements of the transmitted symbol vector $\mathbf{s}$ are assumed to be uncorrelated. The channel matrix is assumed to be known to the receiver, and to be full rank. The decision process involves linear nulling and estimated symbol cancellation. Nulling is performed by linearly weighting the received signals so as to satisfy performance criteria, such as MMSE and ZF. Non-linear technique of symbol cancellation brings superior performance by subtracting out the interference from already-detected components of $\mathbf{s}$, and results in a modified received signal vector, in which fewer interferers are present.

5.5.2.1 Nulling

Denoting the ith column of $\mathbf{H}$ as $\mathbf{H}_i$ the received signal vector can be rewritten as

$$\mathbf{y} = s_1\mathbf{H}_1 + s_2\mathbf{H}_2 + \ldots + s_{\hat{M}}\mathbf{H}_{\hat{M}} + \mathbf{n} \tag{78}$$

where s_i is the transmitted symbol from the ith transmit antenna. For ZF nulling, the nulling vector $\mathbf{w}_i$ is chosen such that

$$\mathbf{w}_i^T\mathbf{H}_j = \delta_{ij} \tag{79}$$

where δ is Kronecker delta. Thus the decision statistic for the ith substream is $y_i = \mathbf{w}_i^T\mathbf{y}$. Then the soft or hard decision can be made on y_i to estimate the transmitted symbol

$$\hat{s}_i = \mathcal{Q}(y_i) \tag{80}$$

where $\mathcal{Q}(\cdot)$ denotes the slicing operation appropriate to the constellation in use.

5.5.2.2 Successive Interference Cancellation

Denoting the received vector $\mathbf{y}$ by $\mathbf{y}_1$, if the nulling vector is $\mathbf{w}_1$, then the decision statistic for the estimation of the first symbol x_1 is

$$d_1 = \mathbf{w}_1^T \mathbf{y}_1. \tag{81}$$

Then the interference from the estimated symbol $\hat{s}_1 = \mathcal{Q}(d_1)$ on the other symbols can be subtracted as

$$\mathbf{y}_2 = \mathbf{y}_1 - \hat{s}_1 \mathbf{H}_1 \mathbf{y}_1. \tag{82}$$

assuming that $\hat{s}_1$ is correctly detected. The next symbols $s_2, \ldots, s_{\hat{M}}$ are detected by finding $\mathbf{w}_2, \ldots, \mathbf{w}_{\hat{M}}$ and subtracting the replica of the previously estimated symbols, $\hat{s}_2 \mathbf{H}_2, \ldots, \hat{s}_{\hat{M}} \mathbf{H}_{\hat{M}}$. The performance of the V-BLAST scheme depends on the error propagation from incorrect symbol decision from the early stages. Consequently, an optimal detection ordering is required to minimize the detection errors in the subsequent detection stages.

5.5.2.3 Detection Ordering

A simple but effective ordering is based on the postdetection SNR of each substream to minimize the error propagation by detecting *stronger* symbols first. The SNR for the ith detected symbol of vector $\mathbf{y}$ is given by [147]

$$\rho_i = \frac{E\{|s_i|^2\}}{\sigma^2(\| \mathbf{w}_i \|^2)} \tag{83}$$

where σ^2 is the noise power. If all the substreams have the same expected signal and noise power, the postdetection SNR is depends on the inverse of the weight vector of each substream. From (79) and $\| \mathbf{w}_i^T \mathbf{H}_i \|^2 = \| \mathbf{w}_i \|^2 \| \mathbf{H}_i \|^2$, a larger $\| \mathbf{H}_i \|^2$ value requires a smaller corresponding $\| \mathbf{w}_i \|^2$. Thus, the optimal detection order is in decreasing order of the *Eucldean* or $l_2 - norm$ of the columns of $\mathbf{H}$.

5.5.2.4 Computation of Nulling Vector

When the channel matrix $\mathbf{H}$ has full rank, the vector $\mathbf{w}_i$ in (79) is unique and is the ith row of the pseudoinverse of channel matrix $\mathbf{H}$

$$\mathbf{w}_i = \left\langle \mathbf{H}^+ \right\rangle_i \tag{84}$$

where $\langle\rangle_i$ and $^+$ denote the ith row and the pseudoinverse, respectively. With the successive cancellation and decoding, $\mathbf{w}_i$ is chosen as the ith row of pseudoinverse of $\mathbf{H}$ of which 1 to $i-1$th columns are set to zero. With optimal ordering, if $(k_1, k_2, \ldots, k_{\hat{M}})$ are the optimal order, the ZF nulling vector $\mathbf{w}_{k_i}$ is

$$\mathbf{w}_{i_{ZF}} = \left\langle \mathbf{H}^{+}_{\overline{k_{i-1}}} \right\rangle_{k_i} \tag{85}$$

where $\mathbf{H}_{\overline{k_{i-1}}}$ is the matrix obtained from $\mathbf{H}$ by zeroing the columns $k_1, k_2, \ldots, k_{i-1}$. With the SNR information in receiver, the k_ith nulling vector with MMSE criterion is ith row of the matrix

$$\mathbf{w}_{i_{MMSE}} = \left(\mathbf{H}^{H}_{\overline{k_{i-1}}} \mathbf{H}_{\overline{k_{i-1}}} + \frac{1}{\rho}\mathbf{I} \right)^{-1} \mathbf{H}^{H}_{\overline{k_{i-1}}} \tag{86}$$

where ρ is the SNR [35].

5.5.2.5 Detection Algorithm

The full detection algorithm for ZF V-BLAST can be summarized as follows [147]:

- initialization:

$$\begin{aligned} i &\leftarrow 1 \\ \mathbf{G}_1 &= \mathbf{H}^{+} \\ k_1 &= \arg\min_j \parallel \langle \mathbf{G}_1 \rangle \parallel^2 \end{aligned}$$

- recursion:

$$\begin{aligned} \mathbf{w}_{k_i} &= \langle \mathbf{G}_i \rangle_{k_i} \\ d_{k_i} &= \mathbf{w}_{k_i}^{T} \mathbf{y}_i \\ \hat{s}_{k_i} &= \mathcal{Q}(d_{k_i}) \\ \mathbf{y}_{i+1} &= \mathbf{y}_i - \hat{s}_{k_i} \mathbf{H}_{k_i} \\ \mathbf{G}_{i+1} &= \mathbf{H}^{+}_{\overline{k_{i-1}}} \\ k_{i+1} &= \arg\min_{j \notin \{k_1, \ldots, k_i\}} \parallel \langle \mathbf{G}_{i+1} \rangle_j \parallel^2 \\ i &\leftarrow i+1 \end{aligned}$$

5.5.3 Capacity in V-BLAST System Model

The capacities discussed in previous section are the limit under ideal conditions. In contrast, real systems achieve portions of that capacity because of imperfect channel estimation. The capacity of a real system is defined as a throughput measured with a particular system architecture. For an example, an uncoded M-ary QAM communication system that is employing ideal Nyquist pulses $Sinc(t/T_s)$ at a bit rate of $R = (log_2 M)/T_s$ occupies a bandwith of $W = 1/T_s$ and yields the throughput of $log_2 M$ bps/Hz. In addition, the errors during the transmission undermines the achievable capacity.

To measure the capacity gain achieved with the SAT method in real systems, we consider a V-BLAST system having the same number of transmit and receive antennas as in the theoretical case. QPSK and 16-QAM signal constellations are employed. The block error rate (BLER) is used as a figure of merit for given system architecture [30]. The BLER can be used in systems employing a block coding techniques. If a data block consists of N_{BL} sub-blocks of length $L_{BL} = L/N_{BL}$, where L is the data packet length, the BLER ϵ_{BL_i} of ith communication link of a MIMO system controlled by the BER ϵ_{b_i} and the number of bit errors N_c in each sub-block which can be corrected by the block coding technique, is

$$\epsilon_{BL_i} = 1 - \left[\sum_{i=0}^{N_c} \binom{L_{BL}}{i} (\epsilon_{b_i})^i (1 - \epsilon_{b_i})^{L_{BL}-i} \right]^{N_{BL}}. \tag{87}$$

The corresponding capacity of the link is [30]

$$\mathcal{C}_i = \log_2 M_i (1 - \epsilon_{BL_i}) \tag{88}$$

where $\log_2 M_i$ is the number of bits per symbol. For a MIMO system transmitting M independent substreams of data from M transmit antennas, the total throughput of the system is then

$$\mathcal{C}_T = \sum_{i}^{m} \mathcal{C}_i. \tag{89}$$

5.6 Rate Adaptive Space-Time Diversity Coding for CCI Mitigation

The SAT scheme is designed to mitigate the capacity loss from high-power interference by redistributing the power over selected antenna subset. Likewise, the space-time diversity

coding (STDC) scheme can be used for the same purpose as the SAT scheme at the cost of increased redundancy ($r_s \leq 1$). One example of STDC scheme is proposed by Alamouti [14]. In Alamouti scheme, two transmit data symbols s_0 and s_1 are transmitted simultaneously from antenna 0 and 1, respectively, during the first symbol period, following which symbols $-s_1^*$ and s_0^* are launched from antenna 0 and 1, respectively. Alamouti scheme with two transmit antennas and one receive antenna achieves a decision metric equivalent to that of a conventional two branch maximum ratio combining (MRC) diversity scheme after combining. Therefore, Alamouti's scheme extracts $2N$th-order diversity with N receive antennas regardless the channel information at the transmitter.

Figure 33 is a schematic of 2×2 Alamouti model. Note that the spatial code rate r_s

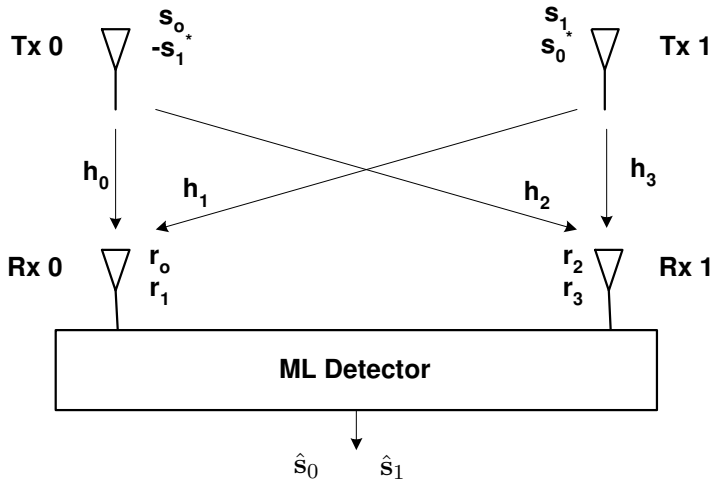

Figure 33: An example of space-time diversity coding MIMO systems: 2×2 Alamouti model.

is 1 in Alamouti scheme. After combining with the known channel information $\mathbf{h}_0$ and $\mathbf{h}_1$, the maximum likelihood detector estimates the transmitted signals:

$$\begin{aligned} \hat{\mathbf{s}}_0 &= \mathbf{h}_0^* \mathbf{r}_0 + \mathbf{h}_1 \mathbf{r}_1^* + \mathbf{h}_2^* \mathbf{r}_2 + \mathbf{h}_3 \mathbf{r}_3^* \\ \hat{\mathbf{s}}_1 &= \mathbf{h}_0^* \mathbf{r}_0 - \mathbf{h}_1 \mathbf{r}_1^* + \mathbf{h}_2^* \mathbf{r}_2 - \mathbf{h}_3 \mathbf{r}_3^*. \end{aligned} \tag{90}$$

Unlike the SAT scheme which controls the power allocation across the antenna, the STDC scheme uses the diversity coding scheme across space-and-time domains. In the viewpoint of power efficiency, the SAT scheme with $\hat{M} = M/2$ and the Alamouti scheme

consume twice as much power per symbol as the full antenna distribution BLAST system with $M = 2$ transmit antennas. The extension of STDC to channels with more than two transmit antennas through orthogonal space-time block coding (OSTBC) with low decoding complexity was proposed [132]. Also, a design of algebraic and convolutional space-time codes operable in the presence of CCI was explored with/without CSI at the transmitter [19]. However, the research on these topics is beyond the interest of this study. Therefore, the performance of an Alamouti based STDC scheme on CCI mitigation is provided for shallow observation on the similarity between the SAT and the STDC in contexts of CCI mitigation.

5.7 Numerical Results

The performance of the proposed SAT method is evaluated by computer simulations. The simulations use 10000 channel realizations for each SIR and SNR condition. For SAT scheme realizations, a 4×4 MIMO system is considered. Based on the number of effective eigenmodes in low SIR conditions, the number of antennas used in the SAT method is fixed to one-half of total number of antennas, i.e., $\hat{M} = M/2 = 2$.

5.7.1 Theoretical Capacity

Figure 34 shows the theoretical capacity of the SAT scheme with four different power allocation schemes at different SIR conditions. The proposed 2-antenna subset algorithm (EP2M) outperforms both equal power distribution over 4 antennas (EP4) and all-power over one antenna (EP1M) schemes in the -5 to 20 dB SIR region. All SAT schemes except EP1R outperform the conventional equal power distribution over 4 antennas (EP4) in -4 to 6 dB SIR region. This result is consistent with the reduced eigenmodes observed in the presence of high-power interference-plus-noise in Section 5.4

5.7.2 4×4 V-BLAST Systems

In the simulations, we employed data blocks of length $L = 360$ or 2400 bits are assumed to be protected by a 1/3 repetition ($L_{BL} = 3$) or a (15,10) shortened Hamming coding ($L_{BL} = 15$. Each channel coding can detect and correct one bit error in each subblock.

In Figure 35 the SAT scheme outperforms the conventional full antenna scheme in V-BLAST systems in the low SIR range (0 to 15 dB). Note that the SAT scheme with higher order modulation (16-QAM) delivers maximum gain while the full-antenna scheme, even with lower order modulation (QPSK), has small capacity in the 8 to 15 dB SIR region. This implies that the SAT scheme can be combined with adaptive modulation schemes to achieve low BLER while transmitting more information with increased modulation orders. In addition, the SAT scheme is less susceptible to channel coding protection than the full antenna distribution is. Compared to the 1/3 repetition coding, the former looses $2 \sim 3$ dB gain while the later suffers $4 \sim 5$ dB loss with the less protective (15,10) shortened Hamming code as illustrated in Figure 36.

The channel impairment from CCI is less severe than that from AWGN with equivalent power if the CSI of CCI is properly exploited. However, in Figure 37, we observe that the CCI imposes $4 \sim 5$ dB and $8 \sim 10$ dB more loss to SAT and full-antenna schemes, respectively, than AWGN does. This results can be foreseen since the transmitter uses no CSI of CCI in antenna selection process. On the other hand, this implies that the SAT scheme is more useful when the most of the channel impairment comes from man-made CCI rather than AWGN.

Also, unlike the theoretical model where the maximum capacity is achieved with $Max\ \mathcal{M}$ antenna subset, the antenna subset with $Min\ \mathcal{R}$ produced the maximum gain in V-BLAST system model, as shown in Figure 38, because of the interference cancelling nature of the V-BLAST system. The SAT scheme consumes the same total power as the full antenna scheme while achieving higher capacity in low-SIR region. So, this scheme is effective for communication system with power-limited source. Furthermore, the capacity gain increases especially in packet communication systems employing ARQ schemes where increase of retransmission rate severely degrades the overall link throughput.

5.7.3 2×2 MIMO systems with STDC and V-BLAST

The performance of a STDC scheme in the presence of high-power CCI is evaluated by using a 2×2 MIMO system with Alamouti scheme. Its capacity is computed from the BLER in

packet communication links with data blocks size of 360 and 2400 bits. This scheme uses twice as much power per symbol as the full antenna distribution 2×2 BLAST system by sending a symbol information twice in predefined way. Thus, the STDC scheme traded data rate for increased transmit power per data symbol. However, as shown in Figure 39 and 40, the STDC scheme exhibits a similar pattern of capacity gain over 2×2 V-BLAST scheme in 5 to 15 dB SIR range by using higher order modulations. Therefore, the STDC scheme can be considered an alternative adaptive transmission technique in interference dominant channel conditions. One drawback of the STDC scheme is that it tends to lose capacity gain as the spatial code rate r_s decreases.

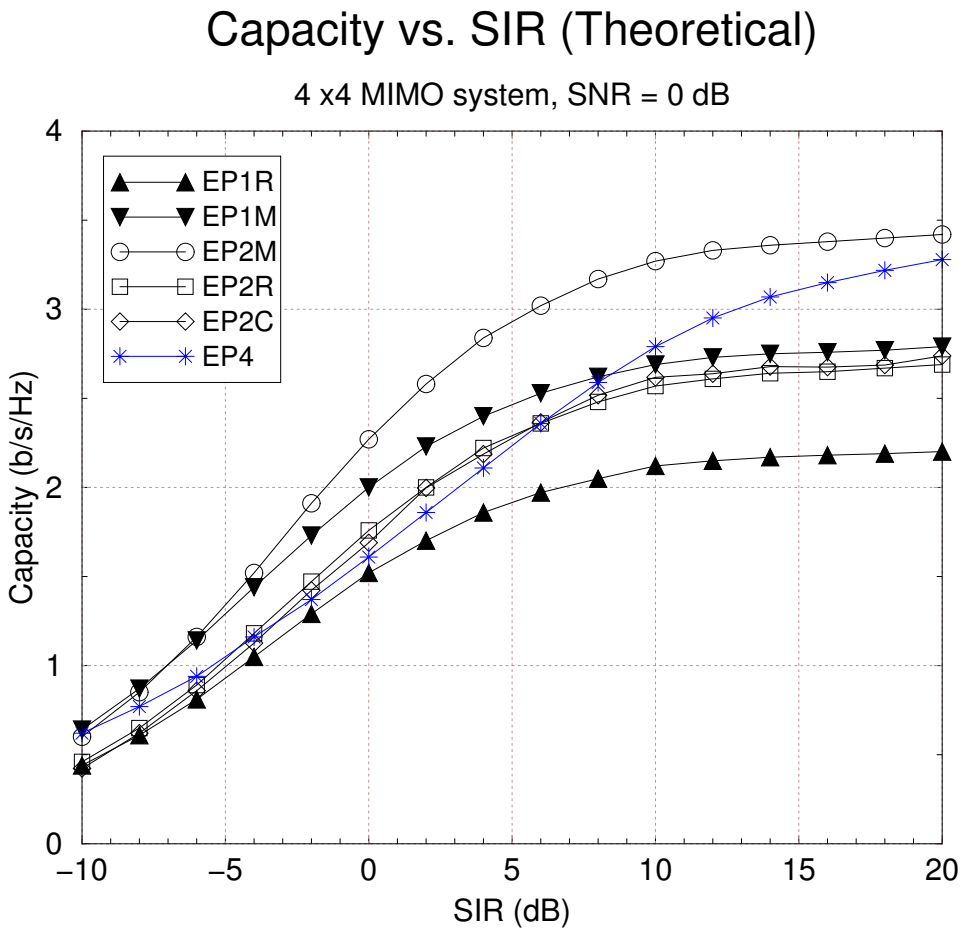

Figure 34: Capacity of a 4×4 MIMO system with given SIR conditions; SNR = 0 dB, Legend: EPxy, x = number of transmit antennas, y = random (R), maximum modulus (M) or minimum cross-correlation (C) antenna selection.

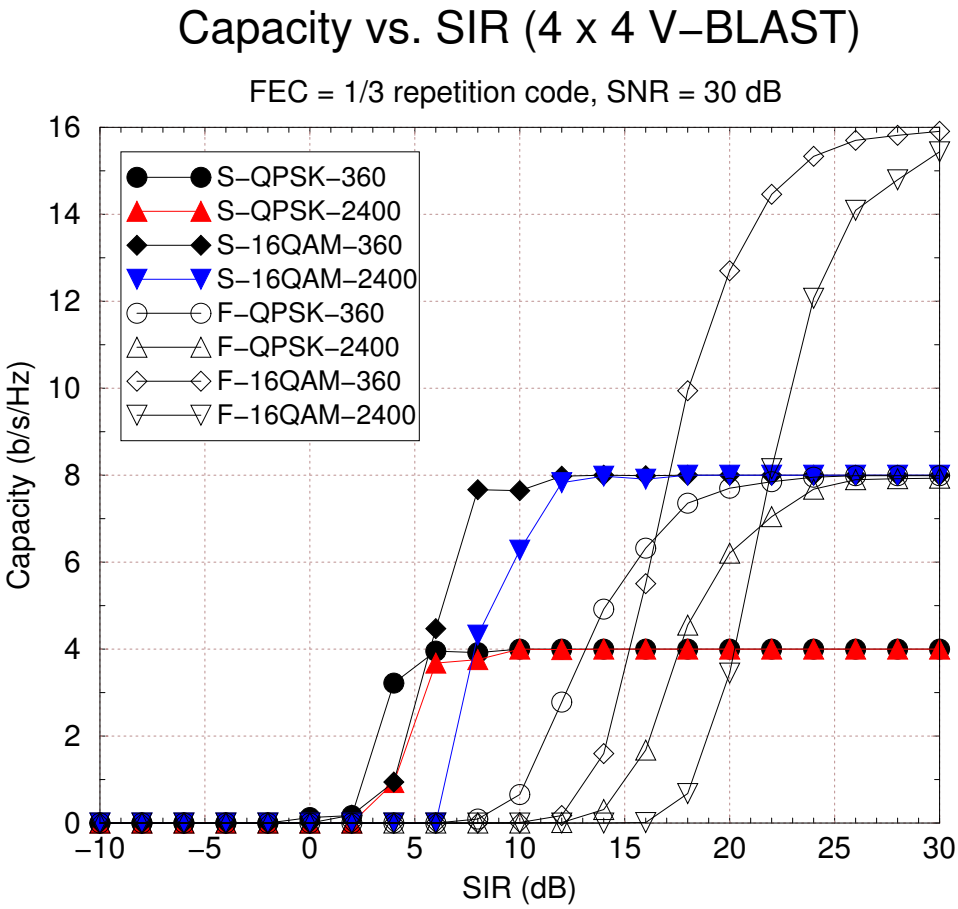

Figure 35: Capacity of a 4×4 V-BLAST system with the SAT scheme; FEC: 1/3 repetition code, L = 360 or 2400 bits, SNR = 30 dB, Legend: full-antenna scheme (F) or SAT scheme with $\hat{M} = 2$(S).

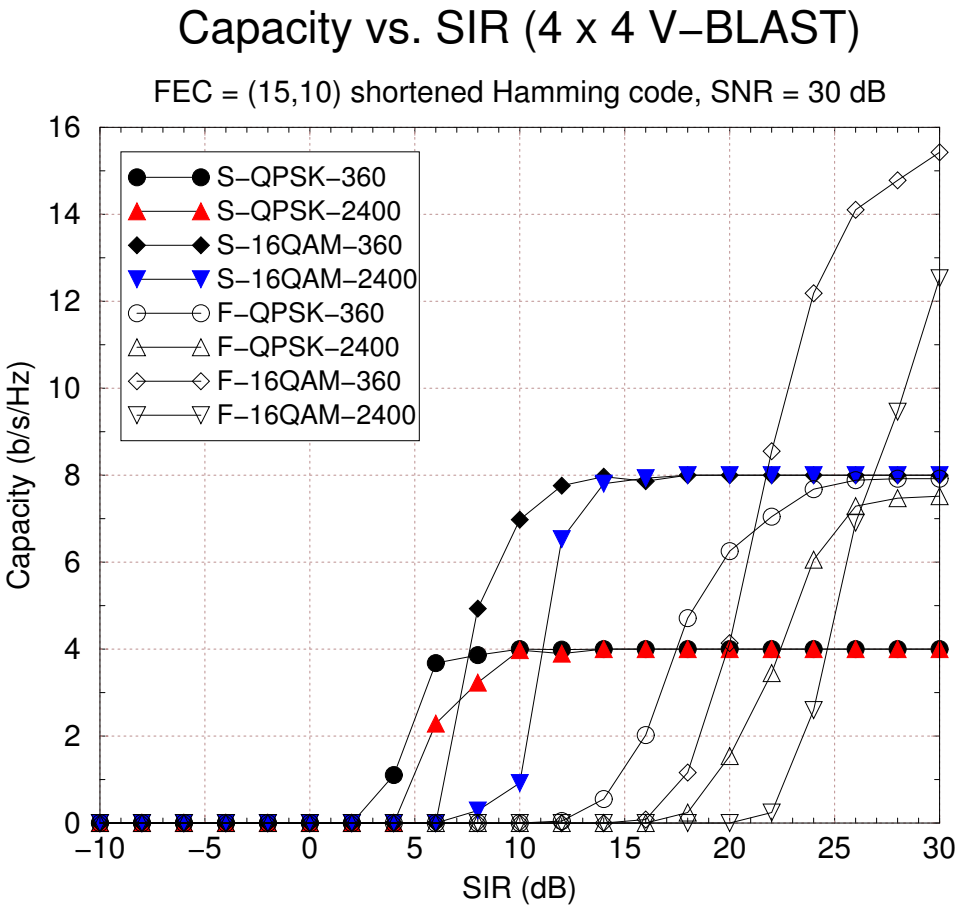

Figure 36: Capacity of 4×4 V-BLAST system with the SAT scheme; FEC = (15,10) shortened Hamming code, L = 360 or 2400 bits, SNR = 30 dB, Legend: full-antenna scheme (F) or SAT scheme with $\hat{M} = 2$(S).

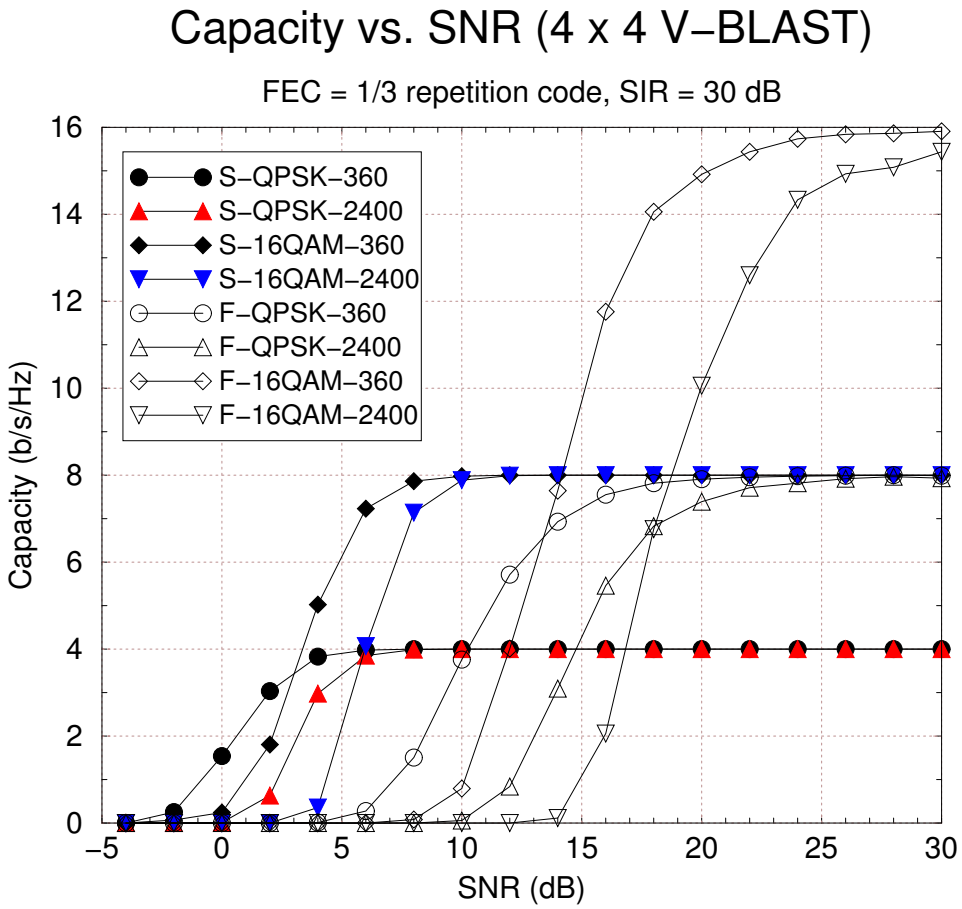

Figure 37: Capacity of a 4×4 V-BLAST system with given SNR conditions; SIR = 30 dB, FEC = 1/3 repetition code, L = 360 or 2400 bits, Legend: full-antenna scheme (F) or SAT scheme with $\hat{M} = 2$(S).

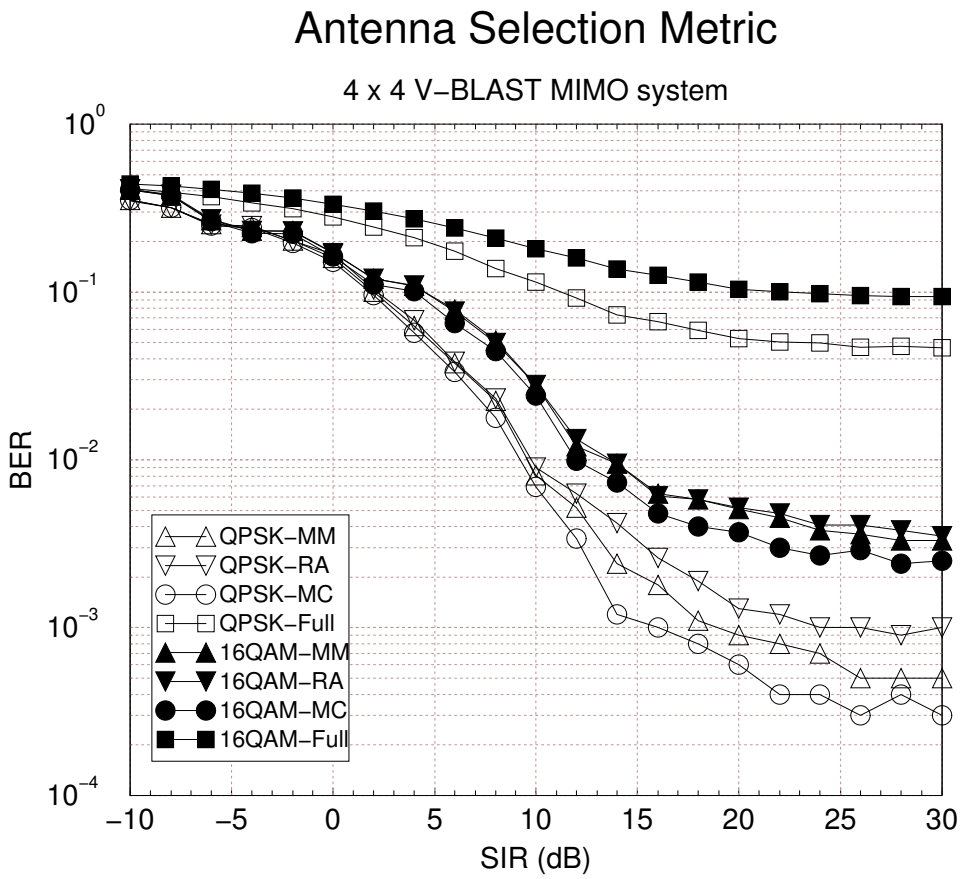

Figure 38: BER performance of antenna subset selection criteria for a 4×4 V-BLAST system with $\hat{M} = 2$; SNR = 30dB, Legend: maximum modulus (MM), random (RA) or minimum cross-correlation (MC) antenna selection.

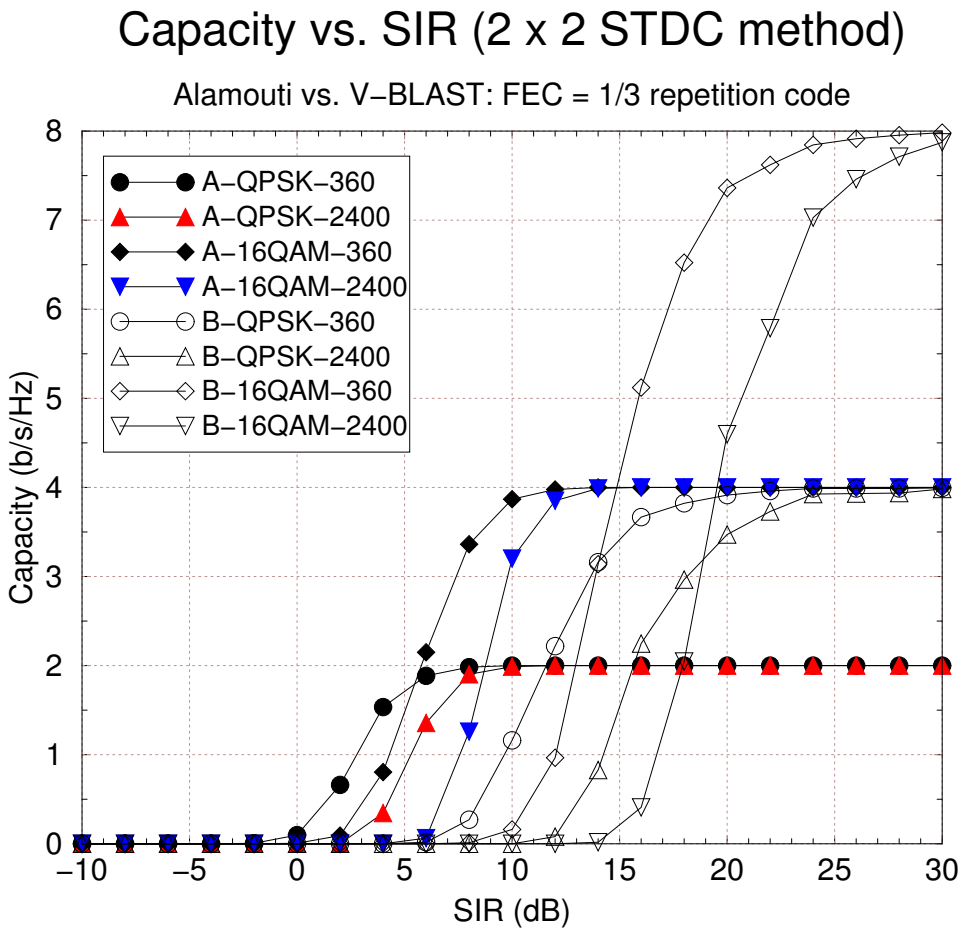

Figure 39: Capacity of a rate adaptive STDC (2×2 Alamouti) scheme; FEC = 1/3 repetition code, L = 360 or 2400 bits, SNR = 30 dB, Legend: Alamouti scheme (A) or V-BLAST scheme (B).

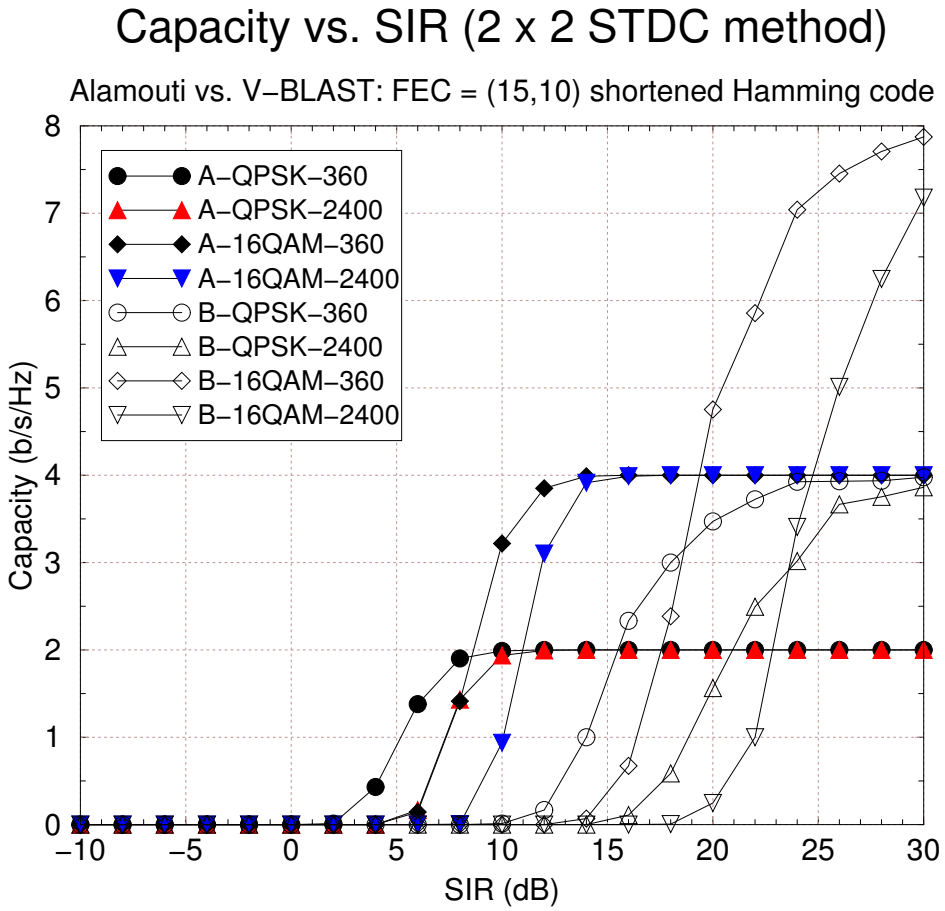

Figure 40: Capacity of a rate adaptive STDC (2×2 Alamouti) scheme; FEC = (15,10) shortened Hamming code, L = 360 or 2400 bits, SNR = 30 dB, Legend: Alamouti scheme (A) or V-BLAST scheme (B).

CHAPTER VI

CONCLUDING REMARKS

This dissertation has considered several topics in interference mitigation for practical wireless communication systems in contexts of receiver design, channel estimation, link-level performance evaluation, and capacity analysis. The research work is primarily focused to address the problems in the design of interference resilient receivers or transmitters in the following areas:

- joint-detection IC-DDF ML Bluetooth receiver
- joint-detection interference rejection combining TDMA receiver
- interference resilient power allocation in MIMO systems

6.1 Summary of Contributions

In Chapter 3, we proposed an interference cancelling dual decision feedback (IC-DDF) receiver that jointly detects two colliding Bluetooth signals to mitigate the packet error probability in the low-Doppler flat fading channels. For a particular case of systems with a single antenna for economic solutions, the dual decision feedback scheme minimizes the CCI and the self interference from the shaping pulse simultaneously. An RLS-type channel estimator, based on the random walk model and constant covariance matrix, is employed to perform joint channel estimation and tracking function with reduced complexity. The proposed receiver achieved large gains in -12 to 4 dB CIR range over a conventional frequency discriminator type receiver, and showed its resilience to channel variations, especially in typical Bluetooth operating environments. In addition, a system level performance evaluation is addressed for an interference resilient receiver in frequent packet collisions by using a geometric approach. In the proposed scheme, the pdf of the received CIR is derived from the traffic load distributions and the network topology of collocated Bluetooth piconets.

For overall link throughput assessment, we also derived a generalized packet collision probabilities for the multiple collocated Bluetooth piconets carrying combined traffics of ACL and SCO links.

In Chapter 4, we proposed a soft output fractionally spaced IRC-DDFSE receiver that jointly detects two co-channel binary (GSM) and non-binary (EDGE) TDMA signals in frequency selective channels for an extended range signal reception. The proposed receiver decodes signals from remote base stations in the presence of strong CCI from a nearby co-channel base station at received CIR less than -10 dB. The joint-detection IRC structure mitigates the influence from a strong CCI. The increased complexity of the joint detection architecture is diminished by using a DDFSE technique. Concatenated Viterbi and Log-MAP algorithms improved the probability of correct sequence estimation by generating soft outputs for the outer code decodings of binary (GMSK) and non-binary (8PSK) symbols. For the completeness of the Log-MAP function, Viterbi algorithm generates a unique covariance matrix and a corresponding decision feedback sequence for each state of the Log-MAP function by using a PSP algorithm. Joint channel estimation with an LS criterion reduces the channel estimation error from the cross-correlation between the TSSs of two co-channel signals. The fractionally-spaced receiver structure whitens the colored noise and reduces the performance degradation from the delay offset between the two co-channel signals. We also showed that an NBAA preprocessing combined with an interference cancelling receiver is effective for the extended range signal reception in TDMA cellular systems. In addition, the proposed receiver showed its resilience to the imbalanced CCI across antenna branches in low-CIR conditions.

In Chapter 5, we proposed an adaptive power allocation scheme for MIMO systems by using subset antenna transmission (SAT) techniques to increase the spectral efficiency in the presence of co-channel interference (CCI). This scheme uses the phenomena of unbalanced eigenmodes in channel matrices often observed in the presence of high-power interference or noise. The phenomena, which can be explained by large condition numbers in channel matrices, results in a capacity loss in the equal power distribution scheme. In the proposed scheme, the capacity loss is reduced by allocating transmit power equally on a selected

subset of the transmit antennas. From the results of numerical analysis, we observed that the proposed scheme achieves larger capacity than that of the all-antenna transmission method when the received SIR is very low, or the channel matrix is ill conditioned. The proposed scheme outperformed the conventional method in low SIR or SNR conditions not only in information theoretic capacity but also in the capacity of V-BLAST MIMO systems. Furthermore, the proposed scheme combined with an adaptive modulation technique outperforms the all-antenna transmission scheme by achieving low BLER even in higher modulation order. For the selection of an antenna subset for transmission in V-BLAST systems, a set of antenna having minimum crosscorrelation produces maximum capacity gain by exploiting the successive interference cancellation nature of the V-BLAST architecture.

6.2 Suggestions for Further Research

Future research can proceed along several lines.

Interference Mitigating Receiver Design:

- In ISM bands, many systems with different radio interface coexist and interfere to each other. Although the issues of coexistence and interference mitigation has received much attention in literature, comparatively little can be found describing practical solutions for inter-system interference. Both PHY and MAC layer approaches can be used in separate or integrative methods.

- In most literature on joint detection or interference mitigation receiver designs, the receiver assumes *a priori* knowledge on the existence of interference. However, when the interference is arriving in asynchronous and variable length burst formats, the detection of interfering signals is an essential function to achieve the desired performance. It becomes a challenging task in frequency bands where the radio spectrum is shared by communication systems with heterogeneous radio interfaces. Furthermore, interference detection can be an important step to the design of a receiver for multi-format signal reception and transmission. A software defined radio (SDR) architecture is an example of possible applications.

Transmitter Design for Interference Resilient MIMO Systems:

- An extended proof of the conjecture that the SAT model achieves capacity gain in low transmit power or small eigenmodes cases needs further research. It includes the study on the distribution of the eigenvalues of the $Wishart$ matrix.

- The SAT scheme is focused on power control over selected antenna subset. It can be extended by using precoding and rate adaptation. Alamouti type STBC is a primitive example of precoding for interference mitigation. Also, the SAT scheme can be extended to multiple antenna-set partitioning combined with rate adaptive STBC techniques in context of overall capacity maximization.

- Interlayer design approaches have received much attention for optimum link throughput in time-varying channel and interference conditions. Its adaptive feature can be extended to interference mitigation by employing subset antenna transmission, adaptive modulation, and interference identification techniques. The open- and closed-loop control for adaptive transmission can be another research concern in interference cancelling interlayer designs. Interference-adaptive interlayer design combined with an SDR architecture can be one realization of the cognitive radio (CR) initiative.

REFERENCES

[1] IEEE, "Wireless LAN Medium Access Control (MAC) and Physical Layer (PHY) Specification," 802.11, 1997.

[2] ETSI, "Digital Cellular Telecommunications System (Phase 2+): Channel Coding," GSM-05.03, 1999.

[3] ETSI, "Digital Cellular Telecommunications System (Phase 2+): Modulation," GSM-05.04, 1999.

[4] ETSI, "Digital Cellular Telecommunications System (Phase 2+): Multiplexing and Multiple Access on the Radio Path," GSM-05.02, 1999.

[5] TIA, "Mobile Station-Base Station Compatibility Standard for Wideband Spread Spectrum Cellular Systems," TIA/EIA-95-B, 1999.

[6] Bluetooth SIG, "Specification of the Bluetooth System," Version 1.0, 1999.

[7] TIA, "Physical Layer Specification for CDMA Spread Spectrum Communications System," TIA/EIA IS-2000, 2000.

[8] 3GPP, "3GPP TSG RAN WG4; Physical Layer Procedures (FDD)," 3GPP TS 25.214, 2000-03.

[9] IEEE, "Air Interface for Fixed Broadband Wireless Access Systems - Medium Access Control and Additional Physical Layer Specifications for 2-11 GHz," 802.16a, 2003.

[10] IEEE, "Low-Rate Wireless PAN Medium Access Control (MAC) and Physical Layer (PHY) Specification," 802.15.4, 2003.

[11] 3GPP, "3GPP TSG GERAN; Radio Transmission and Reception," 3GPP TS 45.005, Release 5.

[12] Aalo, V. A. and Zhang, J., "Performance of Antenna Array Systems with Optimum Combining in a Rayleigh Fading Environment," *IEEE Commun. Lett.*, vol. 4, pp. 387–389, Dec. 2000.

[13] Agrawal, A., Andrews, J. G., Cioffi, J. M., and Meng, T., "Iterative Power Control for Imperfect Successive Interference Cancellation," *IEEE Trans. Wireless Commun.*, vol. 4, pp. 878–884, May 2005.

[14] Alamouti, S., "A Simple Transmit Diversity Technique for Wireless Communications," *IEEE J. Select. Areas Commun.*, pp. 1451–1458, Oct. 1998.

[15] Anderson, S., Hagerman, B., Dam, H., Forssén, U., Karlsson, J., Kronestedt, F., and Mazur, S., "Adaptive Antennas for GSM and TDMA Systems," *IEEE Personal Commun. Mag.*, vol. 6, pp. 74–86, June 1999.

[16] Andrews, J. G., "Interference Cancellation for Cellular Systems: A Contemporary Overview," *IEEE Wireless Commun. Mag.*, vol. 12, pp. 19–29, Apr. 2005.

[17] Andrews, J. G. and Meng, T. H., "Optimum Power Control for Successive Interference Cancellation with Imperfect Channel Estimation," *IEEE Trans. Wireless Commun.*, vol. 2, pp. 375–383, Mar. 2003.

[18] Ariyavisitakul, S. L., Winters, J. H., and Sollenberger, N. R., "Joint Equalization and Interference Suppression for High Data Rate Wireless Systems," *IEEE J. Select. Areas Commun.*, vol. 18, pp. 1214–1220, July 2000.

[19] Arunachalam, A. and Gamal, H. E., "Space-Time Coding for MIMO Systems with Co-Channel Interference," *IEEE Trans. Wireless Commun.*, vol. 3, pp. 1953–1958, Nov. 2004.

[20] Austin, M., "SAIC and Synchronized Networks for Increased GSM Capacity," White Paper, 3G Americas' SAIC working group, Sept. 2003.

[21] Bahl, L. R., Cocke, J., Jelinek, F., and Raviv, J., "Optimal Decoding of Linear Codes for Minimizing Symbol Error Rate," *IEEE Trans. Inform. Theory*, vol. 20, pp. 284–287, Mar. 1974.

[22] Banister, B. C. and Zeidler, J. R., "Transmission Subspace Tracking for MIMO Communications Systems," in *Proc. IEEE Global Communications Conference, GLOBECOM '01*, pp. 1680–1686, Nov. 2001.

[23] Benjebbour, A. and Yoshida, S., "On the Relation between Ordering Metrics for ZF and MMSE Successive Detection in MIMO Systems," *IEICE Transactions on Communications*, vol. E87-B, pp. 2021–2027, June 2004.

[24] Berenguer, I., Wang, X., and Wassell, I. J., "Transmit Antenna Selection in Linear Receivers: Geometrical Approach," *Electronics Letters*, vol. 40, pp. 292–293, Mar. 2004.

[25] Bischl, H. and Lutz, E., "Packet Error Rate in the Non-Interleaved Rayleigh Channel," *IEEE Trans. Commun.*, vol. 43, pp. 1375–1382, Feb. 1995.

[26] Blum, R., "MIMO Capacity with Interference," *IEEE J. Select. Areas Commun.*, vol. 21, pp. 793–801, June 2003.

[27] Bottomley, G. E. and Jamal, K., "Adaptive Arrays and MLSE Equalization," in *Proc. IEEE Vehicular Technology Conference, VTC '95*, pp. 50–54, July 1995.

[28] Bottomley, G. E., Molnar, K. J., and Chennakeshu, S., "Interference Cancellation with an Array Processing MLSE Receiver," *IEEE Trans. Veh. Technol.*, vol. 48, pp. 1321–1331, Sept. 1999.

[29] Buehrer, R. M., Kaul, A., Striglis, S., and Woerner, B. D., "Analysis of DS-CDMA Parallel Interference Cancellation with Phase and Timing Errors," *IEEE J. Select. Areas Commun.*, vol. 14, pp. 1522–1535, Oct. 1996.

[30] Catreux, S., Driessen, P. F., and Greenstein, L. J., "Attainable Throughput of an Interference-Limited Multiple-Input Multiple-Output (MIMO) Cellular System," *IEEE Trans. Commun.*, vol. 49, pp. 1307–1311, Aug. 2001.

[31] Chuang, J., Cimini, L. J., Li, G. Y., Mcnair, B., Sollenberger, N., Zhao, H., Lin, L., and Suzuki, M., "High-Speed Wireless Data Access Based on Combining EDGE with Wideband OFDM," *IEEE Commun. Mag.*, pp. 92–98, Nov. 1999.

[32] Cingular, "SAIC System Level Evaluations Based on GERAN System Simulator." 3GPP TSG-GERAN 15 Tdoc GP-031270, 2003.

[33] Cordeiro, C. M. and Agrawal, D. P., "Piconet Interference Modeling and Performance Evaluation of Bluetooth MAC Protocol," in *Proc. IEEE Global Communications Conference, GLOBECOM '01*, pp. 25–29, Nov. 2001.

[34] Cover, T. M. and Thomas, J. A., *Elements of Information Theory*. New York: John Wiley and Sons, 1991.

[35] Debbah, M., Muquet, B., Courville, M., Muck, M., Simoens, S., and Loubaton, P., "A MMSE Successive Interference Cancellation Scheme for a New Adjustable Hybrid Spread OFDM Systems," in *Proc. IEEE Vehicular Technology Conference, VTC '00*, pp. 745–749, May 2000.

[36] Demirkol, M. F. and Ingram, M. A., "Power-Controlled Capacity for Interfering MIMO Links," in *Proc. IEEE Vehicular Technology Conference, VTC '01*, pp. 187–191, Oct. 2001.

[37] Derryberry, R. T., Gray, S. D., Ionescu, D. M., Mandyam, G., and Raghothaman, B., "Transmit Diversity in 3G CDMA Systems," *IEEE Commun. Mag.*, vol. 40, pp. 68–75, Apr. 2002.

[38] Duel-Hallen, A., "Equalizers for Multiple Input/Multiple Output Channels and PAM Systems with Cyclostationary Input Sequences," *IEEE J. Select. Areas Commun.*, vol. 10, pp. 630–639, Apr. 1992.

[39] Duel-Hallen, A., "Decorrelating Decision Feedback Multiuser Detector for Synchronous Code-Division Multiple Access Channel," *IEEE Trans. Commun.*, vol. 41, pp. 285–290, Feb. 1993.

[40] Duel-Hallen, A., "A Family of Multiuser Decision-Feedback Detectors for Asynchronous Code-Division Multiple Access Channels," *IEEE Trans. Commun.*, vol. 43, pp. 421–434, Feb. 1995.

[41] Duel-Hallen, A. and Heegard, C., "Delayed Decision Feedback Sequence Estimation," *IEEE Trans. Commun.*, vol. 37, pp. 428–436, May 1989.

[42] Edelman, A., *Eigenvalues and Condition Numbers of Random Matrices*. PhD thesis, Massachusetts Institute of Technology, Cambridge, May 1989.

[43] El-Hoiydi, A., "Interference Between Bluetooth Networks-Upper Bound on the Packet Error Rate," *IEEE Commun. Lett.*, vol. 5, pp. 245–247, June 2001.

[44] Eleftheriou, E. and Falconern, D. D., "Tracking Properties and Steady-State Performance of RLS Adaptive Filter Algorithms," *IEEE Trans. Acoust., Speech, Signal Processing*, vol. 34, pp. 1097–1110, Oct. 1986.

[45] Ennis, G., "Impact of Bluetooth on 802.11 Direct Sequence Wireless LANs." IEEE 802.11 Contribution 98/319a, 1998.

[46] Etten, W. V., "Maximum Likelihood Receiver for Multiple Channel Transmission Systems," *IEEE Trans. Commun.*, vol. 24, pp. 276–283, Feb. 1976.

[47] Eyuboglu, M. V. and Qureshi, S. U., "Reduced-State Sequence Estimation for Coded Modulation on Intersymbol Interference Channels," *IEEE J. Select. Areas Commun.*, vol. 7, pp. 989–995, Aug. 1989.

[48] Farrokhi, F. R., Foschini, G. J., Lozano, A., and Valenzuela, R. A., "Link-Optimal Space-Time Processing with Multiple Transmit and Receive Antennas," *IEEE Commun. Lett.*, vol. 5, pp. 85–87, Mar. 2001.

[49] Ferguson, P. and Huston, G., *Quality of Service: Delivering QoS on the Internet and in Corporate Networks*. New York: John Wiley and Sons, 1998.

[50] Forney, Jr., G. D., "Maximum Likelihood Sequence Estimation of Digital Sequences in the Presence of Intersymbol Interference," *IEEE Trans. Inform. Theory*, vol. 18, pp. 363–378, May 1972.

[51] Foschini, G. J., "Layered Space-Time Architecture for Wireless Communication in a Fading Environment When Using Multiple Antennas," *Bell Systems Technical Journal*, vol. 1, pp. 41–59, 1996.

[52] Foschini, G. J. and Gans, M. J., "On the Limits of Wireless Communications in a Fading Environment when using Multiple Antennas," *Kluwer Journal of Wireless Personal Communications*, vol. 6, pp. 315–335, 1998.

[53] Friedlander, B. and Scherzer, S., "Beamforming vs. Transmit Diversity in the Downlink of a Cellular Communications System," in *Proc. IEEE Thirty-Fifth Asilomar Conference*, pp. 1014–1018, Nov. 2001.

[54] Fukawa, K. and Suzuki, H., "Blind Interference Cancelling Equalizer for Mobile Radio Communications," *IEICE Transactions on Communications*, vol. E77-B, pp. 580–588, 1994.

[55] Garg, V. K. and Wilkes, J. E., *Wireless and Personal Communications Systems*. Upper Saddle River, NJ: Prentice Hall, 1995.

[56] Gaston, D., "Overcoming Interference in the Spread Spectrum ISM Bands," in *Proc. of WESCON '95*, pp. 491–496, May 1995.

[57] Gaur, S. and Ingram, M. A., "Transmit/Receive Antenna Selection for MIMO Systems to Improve Error Performance of Linear Receivers," in *Proc. ITC/IEEE Workshop on Smart Antennas, WSA 2005*, Apr. 2005.

[58] Gaur, S., Jiang, J. S., Ingram, M. A., and Demirkol, M. F., "Interfering MIMO Links with Stream Control and Optimal Antenna Selection," in *Proc. IEEE Global Communications Conference, GLOBECOM '04*, pp. 3138–3142, Nov. 2004.

[59] Gerstacker, W. H. and Schober, R., "Equalization Concepts for EDGE," *IEEE Trans. Wireless Commun.*, vol. 1, pp. 190–199, 2002.

[60] Gesbert, D., Shafi, M., Shiu, D. S., Smith, P. J., and Naguib, A., "From Theory to Practice: An Overview of MIMO Space-Time Coded Wireless Systems," *IEEE J. Select. Areas Commun.*, vol. 21, pp. 281–302, 2003.

[61] Getu, B. N., Andersen, J. B., and Faserotu, J. R., "MIMO Systems: Optimizing the Use of Eigenmodes," in *Proc. IEEE Intl. Symposium on Personal, Indoor and Mobile Radio Communications, PIMRC '03*, pp. 1129–1133, Sept. 2003.

[62] Gibson, J. D., *Mobile Communications Handbook, 2nd ed.* Secaucus: Springer-Verlag New York, 1999.

[63] Godara, L. C., "Applications of Antenna Arrays to Mobile Communications. I. Performance Improvement, Feasibility, and System Considerations," in *Proceedings of the IEEE*, vol. 85, pp. 1031–1060, July 1997.

[64] Goldsmith, A. J., Jafar, S. A., Jindal, N., , and Vishwanath, S., "Capacity Limits of MIMO Channels," *IEEE J. Select. Areas Commun.*, vol. 21, pp. 684–702, June 2003.

[65] Golmie, N., Chevrollier, N., and ElBakkouri, I., "Interference Aware Bluetooth Packet Scheduling," in *Proc. IEEE Global Communications Conference, GLOBECOM '01*, pp. 2857–2863, Nov. 2001.

[66] Golmie, N. and Mouveaux, F., "Impact of Interference on the Bluetooth Access Control Performance: Preliminary Results." IEEE 802.15 Contribution 00/322r0, 2000.

[67] Goodman, D. J. and Saleh, A. A. M., "The Near-Far Effect in Local Aloha Radio Communications," *IEEE Trans. Veh. Technol.*, vol. 36, pp. 19–27, Feb. 1987.

[68] Gore, D. A., Gorokhov, A., and Paulraj, A., "Joint MMSE Versus V-BLAST and Antenna Selection," in *Proceedings of The Thirty-Sixth Asilomar Conference*, vol. 1, pp. 505–509, Nov. 2002.

[69] Gore, D. A., R. W. Heath, J., and Paulraj, A., "Transmit Selection in Spatial Multiplexing Systems," *IEEE Commun. Lett.*, vol. 6, pp. 91–493, Nov. 2002.

[70] Gorokhov, A., Collados, M., Gore, D., and Paulraj, A., "Transmit/Receive MIMO Antenna Subset Selection," in *Proc. IEEE Intl. Conference on Acoustics, Speech, and Signal Processing, ICASSP '04*, pp. 13–16, May 2004.

[71] Hafeez, A., Hui, D., and Arslan, H., "Interference Cancellation for EDGE via Two-User Joint Demodulation," in *Proc. IEEE Vehicular Technology Conference, VTC '03*, pp. 1025–1029, Oct. 2003.

[72] Hafeez, A., Molnar, K. J., Bottomley, G. E., and Ramesh, R., "Capacity and Quality Enhancement for ANSI-136 Downlink Using Interference Cancellation and Beamforming," in *Proc. IEEE Vehicular Technology Conference, VTC '00*, pp. 2414–2421, Sept. 2000.

[73] Hamied, K. and Stüber, G. L., "A Fractionally-Spaced MLSE Receiver," in *Proc. IEEE Conference on Communication, ICC '95*, pp. 7–11, May 1995.

[74] Haustein, T. and Boche, H., "Optimal Power Allocation for MSE and Bit-Loading in MIMO Systems and the Impact of Correlation," in *Proc. IEEE Intl. Conference on Acoustics, Speech, and Signal Processing, ICASSP '03*, pp. 405–408, Apr. 2003.

[75] Haykin, S., *Adaptive Filter Theory*. Englewood Cliffs: Prentice-Hall, 1991.

[76] Hoeher, P. A., Badri-Hoeher, S., Deng, S., Krakowski, C., and Xu, W., "Joint Delayed-Decision Feedback Sequence Estimation with Adaptive State Allocation," in *Proc. International Symposium on Information Technology, ISIT 2004*, p. 132, July 2004.

[77] Hoeher, P. A., Badri-Hoeher, S., Xu, W., and Krakowski, C., "Single-Antenna Co-Channel Interference Cancellation for TDMA Cellular Radio Rystems," *IEEE Wireless Commun. Mag.*, vol. 12, pp. 30–37, Apr. 2005.

[78] Horn, R. A. and Johnson, C. R., *Matrix Computations*. Cambridge, U.K.: Cambridge University Press, 1985.

[79] Howitt, I., "WLAN and WPAN Coexistence in UL Band," *IEEE Trans. Veh. Technol.*, vol. 50, pp. 1114–1124, July 2001.

[80] Howitt, I., "Mutual Interference Between Independent Bluetooth Piconets," *IEEE Trans. Veh. Technol.*, vol. 52, pp. 708–718, May 2003.

[81] Howitt, I. and Hawwar, V. K., "Evaluation of Outage Probability Due to Cochannel Interference in Fading for a TDMA System with a Beamformer," in *Proc. IEEE Vehicular Technology Conference, VTC '98*, pp. 520–524, May 1998.

[82] Jakes, W. C., *Microwave Mobile Communications*. New York: IEEE Press, 1994.

[83] Janssen, G. J. M., Stigter, P. A., and Prasad, R., "Wideband Indoor Channel Measurements and BER Analysis of Frequency Selective Multipath Channels at 2.4, 4.75, and 11.5 Ghz," *IEEE Trans. Commun.*, vol. 44, pp. 1272–1288, Oct. 1996.

[84] Joung, J. and Stüber, G. L., "Fractionally Spaced IRC-DDFSE for TDMA Cellular Systems," in *Proc. IEEE Vehicular Technology Conference, VTC '99*, pp. 441–445, Sept. 1999.

[85] Kamerman, A., "Coexistence between Bluetooth and IEEE 802.11 CCK Solutions to Avoid Mutual Interference." IEEE 802.11 Contribution 00/162, 2000.

[86] Karlsson, J. and Heinegøard, J., "Interference Rejection Combining for GSM," in *Proc. IEEE Intl. Conference on Universal Personal Communications, ICUPC '96*, pp. 433–437, Sept. 1996.

[87] Kim, K. and Stüber, G. L., "Interference Mitigation in Asynchronous Slow Frequency Hopping Bluetooth Networks," *Kluwer Journal of Wireless Personal Communications*, vol. 28, pp. 143–159, Jan. 2004.

[88] Kim, K. and Stüber, G. L., "Range Extended Interference Cancelling Joint Detection TDMA Receiver," in *Proc. International Symposium on Wireless Personal Multimedia Communications, WPMC '04*, pp. 315–319, Sept. 2004.

[89] Kim, K. and Stüber, G. L., "Joint Detection Interference Rejection Combining GSM/EDGE Receiver," *Submitted to IEEE Trans. on Wireless Communications Letter*, Jan. 2005.

[90] Kim, S. C., Bertoni, H. L., and Stern, M., "Pulse Propagation Characteristics at 2.4 GHz Inside Buildings," *IEEE Trans. Veh. Technol.*, vol. 45, pp. 579–592, Aug. 1996.

[91] Kohno, R., Meiden, R., and Milstein, L. B., "Spread-Spectrum Access Method for Wireless Communications," *IEEE Commun. Mag.*, vol. 33, pp. 58–67, Jan. 1995.

[92] Lai, J. and Mandayam, N., "Packet Error Rate for Burst-error-correcting Codes in Rayleigh Fading Channels," in *Proc. IEEE Vehicular Technology Conference, VTC '98*, pp. 1568–1572, May 1998.

[93] Laster, J. D. and Reed, J. H., "Interference Rejection in Digital Wireless Communications," *IEEE Signal Processing Mag.*, vol. 14, pp. 37–62, May 1997.

[94] Lee, W. C. Y., *Mobile Communication Engineering*. New York: McGraw-Hill, 1982.

[95] Li, L., Li, H., and Yao, Y. D., "Intersymbol/Cochannel Interference Cancellation for Transmit Diversity Systems in Frequency Selective Fading Channels," in *Proc. IEEE Vehicular Technology Conference, VTC '01*, pp. 678–682, Oct. 2001.

[96] Li, Y., Winters, J. H., and Sollenberger, N., "Spatial-Temporal Equalization for IS-136 Systems with Rapid Dispersive Fading and Co-Channel Interference," *IEEE Trans. Veh. Technol.*, vol. 48, pp. 1182–1194, July 1999.

[97] Liang, J., Paulraj, A. J., and Singh, A., "Two Stage CCI/ISI Reduction with Space-Time Processing in TDMA Cellular Networks," in *Proc. IEEE Thirty Asilomar Conference*, pp. 607–611, Nov. 1996.

[98] Lin, J., Ling, F., and Proakis, J. G., "Fading Channel Tracking Properties of Several Adaptive Algorithms for the North American Digital Cellular System," in *Proc. IEEE Vehicular Technology Conference, VTC '91*, pp. 273–276, May 1993.

[99] Lin, S. C. and Prabhu, V. K., "Diversity Combining and Equalization of Frequency-Selective Fading Signals with Unequal Mean Strengths," in *Proc. IEEE Vehicular Technology Conference, VTC '98*, pp. 753–757, May 1998.

[100] Lo, N. W. K., Falconer, D., and Sheikh, A. U. H., "Adaptive Equalization for Co-Channel Interference in a Multipath Fading Environment," *IEEE Trans. Commun.*, vol. 43, pp. 1441–1453, Feb. 1995.

[101] Lupas, R. and Verdú, S., "Linear Multiuser Detectors for Synchronous Code-Division Multiple-Access Channels," *IEEE Trans. Veh. Technol.*, vol. 35, pp. 123–136, Apr. 1989.

[102] Lupas, R. and Verdú, S., "Near-Far Resistance of Multiuser Detectors in Asynchronous Channels," *IEEE Trans. Commun.*, vol. 38, pp. 496–508, Apr. 1990.

[103] Mallik, R. K., Win, M. Z., and Winters, J. H., "Performance of Dual-Diversity Predetection EGC in Correlated Rayleigh Fading with Unequal Branch SNRs," *IEEE Trans. Commun.*, vol. 50, pp. 1041–1044, July 2002.

[104] Margarita, A., Flores, S. J., Rubio, L., Almenar, V., and Corral, J. L., "Application of MUSIC for Spatial Reference Beamforming for SDMA in a Smart Antenna for GSM and DECT," in *Proc. IEEE Vehicular Technology Conference, VTC '01*, pp. 123–126, May 2001.

[105] Oja, E., *Subspace Methods of Pattern Recognition*. Hertfordshire: Research Studies Press, 1983.

[106] Palomar, D. P., Cioffi, J. M., and Lagunas, M. A., "Uniform Power Allocation in MIMO Channels: a Game-Theoretic Approach," *IEEE Trans. Inform. Theory*, vol. 49, pp. 1707–1727, July 2003.

[107] Park, M., Heath, R. M., and Nettles, S. M., "Improving Throughput and Fairness for MIMO Ad-Hoc Networks Using Antenna Selection Diversity," in *Proc. IEEE Global Communications Conference, GLOBECOM '04*, pp. 3363–3367, Nov. 2004.

[108] Parsons, J. D., *The Mobile Radio Propagation Channel*. London, U.K.: Pentech Press, 1992.

[109] Patel, P. and Holtzman, J., "Analysis of a Simple Successive Interference Cancellation Scheme in a DS/CDMA System," *IEEE J. Select. Areas Commun.*, vol. 12, pp. 796–807, June 1994.

[110] Paulraj, A. J., Gore, D. A., Nabar, R. U., and Bölcskei, H., "An Overview of MIMO Communications-A Key to Gigabit Wireless," in *Proceedings of The IEEE*, vol. 92, pp. 198–218, Feb. 2004.

[111] Payaro, M., Mestre, X., and Lagunas, M. A., "Optimum Transmit Architecture of a MIMO System Under Modulus Channel Knowledge at the Transmitter," in *Proc. IEEE Information Theory Workshop, ITW '04*, pp. 174–178, Oct. 2004.

[112] Petersen, B. R. and Falconer, D. D., "Suppression of Adjacent-Channel, Cochannel, and Intersymbol Interference by Equalizers and Linear Combiners," *IEEE Trans. Commun.*, vol. 42, pp. 3109–3118, Dec. 1994.

[113] Philips, "SAIC Link Performance Simulations." 3GPP TSG-GERAN 15 Tdoc GP-030910, 2003.

[114] Pickholtz, R. L., Schilling, D. L., and Milstein, L. B., "Spread-Spectrum for Mobile Communications," *IEEE Trans. Veh. Technol.*, vol. 40, pp. 313–322, May 1991.

[115] Proakis, J. G., *Digital Communications*. New York: McGraw-Hill Inc., 1995.

[116] Qureshi, S., "Adaptive Equalization," in *Proceedings of IEEE*, vol. 73, pp. 1349–1387, Sept. 1985.

[117] Ranta, P. A. and Escartin, A. M., "Dominant Interference Rejection by Adaptive Antennas in GSM," in *Proc. IEEE Intl. Symposium on Personal, Indoor and Mobile Radio Communications, PIMRC '97*, pp. 85–89, Sept. 1997.

[118] Ranta, P. A., Lappeteläinen, A., and Honkasalo, Z. C., "Interference Cancellation by Joint Detection in Random Frequency Hopping TDMA Networks," in *Proc. IEEE Intl. Conference on Universal Personal Communications, ICUPC '96*, pp. 428–432, Sept. 1996.

[119] Rao, B. D., Wengler, M., and Judson, B., "Performance Analysis and Comparison of MRC and Optimal Combining in Antenna Array Systems," in *Proc. IEEE Intl. Conference on Acoustics, Speech, and Signal Processing, ICASSP '01*, pp. 2949–2952, May 2001.

[120] Sandhu, S., Nabar, R. U., Gore, D. A., and Paulraj, A., "Near-Optimal Selection of Transmit Antennas for a MIMO Channel Based on Shannon Capacity," in *Proceedings of The Thirty-Fourth Asilomar Conference*, vol. 2, pp. 567–571, Oct. 2000.

[121] Sesadri, N. and Winters, J. H., "Two Signaling Schemes for Improving the Error Performance of Frequency-Division-Duplex (FDD) Transmission Systems Using Transmitter Antenna Diversity," *Int. Jr. of Wireless Information Network*, vol. 1, pp. 49–60, 1994.

[122] Shah, A. and Haimovich, A. M., "Performance Analysis of Maximal Ratio Combining and Comparison with Optimum Combining for Mobile Radio Communications with Cochannel Interference," *IEEE Trans. Veh. Technol.*, vol. 49, pp. 1454–1463, July 2000.

[123] Sheikh, K., Gesbert, D., Gore, D., and Paulraj, A., "Smart antennas for broadband wireless access networks," *IEEE Commun. Mag.*, vol. 37, pp. 100–105, Nov. 1999.

[124] Shellhammern, S., "Packet Error Rate of an IEEE 802.11 WLAN in the Presence of Bluetooth." IEEE 802.15 Contribution 00/133r0, 2000.

[125] Shiu, D. S., Foschini, G. J., Gans, M. J., and Kahn, J. M., "Fading Correlation and Its Effect on the Capacity of Multielement Antenna Systems," *IEEE Trans. Commun.*, vol. 48, pp. 502–513, Mar. 2000.

[126] Song, Y. and Blostein, S. D., "Data Detection in MIMO Systems with Co-Channel Interference," in *Proc. IEEE Vehicular Technology Conference, VTC '02*, pp. 3–7, Sept. 2002.

[127] Souissi, S. and Meihofer, E. F., "Performance Evaluation of a Bluetooth Network in the Presence of Adjacent and Co-channel Interference," in *Proc. IEEE ETS on Broadband, Wireless Internet Access*, pp. 1–6, Apr. 2000.

[128] Stüber, G. L., *Principles of Mobile Communication, 2nd ed.* Boston: Kluwer Academic Publishers, 2001.

[129] Stüber, G. L., Barry, J. R., McLaughlin, S. W., L, Y., Ingram, M. A., and Pratt, T. G., "Broadband MIMO-OFDM Wireless Communications," in *Proceedings of IEEE*, vol. 92, pp. 271–294, Feb. 2004.

[130] Suzuki, H., "Signal Transmission Characteristics of Diversity Reception with Least-Squares Combining-Relationship between Desired Signal Combining and Interference Canceling," *Electronics and communications in Japan,* Part I, vol. 76, pp. 80–93, Nov. 1993.

[131] Tarokh, V. and Jafarkhani, H., "A Differential Detection Scheme for Transmit Diversity," *IEEE J. Select. Areas Commun.*, vol. 18, pp. 1169–1174, July 2000.

[132] Tarokh, V., Jafarkhani, H., and Calderbank, A. R., "Space-Time Block Codes for Orthogonal Designs," *IEEE Trans. Inform. Theory*, vol. 45, pp. 1456–1467, July 1999.

[133] Tarokh, V., Seshadri, N., and Calderbank, A., "Space-Time Codes for High Data Rate Wireless Communication: Performance Criterion and Code Construction," *IEEE Trans. Inform. Theory*, vol. 44, pp. 744–765, Mar. 1998.

[134] Telatar, E., "Capacity of Multi-Antenna Gaussian Channels," *European Transactions on Telecommunications*, vol. 10, pp. 585–596, Nov. 1999.

[135] Uesugi, M., Futagi, S., and Homma, K., "Interference Cancellation Method using DFE," in *Proc. IEEE Vehicular Technology Conference, VTC '96*, pp. 1190–1194, May 1996.

[136] Unawong, S., Miyamoto, S., and Morinaga, N., "Effects of Microwave Oven Interference on the Performance of ISM-Band DS/SS System," in *Proc. IEEE Intl. Symposium on Electromagnetic Compatibility*, pp. 51–56, Aug. 1998.

[137] Ungerboeck, G., "Channel Coding with Multilevel Phase Signals," *IEEE Trans. Inform. Theory*, vol. 28, pp. 55–67, Jan. 1982.

[138] Valenti, M. C. and Woerner, B. D., "Iterative Multiuser Detection, Macrodiversity Combining, and Decoding for the TDMA Cellular Uplink," *IEEE J. Select. Areas Commun.*, vol. 19, pp. 1570–1583, Aug. 2001.

[139] Van Dyck, R. E., "Collaborative Co-located Coexistence Mechanism." IEEE P802.15 Contribution 01/327r0, 2001.

[140] Varanasi, M. and Aazhang, B., "Multistage Detection in Asynchronous Code-Division Multiple Access Communications," *IEEE Trans. Commun.*, vol. 38, pp. 509–519, Dec. 1990.

[141] Varanasi, M. and Aazhang, B., "Near-Optimum Detection in Synchronous Code-Division Multiple Access Systems," *IEEE Trans. Commun.*, vol. 39, pp. 725–736, Dec. 1991.

[142] Veen, B. V. and Buckley, K., "Beamforming: A Versatile Approach to Spatial Filtering," *IEEE ASSP Mag.*, vol. 5, pp. 4–24, Apr. 1988.

[143] Verdú, S., "Minimum Probability of Error for Asynchronous Gaussian Multiple Access Channels," *IEEE Trans. Inform. Theory*, vol. 32, pp. 85–96, Jan. 1986.

[144] Viterbo, E. and Boutros, J., "A Universal Lattice Code Decoder for Fading Channels," *IEEE Trans. Inform. Theory*, vol. 45, pp. 1639–1642, July 1999.

[145] Walker, E., Zepernick, H. J., and Wysocki, T., "Fading Measurements at 2.4 GHz for the Indoor Radio Propagation Channel," in *Proc. of Intl. Zurich Seminar on Broadband Communications*, pp. 171–176, Feb. 1998.

[146] Winters, J. H., "Optimum Combining in Digital Mobile Radio with Cochannel Interference," *IEEE J. Select. Areas Commun.*, vol. 2, pp. 528–539, July 1984.

[147] Wolniansky, P. W., Foschini, G. J., Golden, G. D., and Valenzuela, R. A., "V-BLAST: an Architecture for Realizing very High Data Rates over the Rich-Scattering Wireless Channel," in *Proc. IEEE Intl. Symposium on Signals, Systems, and Electronics, ISSSE '98*, pp. 295–300, Sept. 1998.

[148] Xie, Z., Short, R., and Rushforth, C. K., "A Family of Suboptimum Detectors for Coherent Multiuser Communications," *IEEE J. Select. Areas Commun.*, vol. 8, pp. 686–690, Oct. 1990.

[149] Yao, Y. D. and Sheikh, A. U. H., "The Capture Effect in Frequency-Hop Spread-Spectrum Multiple-Access Communications over Fading Channels with Near/Far Problem," in *Proc. IEEE Intl. Conference on Communications, ICC '88*, pp. 194–198, June 1988.

[150] Yoshino, H., Fukawa, K., and Suzuki, H., "Adaptive Equalization with RLS-MLSE for Fast Fading Mobile Radio Channels," in *Proc. IEEE ISCAS '92*, pp. 501–504, June 1992.

[151] Yoshino, H., Fukuwa, K., and Suzuki, H., "Interference Cancelling Equalizer (ICE) for Mobile Radio Communication," *IEEE Trans. Veh. Technol.*, vol. 46, pp. 849–861, Nov. 1997.

[152] Zeng, H. H., Li, Y., and Winters, J., "Improved Spatial-Temporal Equalization for EDGE: a Fast Selective-Direction MMSE Timing Recovery Algorithm and Two-Stage Soft-Output Equalizer," *IEEE Trans. Commun.*, vol. 49, pp. 2124–2134, Dec. 2001.

[153] Zhang, Y. B. and Letaief, K. B., "Optimizing Power and Resource Management for Multiuser MIMO/OFDM Systems," in *Proc. IEEE Global Communications Conference, GLOBECOM '03*, pp. 179–183, Dec. 2003.

[154] Zorzi, M., Rao, R. R., and Milstein, L. B., "Error Statistics in Data Transmission over Fading Channels," *IEEE Trans. Commun.*, vol. 46, pp. 1468–1477, Nov. 1998.

[155] Zurbes, S., Stahl, W., Matheus, K., and Haartsen, J., "Radio Network Performance of Bluetooth," in *Proc. IEEE Intl. Conference on Communications, ICC '00*, pp. 1563–1567, June 2000.

[156] Zyren, J., "Reliability of IEEE 802.11 WLANs in Presence of Bluetooth Radios." IEEE 802.15 Contribution 99/073r0, 1999.

VITA

Kihong Kim received the B.S. and M.S. degrees in electrical engineering from Yonsei University in Seoul, Korea, in 1987 and 1989, respectively. From 1989 to 1998, he was a Senior Research Staff at Electronics and Telecommunication Research Institute (ETRI), Taejeon, Korea, where he was involved on the development of a code division multiple access (CDMA) digital cellular system. Since 1998, he has been at Georgia Institute Technology, Atlanta, GA, working toward his Ph.D. in electrical and computer engineering. His current research interest is the wireless communications technology specifically in the design of interference cancelling receivers.